IN VIVO X-RAY FLUORESCENCE OF BONE LEAD IN THE STUDY OF HUMAN LEAD METABOLISM

IN VIVO X-RAY FLUORESCENCE OF BONE LEAD IN THE STUDY OF HUMAN LEAD METABOLISM

by

KATRINA CAKE, B.Sc.

A Thesis

Submitted to the School of Graduate Studies

in Partial Fulfilment of the Requirements

for the Degree

Master of Science

(Medical Physics)

McMaster University

August 1994

MASTER OF SCIENCE (1994)
(Medical Physics)

McMASTER UNIVERSITY
Hamilton, Ontario

TITLE: *In Vivo* X-Ray Fluorescence of Bone Lead in the Study of Human Lead Metabolism

AUTHOR: Katrina Cake, B.Sc. (University of Prince Edward Island)

SUPERVISOR: Dr. D.R. Chettle

NUMBER OF PAGES: 156

ABSTRACT

It is well known that lead is toxic. Since the full effects, particularly of long term, low level exposure are not well understood, further knowledge of lead metabolism has significant public health implications.

Traditionally, clinical studies of lead's effect on health have relied heavily on blood lead levels as an indicator of lead exposure. However, this is unsatisfactory, because blood lead levels principally reflect only recent exposure and lead in serum is more readily bioavailable than whole blood. Over 90% of the lead body burden is in bone, where it has a long residence time. Therefore, bone lead measurements are reflective of cumulative exposure.

The bone lead detection system at McMaster University uses a ^{109}Cd source, which is positioned at the centre of the detector face (HPGE). This arrangement allows great flexibility, since one can sample lead in a range of different bone sites due to a robust normalization technique that eliminates the need to correct for bone geometry, thickness of overlying tissue, and other related factors.

Lead in both the tibia and the calcaneus, whole blood lead, and serum lead have been measured in a group of 49 active lead workers (Nova Pb bone lead survey). Before studying the interrelationships between the above measurements, work was done to improve the programs which fit the bone lead spectra. That is, work was done to link the amplitudes of the alpha and beta peaks and to investigate the

sensitivity of the analysis on the channel ranges and start parameters.

The main goal of this project was to carefully study the interrelationships between the major components of any human lead metabolism model, bone, whole blood, and serum, in order to establish a solid basis for computer modelling of lead metabolism.

ACKNOWLEDGEMENTS

During the past two years, a great number of people have influenced and enriched both my academic and personal life. I would like to thank my supervisor, Dr. David R. Chettle, who has been both helpful and supportive in my pursuit for a Master of Science degree. I would also like to thank the members of my supervisory committee, Drs. C.E. Webber, W.V. Prestwich, and T.J. Kennett for all their advice.

I also want to thank my parents for all the encouragement and support they gave me when course work and research gave me serious problems. The care packages that my Mom sent to me were always great anti-depressants.

Last but not least, I would like to thank my office-mate, Dave Kornylo, for all his support and love. Friends like him are a rarity to be treasured.

TABLE OF CONTENTS

LIST OF FIGURES

LIST OF TABLES

Chapter 1

Introduction

1.1 **The Effects of Lead on Human Health**

> *"Lead is the oldest of the industrial poisons except carbon monoxide, which must have begun to take its toll soon after Prometheus made the gift of fire to man* [1] *."*

Because of the heightened public awareness of the toxicological effects of lead on human health, much effort has been put into characterizing the biological behaviour of lead in great detail. Lead is a recognized occupational hazard and became the first designated substance, in 1981, to be regulated by the Ontario Occupational Health and Safety act. Lead is often referred to as a subclinical toxin, because relatively low dose exposures may cause harmful effects to health that may not be apparent with a standard clinical examination. Clinically obvious manifestations of lead poisoning like wrist drop, anaemia, and renal failure define the upper limits of the toxicity range while effects such as slowed nerve conduction, impaired biosynthesis of haem, and altered excretion of uric acid are the subclinical alternatives.

1.1.1 **Haematological Effects**

As mentioned above, anaemia is a clinical manifestation of lead toxicity in red blood cells, where the severity correlates directly with blood lead concentrations. Quite simply, lead inhibits the body's ability to produce haemoglobin which leads to a decreased production of red blood cells. The impairment of haem biosynthesis first begins with the inhibition of δ-aminolevulinic acid dehydratase (ALAD), a cytoplasmic enzyme which acts as a catalyst for the condensation of two molecules of δ-aminolevulinic acid (ALA) to form one molecule of porphobilinogen (PGB), a precursor of haem. (Figure 1.1) The lead ions can replace the enzyme activating zinc ions at a few sites on ALAD, and thus inactivate ALAD and elevate ALA in blood and urine. Urinary ALA increases nonlinearly with increases in the blood lead concentration, perhaps exponentially, for blood lead concentrations exceeding 30-40 μg/dl [2,3]. The inhibition of ALAD is noted initially at blood lead concentrations of 10-20 μg/dl and is complete at concentrations of 70-90 μg/dl [4]. Lead also inhibits ferrochelatase, a mitochondrial enzyme, which catalyses the transfer of iron from ferritin into protoporphyrin to form haem. This results in an accumulation of protoporphyrin in the erythrocytes and an increased excretion of coproporphyrin in the urine. The concentration of erythrocyte protoporphyrin (EP) begins to rise above background levels, in adult men, at blood lead concentrations of 30-35 μg/dl [5]. EP has a much higher affinity for zinc than for iron and measuring zinc protoporphyrin (ZPP) would be another indicator of lead exposure.

The haem protein is also an important part of cytochrome A^3, a compound that is responsible for the production of adenosine triphosphate (ATP). Because ATP provides energy for cells to function, interfering with cytochrome production can lead to decreased cell efficiency [6].

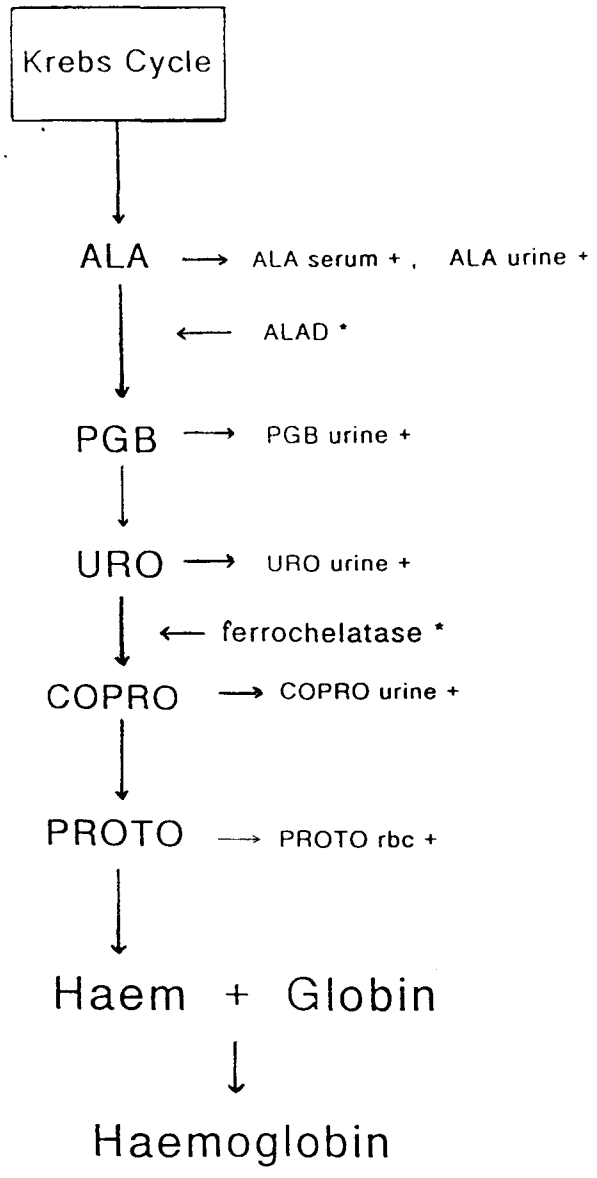

Figure 1.1: Effects of lead on haem synthesis. The * indicates the enzymes inhibited by lead. URO is the abbreviation for uroporphyrin and COPRO is the abbreviation for coproporphryin.[7]

1.1.2 **Neurological Effects**

With respect to the nervous system, lead principally targets the motor axons. The clinical manifestation is extensor muscle palsy with ankle and wrist drop, but lead also induces pathological changes in the axons like axonal degeneration and segmental demyelination. Recent studies have reported a slowing of nerve conduction in lead exposed workers without displaying any signs of weakness at blood lead levels below 60 μg/dl [8,9].

Neurological illnesses like dementia may also be linked to chronic lead exposure, because lead appears to enter the brain readily and to be selectively deposited in the hippocampus, cortex, and in nonneuronal elements that are necessary to maintain the blood-brain barrier functions. More work needs to be done to investigate this possible connection.

1.1.3 **Renal Effects**

In the kidneys, the clinical manifestation of lead toxicity is chronic nephropathy which can lead to kidney failure after high dose, long term exposure to lead. Blood lead concentrations of approximately 40-60 μg/dl have been linked with subsequent renal disease [10,11,12]. Specifically, it is the cells lining the proximal tubules that are sensitive to lead. In these cells, blood lead concentrations below 25 μg/dl inhibit the metabolic activities of vitamin D [13], and at blood lead concentrations of 40-80 μg/dl, lead induces the formation of dense intranuclear

inclusion bodies [14]. The formation of these bodies is a protective mechanism, because it helps to lower the concentration of lead in the cytoplasm. The fact that these bodies can be shed is another useful attribute.

1.1.4 **Reproductive Effects**

Animal studies (male and female) have shown lead at high doses to be toxic to the reproductive system [15]. Decreased sperm count and an increased occurrence of morphologically abnormal sperm has been reported in male workers who have been heavily exposed to lead (blood lead $>$ 58.2 μg/dl) [16]. Findings have also been reported which link blood lead concentrations of 15-20 μg/dl with neurological damage to the fetus [17,18,19].

1.2 **The Multiple Pathways for Lead Absorption**

The most significant pathways for lead absorption are by direct air inhalation, direct ingestion or inhalation of settled dust, and ingestion of food and water. In other words, both the respiratory and gastrointestinal tracts play a very important role in lead uptake. For example, 30% - 50% of inhaled lead is absorbed by the lung and then enters the circulatory system [6]. Of course, particle size and ventilation rates must be taken into consideration.

For small children, the main routes leading to exposure are lead in soil and paint chips. This is the case because gastrointestinal absorption is age-dependent. Adults absorb about 10% [20] of ingested lead while children absorb as much as 50% [21]. Although, it is important to note that the amount of lead absorbed by the gastrointestinal tract does vary with gut content [22,23].

Why do soil and paint chips pose a potential health risk with respect to lead? In older homes, lead-based paints were used both for the interior and exterior, and before the switch from leaded to unleaded gasoline, the fallout from motor vehicles greatly enriched the lead concentration in soil, especially in urban areas. Older homes are also known to have lead pipes which can raise the lead concentration in the tap water above standard limits. To a lesser degree, modern copper and brass pipes also elevate the concentration of lead in water due to the leaching of lead from the solder in the joints. Lead particles in air can also deposit on fruits and vegetables and leave residues that can be ingested. As well, growing plants can absorb lead from the soil.

With respect to occupational exposure, inhalation is the primary route, but the consumption of tobacco, food, and beverages can also increase exposure if such products become contaminated with lead from the work environment.

1.3 The Distribution of Lead in the Human Body

Lead competes with calcium for deposition in bone. That is, lead becomes incorporated into the crystalline structure of bone where it replaces calcium ions at some sites. Lead also distributes similarly to calcium and other alkaline earth elements among different bones [24,25,26] and is eventually distributed throughout the bone volume [27,28,29].

With respect to the skeleton, there are two distinctive bone types, cortical (80%) and trabecular (20%) [30,31]. Cortical bone is characterized by being very dense and compact with only 5-30% of its volume being occupied by vascular and marrow space [32] and is found at the outer surfaces of many bones like vertebrae and the ribs and in the shafts of the long bones. O'Flaherty describes trabecular bone as consisting "of an intricate network of leaves and struts of marrow-free bone surrounding small communicating pockets of marrow-vascular space [32]." Trabecular bone is often referred to as spongy bone because of its porous nature. It is important to realize that no bone is a 100% pure in composition, although several bones like the calcaneus and the tibia approach 90-95% purity.

Less than 10% of all lead stored in the body is deposited in the soft tissues, where it is distributed unequally [33]. Ingested lead that is not absorbed by the body passes through the gastrointestinal tract and is eliminated in the feces. Lead that is absorbed into the circulating blood can be excreted through the renal system or the

gastrointestinal tract. Human lead metabolism studies, in adults, have demonstrated that short term lead excretion amounts to 50-60% of the absorbed lead fraction [34].

TABLE 1.1

Concentration of Lead in Tissues of Subjects

With No Known Occupational Exposure to Lead

Male Adults - Cadavers [35]

Tissue	No. of Samples	Mean Value (ppm wet weight)
Bone		
Tibia	60	23.40 +/- 15.96
Rib	60	8.85 +/- 5.81
Calvarium	31	20.17 +/- 16.00
Liver	58	1.03 +/- 0.62
Pancreas	58	0.37 +/- 0.26
Kidney		
Cortex	59	0.78 +/- 0.38
Medulla	59	0.50 +/- 0.25
Skin	26	0.19 +/- 0.14
Lung	59	0.22 +/- 0.11
Heart	59	0.07 +/- 0.05

With respect to table 1.1, how does Barry's tibia wet weight measurement convert to bone mineral. In the ICRP publication, "Report of the Task Group on Reference Man", table 21 lists the composition of tibia, ulna, and rib for two male skeletons. The mean % ash value for the tibia is 42.8 [36]. To correct a tibia wet weight measurement to a bone mineral measurement, one has to divide the wet weight measurement by 0.428.

In order to make a useful comparison with contemporary results in Hamilton, one had to look at Barry's age dependent table which lists a value of 16.40 ppm wet weight for the tibia [35]. The age group was 30-39, male, and included only 5 measurements. The corresponding value for the lead concentration in units of μg Pb / g bone mineral is 38.32. Hoe does this compare with results of non-occupationally exposed people in Hamilton? Gamblin et al measured the tibia bone lead concentration in 111 non-occupationally exposed subjects from this region [37]. The mean tibia lead value for males with respect to this age range was 7.00 μg Pb / g bone mineral [37]. Based on the Nova Pb bone lead survey (exposed factory workers), the mean tibia lead value for this age range was 35.83 μg Pb / g bone mineral.

The two values which one should most be concerned about are the Nova Pb bone lead survey result and the result by Gamblin et al, because Barry results were published in 1975, where the collection dates for samples ranged from May 1966 to May 1973. The 1986 EPA criteria document had shown that the average blood lead level for the general public dropped dramatically during the years 1976 to 1980

which is mostly likely due to the phasing out of leaded gasoline [38]. Therefore, different environmental conditions existed for the general public in 1975 and would explain the discrepancy between Barry and Gamblin et al values for non-occupationally exposed workers.

The amount of lead that enters the blood stream depends upon the chemical and physical parameters of lead, the different routes of absorption, individual variability, and on factors like nutritional status and age. In adults, around 10-15% of ingested lead will be absorbed, but this absorption rate can increase to 45% under fasting conditions [39,40]. Traditionally, whole blood lead concentrations and EP levels have been used as indicators of exposure. Such measurements are only representative of recent exposure because of the short half-lives. For example, the half-life of lead in blood is approximately 35 days [41]. With respect to EP, an increase is observable at blood lead concentrations between 20-25 μg/dl [42], and the half-life is roughly 1-2 months following a specific exposure [4]. Blood contains lead in two forms, non-diffusible (bound to the erythrocytes) and diffusible (plasma). Thus, plasma is the component of blood which contains the more biologically active fraction of lead, where the concentration depends mainly on the balance between absorption, elimination, and transfer of lead to and from bone.

90-95% of the total lead body burden in adults (73% for children) is in bone [43,44], thus bone lead measurements would be reflective of cumulative exposure. Bone was once considered as a physiological sink for lead, a storage site, where lead

is permanently removed from the circulation and any possible contact with soft tissue. Such a concept was proven to be incorrect. The current train of thought is that bone lead storage is a two-way process of active influx and efflux which closely models the physiology of calcium metabolism and that bone mineralization is an active process with uniquely different developmental stages during skeletal growth. Skeletal lead stores are not inert. Clinical studies have illustrated quite clearly that lead can be remobilized from bone into blood. Therefore, bone lead can be considered as an endogenous source and can have a dramatic effect on blood lead levels, especially for those individuals who have had long term exposure to lead. A good example is the survey of 30 retired lead workers conducted by Gerhardsson et al where strong correlations were observed between tibia and calcaneus lead concentrations and blood lead concentrations [45]. Based on a set of serial measurements of retired lead workers, Nilsson et al observed that blood lead concentrations were, in general, higher than the values observed in non-occupationally exposed individuals which implies that aging is associated with a slow efflux of lead from bone [46]. Physiologic states like kidney disease, bone disease, aging, and nutritional deficiencies in calcium intake have also been shown to have an effect on blood lead levels. As well, pregnancy and lactation have been shown to heighten the release of bone lead stores into blood. A Swedish group measured the blood lead concentrations of 120 women during their pregnancy, and it was observed that the blood lead levels increased significantly during the latter stages of pregnancy [47]. Another example is

postmenopausal women. Silbergeld observed that significantly higher blood lead concentrations were observed in postmenopausal women than premenopausal women [48].

1.4 The Mechanisms for Lead Detection

a. Calcium Disodium Edetate Lead Mobilization Test

There are two common methods of assessing lead exposure, calcium disodium edetate lead mobilization test (EDTA) and *in vivo* x-ray fluorescence. Even though the EDTA lead mobilization test is no longer considered to be reflective of the total body burden of lead, it is still a commonly used technique.

The EDTA lead mobilization test is impractical for repeat measurements or widespread screening, because it requires injections and 24 hour urine collections. Another common chelating agent used is penicillamine (PCA). It can be administered orally, but since it is less potent than calcium disodium edetate, the chemical yield is reduced. The chelated lead concentration is representative of the portion of the total lead body burden that is readily mobilized and is equivalent to the more exchangeable lead pools like blood, soft tissue, plasma, trabecular bones, and the outer surface layer of cortical bones. Another problem associated with this method is that the exact location from which the chelatable lead is derived is unknown and can vary with

different metabolic conditions [49]. Based on animal studies, Hammond reports that calcium disodium edetate mainly releases bone deposits of lead, [50] but alternatively, Castellino and Aloj report that calcium disodium edetate primarily releases lead stores from soft tissues like the liver and kidneys [51]. Even though several human studies have reported a wide discrepancy between calcium disodium edetate results and bone lead content [52,53], Batuman et al have shown that the EDTA lead mobilization test did achieve a substantial reduction in the bone lead concentration for a patient with a longstanding exposure to lead. Both chemical tests of bone biopsies and *in vivo* x-ray fluorescence measurements support Batuman's claim [54], but it has been shown that the amount of chelated lead does not equal the amount of bone lead. A recent paper by Tell et al has reported that the amount of chelatable lead is mainly due to the blood and the soft-tissue lead pools which are partially dependent upon the lead content in the skeleton. [55]

b. *In Vivo* X-Ray Fluorescence

The technique of *in vivo* x-ray fluorescence is a safe, fast, and noninvasive alternative to the EDTA lead mobilization test. For a long time, laboratory diagnosis of lead poisoning depended heavily on the concentration of lead in blood and urine samples. Using *in vivo* x-ray fluorescence, one can measure bone lead concentrations and thus quantify the extent of cumulative lead exposure. Bone lead measurements are

important, because it allows one to monitor individuals who are not eligible for monitoring by other techniques and to estimate past exposure which is important for epidemiological studies of adverse health effects. As well, field studies have shown that the technique of *in vivo* x-ray fluorescence is transportable, convenient for subjects, and accurately measures bone lead content. For example, in one study of 6 intact leg specimens, the correlation coefficient was 0.98 when relating K x-ray fluorescence bone lead measurements with the results obtained by atomic absorption spectroscopy [56].

X-ray fluorescence (XRF) involves using photons to fluoresce atoms of a particular element. These atoms can then emit x-rays of energies that are specific to that element (characteristic x-rays). Of course, the number of x-rays is proportional to the amount of element present in the sample. The concept is easy to understand if one considers the atom as consisting of electrons in layers or shells surrounding the nucleus. The standard procedure is to give a letter designation to the electrons existing in the same shell, where electrons in the innermost shell ($n = 1$) are called K electrons, electrons in the second shell ($n = 2$) are called L electrons, electrons in the third shell are called M electrons, and so forth (Figure 1.2).

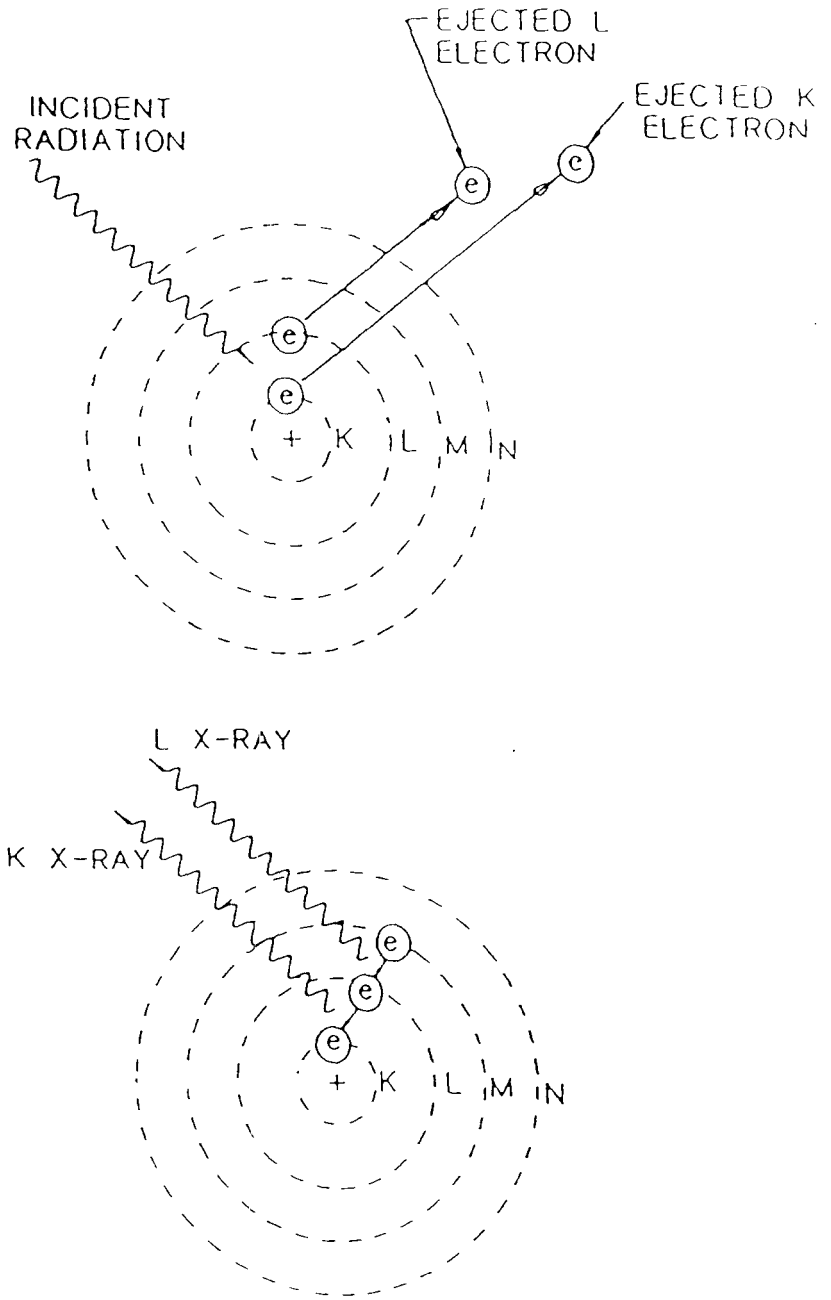

Figure 1.2: X-ray fluorescence [28]

In 1976, Ahlgren et al reported the first noninvasive measurements of bone lead in humans, where gamma-rays from ^{57}Co were used to excite the K series x-rays of lead in finger bones with a 90^0 geometry and obtained a detection limit of 20 (μg Pb/g bone wet weight) for a dose of 2.5 mGy at the midpoint of the phalanx [57]. Price et al adopted the same method to measure lead in the phalanx as well [58]. Around the same time, Bloch et al independently measured lead in teeth using ^{57}Co and obtained results very similar to Ahlgren et al [59]. The choice of isotope for K series x-ray fluorescence quickly became ^{109}Cd with a backscatter geometry, because such an approach permitted great flexibility in sampling lead in a range of different bone sites and involved a rigorous normalization technique which eliminated the need to correct for thickness of overlying tissues, bone geometry, and other related factors. The tibia and the calcaneus soon became the principal target sites because of easy accessibility, purity of bone type, and the preference for avoiding radiosensitive organs. Better precision was obtained using ^{109}Cd than ^{57}Co, $\sim$ 10 μg Pb / g bone mineral versus 50 μg Pb / g bone mineral, but ^{109}Cd results in a higher effective dose equivalent, 2.1 μSv versus 0.1 μSv [60,61].

L series x-rays can also be used where either radioactive sources or polarized x-rays are the source of incident radiation. For example, Wielopolski et al used silver K series x-rays from ^{109}Cd or telurium K series x-rays from ^{125}I to excite the lead L series x-rays (10.5 keV, 12.6 keV) in the tibia [62]. A detection limit comparable to the above systems which used ^{57}Co was obtained, but the dose was much larger, 10

mGy [62]. Because of the low energies, attenuation of the signal by the overlying skin must be taken into account. Based on the mass attenuation coefficients from Robinson and bone composition and density figures from Woodard, the attenuation mean free paths (the average distance travelled by a photon before undergoing some form of interaction) for 11.5 keV and 75 keV photons were calculated to be 0.028 and 2.2 cm. [63,64] Using the data from the ICRP, for soft tissue, the corresponding figures are 0.31 and 5.4 cm. [65] Therefore, by using K x-rays, one is ensuring that the measurement is over as large a bone volume as possible.

The lead detection system at McMaster University uses a ^{109}Cd source which emits gamma-rays of 88.035 keV in 3.6% of its decays. The energy of these gamma rays is just above the energy threshold for the K shell absorption edge in lead (88.005 keV) and thus maximizes the x-ray fluorescence yield per incident photon [66]. The gamma rays can interact with a K shell electron in lead and eject it. The resulting vacancy can then be filled by less tightly bound electrons, and energy being released as K series x-rays (96% of transitions) or Auger electrons. ^{109}Cd also emits silver x-rays in its decay (^{109}Cd decays by electron capture to ^{109m}Ag) but are filtered out by placing a thin piece of copper in front of the source.

Compton scattering of the incident gamma-rays can occur in the subject and results in scattered photons of reduced energy, where the amount of energy is dependent upon the angle of scatter. Because of the backscatter geometry ($\sim 160^0$) used (Figure 1.3), the Compton scattered photons have a mean energy of 66.5 keV

[66]. Unfortunately, scattered photons produce relatively intense background in the energy spectrum and thus limit measurement precision. There will be a distribution of energies about this mean due to the range of detection angles possible during bone lead measurements which emphasizes the point that it is important to have the Compton scatter peak as far away as possible from the lead K x-rays in order to minimize the background beneath them. Earlier, it was mentioned that using ^{109}Cd with a backscatter geometry was advantageous. This is the case, because the Compton scatter peak would be well below the lead x-ray peaks. For example, if a 90^0 geometry was used, then the Compton scattered photons would have an energy of 75.1 keV and would obscure the lead K_α x-rays [66].

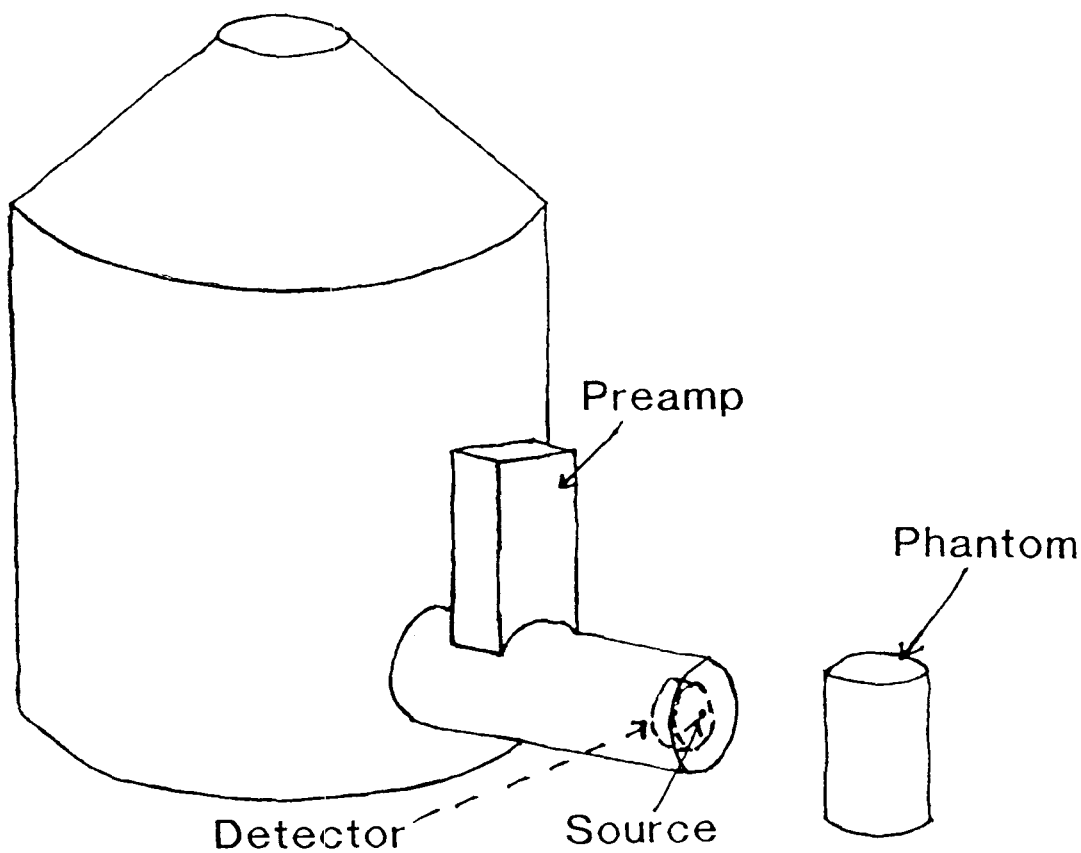

Figure 1.3: Equipment arrangement for *in vivo* K x-ray fluorescence [67].

In contrast to inelastic scattering, elastic scattering results in a scattered photon of virtually unchanged energy. When looking at the spectrum of a bone lead measurement, the most dominant feature is the Compton scatter peak, but the elastic (coherent) scatter peak at 88 keV is also clearly visible. The energies of the lead K x-rays are listed below (Figure 1.4): [66]

$K_{\alpha 1}$ = 75.0 keV
$K_{\alpha 2}$ = 72.8 keV
$K_{\beta 1}$ = 85.0 keV
$K_{\beta 2}$ = 87.3 keV
$K_{\beta 3}$ = 84.5 keV

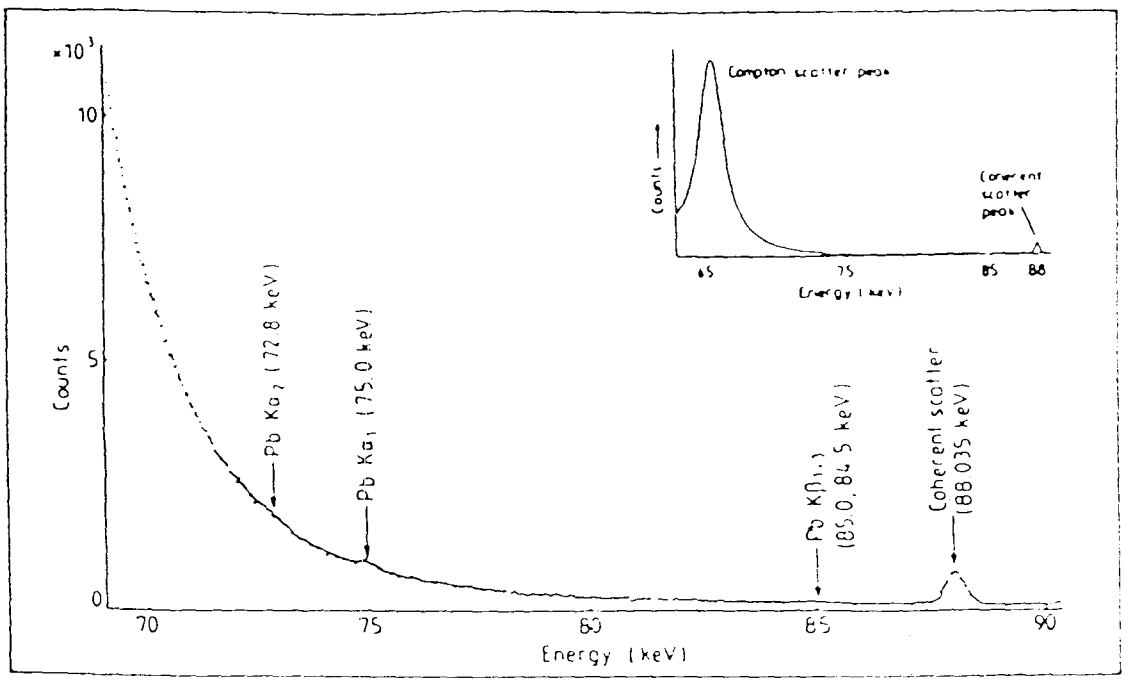

Figure 1.4: Typical spectra obtained using the K x-ray fluorescence technique [68].

The $K_{\alpha 1}$ and $K_{\alpha 2}$ x-ray peaks are the most intense, but since the background below the $K_{\beta 1}$ and $K_{\beta 3}$ is much less than the alpha peaks, there is still valuable information to be gained. The relative intensities of the x-rays are 100%, 59.3%, 22.8%, and 11.9% for $K_{\alpha 1}$, $K_{\alpha 2}$, $K_{\beta 1}$, and $K_{\beta 3}$ respectively [66]. Due to the resolution of the detector, one does not see the $K_{\beta 1}$ and $K_{\beta 3}$ peaks separately. One refers to this sum peak as $K_{\beta 1,3}$. In order to analyze this peak, one has to take into account a calcium edge at 84.0 keV [61], a phosphorus edge at 85.9 keV in the case of bone mineral [66], and a sulphur edge at 85.6 keV in the case of plaster of Paris phantoms [66]. Although the $K_{\beta 2}$ peak is used in in-vitro analyses, it is not used in in-vivo studies, because there is an oxygen edge that interferes with it. It is a tricky feature to correct for since the height is dependent on the amount of soft tissue.

Although elastic scattering at these large angles is a low probability event compared to Compton scattering, the cross-section at this energy and angle varies very strongly with the atomic number (Z) of the target atom. Because the cross-section depends on the fifth or sixth power of Z, the elastic scatter peak is predominantly due to the higher Z elements. For example, the elastic scattering cross section is 28 times greater for cortical bone than soft tissue [69]. Therefore, with respect to bone, 98-99% of the elastic scatter peak arises from bone mineral.

It is important to note that the lead x-ray peaks arise from bone as well, since it is the main storage site for lead and that the kidney and liver will not be in view during a bone lead measurement. The concentration of lead in bone is essentially uniformly distributed on the scale defined by the penetration of lead K x-rays which is approximately 30 mm, although the lead concentration has been shown to vary sharply over distances of the order of 100 μm [29]. Another relevant fact is that only uncollided gamma-rays can produce lead K x-rays, since the energy of the ^{109}Cd gamma rays are only 30 eV above the lead K shell absorption edge. For example, a Compton scatter of greater than 3.6^0 will result in a scattered photon with energy below the lead photoelectric K edge [70]. Therefore, the same photon fluence gives rise to both the elastic scatter peak and the lead K x-ray peaks. Although, it is important to note that a very small angle Compton scatter can give rise to an elastic scatter which would still be within the resolution of the detector, but since this is a second order process, the effect is quite small. By combining the points mentioned above, a rigorous method for normalizing lead to bone mineral is obtained by taking the ratio of the amplitudes of the lead K x-ray peaks and the elastic scatter peak (Figure 1.5). Such a ratio is insensitive to either source to sample distance, thickness of overlying tissue, and bone geometry in spite of marked variations in lead x-ray counts.

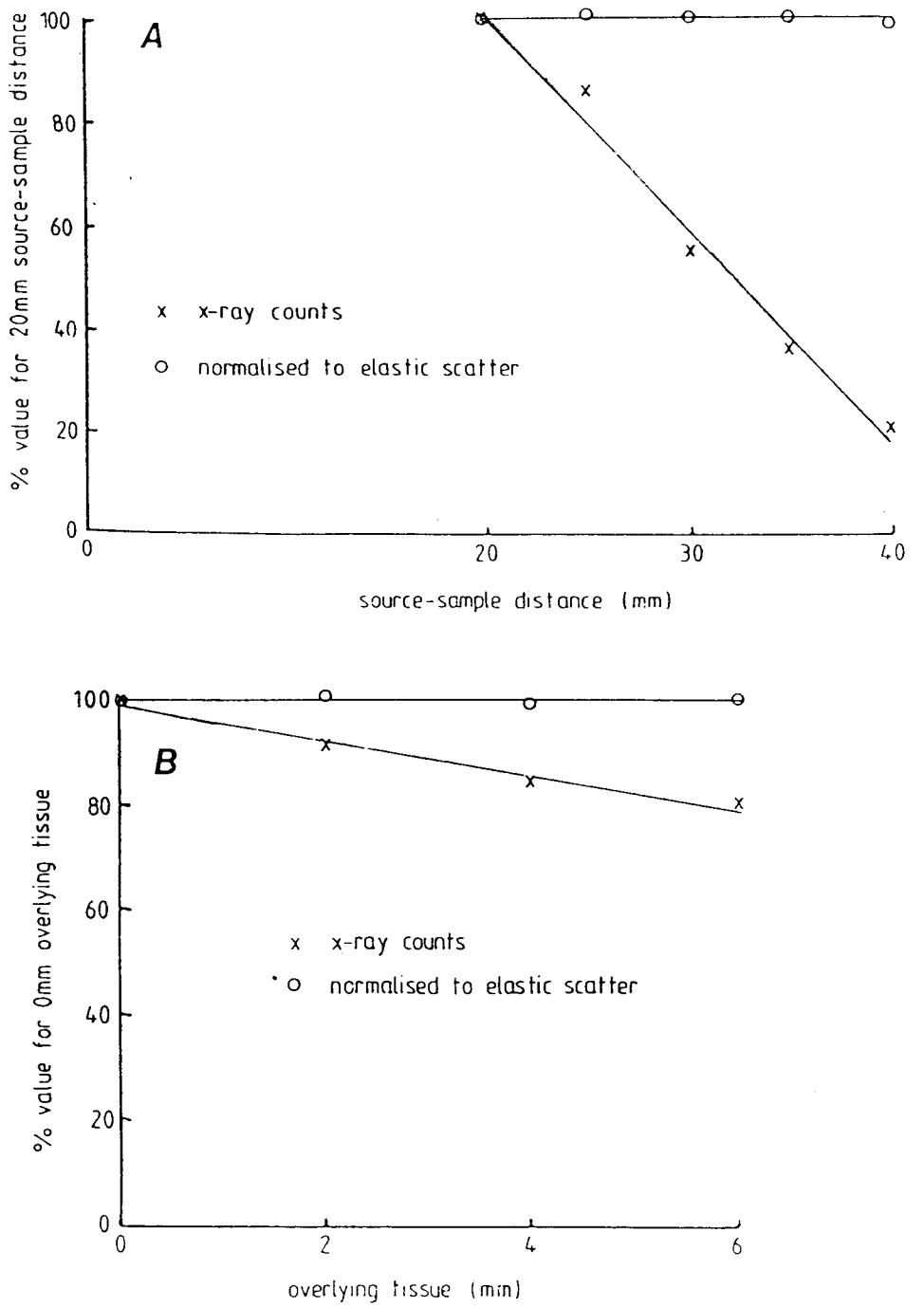

Figure 1.5: Elastic scatter normalization. (A.) Source to sample distance (B.) Thickness of overlying tissue [66].

In order to obtain bone lead concentrations, the x-ray to coherent ratio is calibrated against a series of plaster of Paris phantoms (calcium sulphate) which have been doped with various quantities of lead. Of course, there needs to be a correction factor to take into consideration the fact that the elastic scatter cross section differs between bone mineral and plaster of Paris. Essentially, all one has to do is multiply the calibrated ratio by 1.46 [66]. Since the cross sections are also a weakly varying function of angle, the fact that a range of angles is subtended does not erode the normalization.

The best way to conclude this section is to discuss precision and accuracy. Accuracy is a measure of how close the result of the experiment comes to the true value while the precision is a measure of how exactly the result is determined. With respect to *in vivo* x-ray fluorescence, the precision is dependent on the amount of overlying tissue. That is, the precision worsens with increasing tissue thickness. For ^{109}Cd K x-ray fluorescence, the precision worsens by 5% when comparing 3 mm to 6 mm of overlying tissue [71]. In other words, the number of x-ray counts limits the precision. The accuracy depends on the quality of the phantoms, the assumption that the lead concentration in tissue is zero, and the assumption that lead is homogenously distributed in the bone. The first assumption is not entirely correct. In the previous section, it was mentioned that less than 10% of lead stored in the body is deposited in the soft tissues. The second assumption is true. A study by Wittmers et al indicated that the concentration of lead was relatively uniform along the length of the tibia [72].

The accuracy is also dependent on the normalization technique, because it removes potential problems associated with source to subject distance, bone size, bone geometry, bone density, overlying tissue thickness, and minor subject movement.

The ^{109}Cd K x-ray fluorescence technique has been tested by analyzing sets of bone samples using both atomic absorption spectroscopy and x-ray fluorescence [73,74]. The results are summarized below [66]:

TABLE 1.2

Comparison of Atomic Absorption and X-Ray Fluorescence Results

Bone Sample	n	Mean Difference
Metatarsal	6	-3.4 +/- 4.1
Tibia section	3	4.9 +/- 4.3
Tibia section	16	1.0 +/- 7.6
Tibia section	22	-1.0 +/- 9.9
Tibia fragment	11	-3.0 +/- 6.2
Calcaneus	22	2.0 +/- 23.7
Combined sets		0.2 +/- 23.7
Tibia section	41	0.2 +/- 8.8
All bones	80	0.0 +/- 14.1

1.5 McMaster University Lead Detection System

The lead detection system at McMaster University consists of a high purity germanium (HPGe) detector (horizontal integral type), a fast spectroscopy amplifier, a Wilkinson analog-to-digital converter (ADC), and a multichannel analyzer (MCA). All the equipment was made by Canberra, a nuclear electronics company. Specifically, the model 2024 fast spectroscopy amplifier, model 8077 Wilkinson ADC, and the Accuspec MCA was used. With respect to the detector, it has an active diameter of 50.5 mm, an active area of 2000 mm^2, a sensitive volume 20 mm thick, a 0.5 mm beryllium window, and requires a bias voltage of -2500 V dc [75]. The manual specifications for this detector define the energy resolution by referring to the FWHM of three isotopes, ^{55}Fe, ^{57}Co, and ^{133}Ba. For example, with a time constant of 4 μs, the FWHM is 564 eV for the 81 keV gamma ray of ^{133}Ba [75].

The ^{109}Cd source is positioned in a tungsten collimator at the centre of the detector face, so that the 88 keV photons cannot directly enter the detector. For a bone lead measurement, the person's tibia or calcaneus is positioned approximately 20-30 mm away depending on the activity of the source. The 1.11 GBq source was prepared by Amersham Canada and placed in a stainless steel capsule. The collimator was fitted with a 0.5 mm thick copper filter to absorb the Ag K x-rays associated with the decay of ^{109}Cd.

In order to protect the beryllium window, a cylindrical iron sleeve with a

closed end of styrene slides over the horizontally mounted detector and is held in place by grub screws. At the centre of the styrene face, a lucite source holder was glued into place. An additional iron sleeve slides over the inner sleeve and is held in place by grub screws as well. The shutter for the source, a tungsten alloy, is mounted on the outer sleeve. The detector was then mounted on a table which allowed movement of the detector in three orthogonal directions.

Before the Nova Pb bone lead survey, there was only one operational lead detection system at McMaster University which was, and still is, in constant use, therefore a second system needed to be assembled. Specifically, a MCA was needed, but a general review of what the market had to offer for gamma spectroscopy systems was done. The latest equipment by Canberra, Aptec, and EG&G was tested. In the next chapter, I will discuss the results of these tests.

1.6 **Nova Pb Bone Lead Survey**

At the end of May 1993, the lead research team went to a lead recycling plant, Nova Pb, in St. Catherine, Quebec. Each factory worker had their tibia and calcaneus measured, where each measurement took 30 minutes for a total effective dose of 70 nSv [76]. By the end of the survey, 65 people had both measurements done. Great care was taken to ensure that there was no external contamination. That is, the measurement site was swabbed very carefully with rubbing alcohol, the

workers showered, if possible, before having their bone lead measured, and the system was set up in one of the conference rooms in an office building which is separate from the plant. As well, each subject had to answer a comprehensive questionnaire which inquired about previous lead exposure, other than current employment, and about such factors like drinking, smoking, and eating disorders that might affect the metabolism of lead.

The factory has in its employ a physician, Dr. Vaillancourt, who provided us with whole blood lead information at monthly intervals, but there were often interruptions in the monitoring. It is also important to note that the monitoring programme began in 1987, but the majority of the workers had been at the plant long before this time. Therefore, the blood lead records can be divided into two groups, incomplete and complete. For example, of the 65 individuals who had bone lead measurements done, 53 had blood lead records, but only 11 of the 53 were complete blood lead records.

Serum samples were collected later in June and sent to McMaster University where they were analyzed for lead content by Bowins and McNutt [77]. It is very unfortunate that the serum lead was not routinely measured. Since it is considered to be the biologically most readily available compartment for lead, it would have been interesting to have seen how serum concentrations varied with time. As the technique improves, it may someday be possible to make routine serum lead measurements. It would also have been ideal to have had information on urine lead levels for a more

complete picture. In order to develop a realistic model for human lead metabolism, one has to look at all the relevant components.

The Nova Pb bone lead survey provided the raw data for this thesis, and in future chapters, the relationships between bone lead (calcaneus and tibia), serum lead, and whole blood lead will be explored in great detail in order to further the understanding of human lead metabolism.

Chapter 2

Testing of New Equipment

2.1 The Need for a Second Lead Detection System

In section 1.6 of chapter 1, it was mentioned that the lead research team went to the Nova Pb lead recycling plant in St. Catherine, Quebec to measure both tibia and calcaneus bone lead concentrations in the factory workers. In order to be able to make such measurements, a second system had to be assembled. Specifically, a MCA was needed, but a general review of what the market had to offer for amplifiers and ADCs was done. The latest equipment by Canberra, Aptec, and EG&G (Ortec) was tested [78,79,80].

2.2 The Basic Components of a Gamma Spectroscopy System

a. Overview

A common nuclear measurement is to record the amplitude distribution of the pulses produced by a detector. Figure 2.1 is an illustration of the various components in a gamma spectroscopy system.

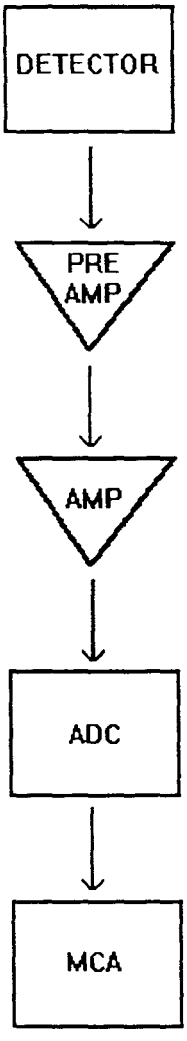

Figure 2.1: Pulse height analysis system.

b. Detector

It was mentioned in section 1.5 of chapter 1 that a HPGe detector was used. Simply put, germanium detectors are semiconductor diodes, where the depletion region is sensitive to ionizing radiation. When under a reverse bias, an electric field extends across the depleted region. If a photon interacts with the material in the depleted volume of the detector, charge carriers, electrons and holes, are formed. These carriers are then swept by the electric field to the P and N electrodes of the detector. Such a charge is proportional to the energy deposited in the detector which is proportional to the energy of the incident photon and can be converted into a voltage pulse by an charge sensitive preamplifier.

The time it takes the carriers to travel to the electrodes is often referred to as the charge collection time. When a second event takes place before the completion of the first, the energy of the two events is summed together. Therefore, if the detector starts reporting more sum peaks than valid events, then the count rate capability of the system has been exceeded.

Since germanium has a relatively low band gap, this kind of detector must be cooled with liquid nitrogen to reduce the thermal generation of charge carriers, leakage current, which can seriously affect the energy resolution of the detector. Two other note-worthy features of germanium detectors are the cryostat which consists of a vacuum chamber that houses the detector element and a dewar for containing the liquid nitrogen. The HPGe detector used in the Nova Pb bone lead survey was a

horizontal integral type where the dewar and the detector chamber are permanently attached together.

c. Preamplifier

In the previous section, it was discussed how incident radiation could produce a burst of charge in the detector. For most detectors, this charge is so small that the signal pulses are useless without some amplification. Therefore, the first step, as indicated by figure 2.1, is a preamplifier, and its job is to convert the ionization charge that was developed in the detector during each absorbed event to a step-function output pulse whose amplitude is proportional to the charge accumulated in that event.

If a second pulse arrives before the first has completely decayed, then it rides upon the tail of the first pulse, and causes the signal baseline to rise slightly. Although, as long as the sum of the amplitudes of the pulses and any residual tailing does not exceed the dynamic range of the preamplifier, then the preamplifier will not reach saturation. When the preamplifiers saturates, it simply stops working until the feedback resistor has time to draw the baseline dc level back down to within the operating voltage.

Since small pulses represent low energy events while large pulses are indicative of high energy events, it takes more low energy events to result in the same dc level increase as would be caused by a few high energy events. Therefore, the

throughput capabilities of a preamplifier decrease as the energy of the events increases.

d. Amplifier

Depending on one's outlook, the key element or weakest feature of any gamma spectroscopy system is the amplifier. Its duty is to shape the pulses from the preamplifier to match the input span for which the MCA has been designed or in other words, pulse shaping and amplitude gain. Specifically, it is the shaping functions of the amplifier that will dictate how well it will perform. At high count rates, there can be serious problems in trying to optimize the system. That is, the parameters chosen to minimize pulse pileup and to assure rapid return of the pulse to the baseline conflict with the choices that would need to be made about signal-to-noise.

Differentiators and integrators play an important role in how amplifiers perform their jobs. The differentiator allows the energy information contained in the leading edge of a signal to be passed through while the trailing edge is clipped sharply to the baseline. The integrator recovers the energy information from the signal and produces a Gaussian shaped pulse, where the amplitude of the pulse is directly proportional to the energy information of the preamplifier pulse. With respect to the differentiator, shorter time constants result in higher throughout rates, since the tails of the preamplifier pulses will be pulled down much more quickly. Although, shorter

time constants will cause the integrator to pass more high frequency noise which will degrade the quality of the signal. Therefore, any adjustments to the amplifier to improve throughput capabilities will do so only at the expense of decreased resolution. If the full amplitude of the preamplifier pulse is to be preserved through the shaping process, the shaping time constants must be large compared with the rise time of the preamplifier. If not, the amplitude of the amplifier's output pulse will be too low, and thus there will be a loss of resolution in the data. This pulse height distortion which is caused by too short of a time constant is called ballistic deficit. There is no simple solution. If the time constant is too long, then the throughput capabilities of the system are reduced.

e. ADC

Quite simply, the ADC converts the amplitude of the pulse presented at its input into a digital value that can be processed by the MCA. There are two commonly used kinds of ADCs, fixed conversion time and Wilkinson. With respect to a Wilkinson ADC, the time needed to convert a pulse is proportional to the amplitude (energy) of that pulse ; higher energies imply longer conversion times. First, the input pulse is sent to a comparator circuit which continuously compares the amplitude with that of a linearly increasing ramp voltage. The output of the comparator circuit is a gate pulse that begins at the same time as the initiation of the ramp voltage. This gate voltage is maintained until the comparator senses that the linear ramp has reached the

amplitude of the pulse. The gate pulse is then used to operate a linear gate that receives periodic pulses from a constant frequency clock. Thus, a number of these pulses pass through the gate and are counted by the address register. Since the gate is opened for a period of time that is proportional to the input pulse amplitude, the number of pulses stored in the register is proportional to the input amplitude.

The fixed conversion time or successive approximation ADC will always take the same amount of time to make a conversion regardless of the amplitude of the pulse being converted. In the first stage, a comparator is used to determine whether the amplitude of the input pulse lies in the upper or lower range of the ADC. If it lies in the lower half, a zero is entered in the first bit of the binary word which represents the output of the ADC. If the amplitude is in the upper half, the circuit subtracts a value equal to 1/2 the ADC range from the pulse amplitude and passes the remainder on to the second stage. A one is then entered as the first bit. The second stage involves making a similar comparison but over half the range of the ADC. A zero or a one is then entered as the second digit depending on the size of the remainder passed on from the first stage. The remainder from the second stage is then passed on to the third stage and etc. If there are ten stages, the binary word is ten bits long which will cover a range of 2^{10} or 1024 channels [81]. Wilkinson ADCs generally have better linearity than fixed conversion time ADCs, because linear ramp generators can be designed to be very precise. As well, the cumulative errors arising from the subtraction process in fixed conversion time ADCs will degrade the linearity.

Of course, piled up events are invalid and will only increase the background, thus it is best that they are not processed by the ADC. A pileup rejector circuit is the answer. If a new pulse arrives from the preamplifier before the amplifier has finished processing the previous pulse, the pileup rejector circuit will generate a reject signal which will tell the data acquisition system that the event is invalid and should be ignored. However, the ADC does not indiscriminately reject data every time its receives a reject signal. For example, with respect to trailing edge pileup, once a pulse in the ADC has risen from its baseline to its peak and returned to its 90% point, then the ADC accepts the event for conversion [81]. In the case of leading edge pileup, since the reject is generated before the ADC has detected a peak, this event is obviously invalid and will be rejected.

f. MCA

The multichannel analyzer (MCA) records and stores pulses according to their height, where each storage unit is referred to as a channel. Since each pulse is stored in a particular channel corresponding to a certain energy, the distribution of the pulses in the channels is an image of the distribution of the energies of the particles.

2.3 **Experimental Design**

Before describing the method used to test the different equipment, there are a few important points to keep in mind. Since the lead research team uses this technology to make *in vivo* measurements of human bone lead concentrations, a blank plaster of Paris phantom and an aluminum resin phantom were used to test the equipment. The blank plaster of Paris phantom was chosen, because the concentration level ($\sim$ 0 ppm Pb) is indicative of what one would expect in a non-occupationally exposed person and a series of lead doped plaster of Paris phantoms were used to calibrate the ratios of the amplitudes of the K x-ray peaks and the coherent (elastic) scatter peak in terms of parts per million. The aluminum resin phantom was chosen, since its chemical composition and size is similar to human bone and the dead time of the system is comparable to what is obtained when bone lead measurements are done. Another relevant point to make is that each bone lead measurement takes thirty minutes. Such a decision involved taking into consideration the comfort of the subject and the necessity of having enough counts to reduce the %error in the area of the coherent peak to approximately 1%. Of course, more information could be obtained if the acquisition time was increased, but this is not practical in an *in vivo* bone lead survey. The experimental design was quite simple. In each case, the phantom was placed 20 mm away from the ^{109}Cd source and a 30 minute real time acquisition was then started. The resulting spectrum was then analyzed using a program called

PBCOFWH.FOR which fits the coherent scatter peak. The main criteria for ranking the various equipment were the area and its % error, the background, and the FWHM.

2.4 **Results**

The results are summarized in table 2.1. One should note that TC is the abbreviation for time constant, the first number refers to the amplifier model, and the second number refers to the ADC model. The words, S100 and Accuspec, are used to describe Canberra's different MCAs.

With respect to APTEC, their system was tested several times, because the engineers continued to make design changes with hopes of improving the performance of their system. Version #1 of Aptec is their first offering. #2 involved adjustments with the pileup reject, and #3 and #4 involved changes to the amplifier. The exact nature of the changes and adjustments is unknown, because I only received the modified product. There was no verbal or written explanation of the changes made.

Canberra and EG&G systems both offered gated integration (GI). Previous work has shown that Canberra's GI mode does not significantly improve throughput [82], therefore only EG&G's version was tested.

In order to simplify the analysis program, the width was defined to be equal to $\sqrt{2} \times \sigma$, where σ is the gaussian width. Such a unit was used to simplify the spectral analysis program. The FWHM is equal to $2.35 \times \sigma$. The area under the coherent peak is equal to $\sqrt{2\pi}\ a\ \sigma$, where a is the amplitude of the peak ; the uncertainty is equal to $\sigma_{AREA}^2 = AREA^2 \left(\frac{\sigma_a^2}{a^2} + \frac{\sigma_w^2}{w^2} + 2\frac{\sigma_{aw}^2}{aw} \right)$. Even though the uncertainty equation for the area includes a covariance term, it was not used in the final determination of the uncertainty, because the covariance term was assumed to be scaling with the other two terms. The % error is defined by the equation:

% error $= \frac{\sigma_{AREA}}{AREA} \times 100$. BKG is the abbreviation for the background under the coherent peak which can be calculated using the equation : $\frac{A_4}{A_5} \left(e^{A_5 X_2} - e^{A_5 X_1} \right)$,

where A_4 represents the initial exponential background and A_5 is the exponent coefficient of the exponential background. As well, $x_1 = A_1 - 2A_6$ and

$x_2 = A_1 + 2A_6$, where A_1 is the centroid and A_6 is the width of the coherent peak. GCR is the abbreviation for the gross counting rate ; %Dead is the short form for dead time. Figure 2.2 illustrates some of the above definitions.

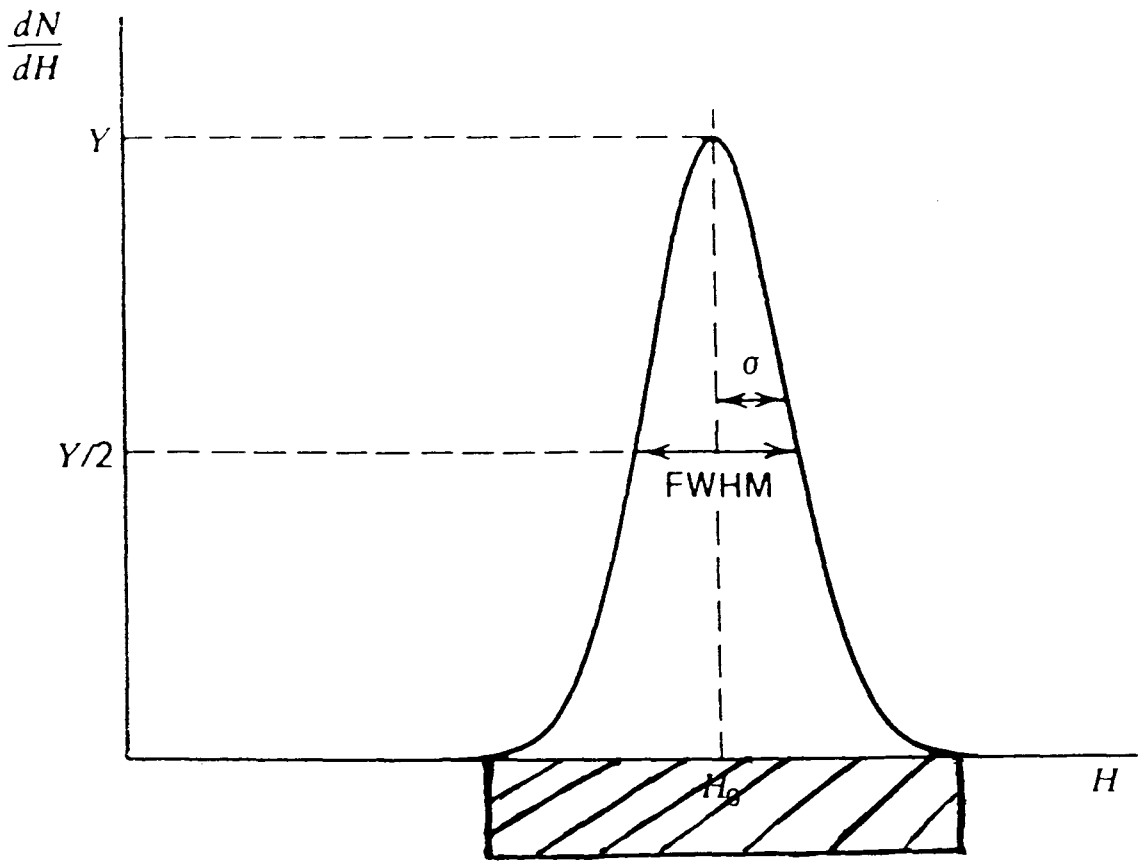

Figure 2.2: Illustration of the terms used to characterize a peak. The box with lines drawn through it represents the background underneath the peak. [80]

To help prevent confusion, the following lines list all the equipment tested with respect to each manufacturer:

1.) Canberra Industries Inc.

a.) S100 System

- 2024 amplifier
- 8077 ADC -- Wilkinson
- S100 MCA -- Windows version

b.) Accuspec system

- 2025 amplifier
- 8715 ADC -- Fixed Conversion Time
- Accuspec MCA -- DOS version

2.) Aptec Engineering Limited

a.) Flatpack

- a single unit package -- high voltage bias supply, amplifier, and ADC (900 ns)

b.) 6300 amplifier

3.) EG & G Nuclear Instruments

a.) 673 Spectroscopy Amplifier and Gated Integrator

b.) 973U Ultra High Rate Amplifier

TABLE 2.1

TEST RESULTS

*** P - Plaster of Paris Phantom, A - Aluminum Resin Phantom**

SYSTEM	FILE	FWHM (eV)	AREA	%ERROR	BKG	GCR	%DEAD
2024, 8077	P	721	35,715 +/- 303	0.849	616	26.015	32
S100 MCA	P - REPEAT	712	36,745 +/- 304	0.828	540	26.950	33
TC = 1.0 µs	A	724	21,019 +/- 286	1.363	6,299	37.667	56
	A - REPEAT	711	21,737 +/- 294	1.352	6,751	38.681	60
2024,8715	P	727	36,964 +/- 306	0.827	464	27.883	34
S100 MCA	P - REPEAT	727	37,637 +/- 308	0.818	482	28,391	35
TC=1.0 µs	A	722	21,979 +/- 294	1.336	6,507	39,217	58
	A - REPEAT	722	21,807 +/- 293	1.344	6,736	39,346	58
2024, 8715	P	723	35,992 +/- 318	0.883	650	27,355	32
ACCUSPEC MCA	P - REPEAT	725	36,359 +/- 307	0.845	504	27,378	33
TC = 1.0 µs	A	769	20,941 +/- 317	1.512	8,692	38,636	54
	A - REPEAT	786	21,140 +/- 320	1.512	8,964	39,213	55
2024,8077	P	722	32,981 +/- 286	0.868	439	24.548	30
ACCUSPEC MCA	P - REPEAT	727	32,691 +/- 285	0.872	342	24,774	30
TC = 1.0 µs	A	784	19,896 +/- 300	1.507	7,527	36.742	53
	A - REPEAT	767	19,064 +/- 291	1.527	7,151	36,280	52
2025, 8715	P	721	34,851 +/- 308	0.884	1,291	26,395	26
ACCUSPEC MCA	P - REPEAT	723	35,343 +/- 309	0.861	1,400	26,986	27
TC = 1.0 µs	A	699	21,920 +/- 414	1.889	33,081	41.908	48
	A - REPEAT	719	22,016 +/- 420	1.909	33,394	41.824	48
FLATPACK	P	860	36,268 +/- 331	0.912	2,302	26.975	41
APTEC	P - REPEAT	851	34,732 +/- 325	0.936	2,331	26.324	41
TC=0.50 µs	A	857	24,656 +/- 493	2.001	42,445	42.998	57
#1	A - REPEAT	889	25,104 +/- 509	2.026	46,989	43.479	58

FLATPACK	P	742	34,144 +/- 306	0.895	1,650	25,917	43
APTEC	P - REPEAT	749	33,186 +/- 305	0.920	1,479	25,238	43
TC=0.75 µs	A	736	18,771 +/- 365	1.946	23,309	34,174	60
#1	A - REPEAT	764	19,619 +/- 390	1.985	26,775	34,959	63
FLATPACK	P	680	30,454 +/- 279	0.912	961	23,140	42
APTEC	A	697	15,750 +/- 326	2.073	18,673	29,187	67
TC = 1.0 µs							
#1							
APTEC 6300	P	908	38,106 +/- 350	0.917	2,364	28,009	28
TC=0.50 µs	P - REPEAT	906	37,408 +/- 347	0.927	1,143	27,961	19
#2	A	927	28,136 +/- 554	1.969	45,446	48,258	44
	A - REPEAT	929	27,450 +/- 553	2.013	42,419	49,648	42
APTEC 6300	P	788	35,236 +/- 316	0.897	986	26,414	26
TC=0.75 µs	P - REPEAT	797	35,230 +/- 316	0.897	1,159	26,207	27
#2	A	827	24,375 +/- 506	2.078	39,361	45,368	51
	A - REPEAT	822	25,000 +/- 472	1.886	34,624	43,761	48
APTEC 6300	P	710	34,559 +/- 302	0.875	1.314	25,836	36
TC = 1.0 µs	P - REPEAT	715	33,750 +/- 298	0.883	918	25,306	39
#2	A	723	19,654 +/- 407	2.071	31,547	37,515	61
	A - REPEAT	748	19,891 +/- 415	2.087	30,624	37,592	59
APTEC 6300	P	954	36,813 +/- 357	0.971	748	27,490	23
TC=0.50 µs	P - REPEAT	933	35,804 +/- 350	0.976	749	27,279	22
LL-#3	A	978	23,035 +/- 465	2.017	15,571	45,320	40
	A - REPEAT	985	22,721 +/- 466	2.053	15,153	45,204	40
APTEC 6300	P	759	35,137 +/- 301	0.857	693	25,930	26
TC=0.75 µs	P - REPEAT	758	34,718 +/- 299	0.862	514	26,190	27
LL-#3	A	742	22,048 +/- 340	1.542	14,195	41,471	47
	A - REPEAT	759	21,586 +/- 336	1.556	13,277	40,711	46

APTEC 6300	P	705	31,434 +/- 284	0.902	815	23,427	28
TC = 1.0 µs	P - REPEAT	708	32,454 +/- 288	0.886	914	24,079	29
LL-#3	A	705	19,260 +/- 365	1.893	22,923	36,558	50
	A - REPEAT	697	19,036 +/- 359	1.884	21,360	36,167	49
APTEC 6300	P	896	36,240 +/- 329	0.908	1,045	26,844	24
TC=0.50 µs	P - REPEAT	895	35,680 +/- 327	0.917	1,070	26,460	23
#4	A	904	24,723 +/- 392	1.587	17,511	44,942	35
	A - REPEAT	901	24,609 +/- 398	1.619	17,192	45,282	35
APTEC 6300	P	775	33,025 +/- 297	0.899	755	24,688	28
TC=0.75 µs	P - REPEAT	776	32,865 +/- 297	0.903	925	24,757	28
#4	A	763	22,098 +/- 365	1.652	19,033	40,477	43
	A - REPEAT	767	22,004 +/- 366	1.661	19,342	40,697	43
APTEC 6300	P	715	31,050 +/- 284	0.916	868	23,211	36
TC = 1.0 µs	P - REPEAT	712	30,708 +/- 282	0.919	939	23,071	35
#4	A	703	18,895 +/- 361	1.912	22,486	35,255	51
	A - REPEAT	699	18,797 +/- 357	1.898	22,296	35,096	51
ORTEC 973U	P	1044	40,966 +/- 451	1.100	850	31.548	15
GI – 1.5 µs	A	1132	23,278 +/- 1369	5.880	39,414	54,397	28
ORTEC 973U	P	816	37,978 +/- 329	0.866	908	28,542	24
GI – 3.0 µs	A	917	22,146 +/- 570	2.574	31,960	46,260	42
ORTEC 673	P	771	30,687 +/- 288	0.939	388	22,933	31
GAUSSIAN - 1.0 µs	A	874	10,559 +/- 341	3.227	9,011	27,426	58
ORTEC 673	P	1027	38,917 +/- 410	1.053	916	28,845	26
GAUSSIAN - 0.5 µs	A	1120	15,623 +/- 1466	9.383	27,344	43,621	46

The systems which performed the best were both built by Canberra, S100 and Accuspec. It was found that the Canberra's 2025 amplifier was no improvement over the 2024 and that there was no significant difference in performance between the 8077 and the 8715 ADC.

Both the S100, Accuspec, and the combinations of the S100 and Accuspec yielded similar results for energy resolution (FWHM). It is worthy to note that the different generations of the Aptec equipment at a time constant of 1 μs had similar energy resolution as the Canberra systems, but other factors like the background and the %error in area of the peak forced one to reject the equipment. Generally, anything that one does to the amplifier to improve the count rate capabilities will do so only at the expense of decreased resolution, and such a statement is clearly supported by the results obtained for the other systems with poor energy resolution.

It is important to remember that energy resolution is dependent on pulse shaping. Since noise created in the detector and the early amplifier stages accompanies the detector signal, appropriate pulse shaping can enhance the signal while at the same time reduce the noise. Gaussian pulse shaping is a popular choice in gamma spectroscopy systems utilizing high resolution germanium detectors because of reduced pulse pileup at high counting rates and improved signal-to-noise ratio. All the systems studied used Gaussian pulse shaping. The results of a paired t test analysis of the values obtained for the resolution using the 2024 and 2025 amplifiers with the 8715 ADC and Accuspec MCA show that the values obtained for the resolution are

not statistically different with respect to the plaster of Paris phantoms, but the results for the aluminum resin phantom are statistically different at the 5% test of significance level. Such results imply that the resolution is marginally better when using the 2025 amplifier, but it is important to note that both amplifiers are very sensitive to the pole-zero adjustment. Therefore, the difference in resolution may be attributed to the pole-zero not being properly adjusted.

Another advantage of the Canberra systems is that they are characterized by low background which implies that the pile-up rejector is working quite well. While the use of shorter shaping time constants minimizes pileup, there will always be some upper incoming count rate limit beyond which the amplifier will produce more piled up events than valid events. Assuming a properly set up amplifier, there is no way to avoid pileup other than reducing the incoming count rate. But, by using a pileup rejector circuit, one can ensure that the piled-up events are not processed by the ADC.

The results of a paired t test analysis of the values obtained for the background using the 2024 and 2025 amplifiers with the 8715 ADC and Accuspec MCA show that the values are not statistically different with respect to the plaster of Paris phantom, but the results for the aluminum resin phantom are statistically different at the 1% test of significance level. As the dead time and the gross counting rate values indicate, the system is operating at higher count rates when the aluminum resin phantom is used. It is important to remember that the aluminum resin phantom was

chosen, because it mimics the demands on the systems by *in vivo* bone lead measurements. The values for the background are higher when the 2025 amplifier is used instead of the 2024 amplifier which implies that the pileup rejector is working more efficiently in the 2024 amplifier unit.

The area under a peak is representative of the absolute intensity of a particular gamma energy. In this case, the coherent scatter peak represents the intensity of the elastic scatter photons which are of the same energy as the gamma ray source ($\sim$88 keV). Therefore, the system with the lowest % error in the area is the best (Canberra), because one is limiting the counting rate error in the coherent peak.

Based on the above analysis and discussion, the Accuspec MCA and the 8715 ADC were purchased for the Nova Pb bone lead survey, where the 8715 ADC was used as a spare.

Chapter 3

Spectral Analysis

3.1 **Introduction**

The coherent scatter and x-ray peaks of the spectra collected during the Nova Pb bone lead survey were analyzed using a non-linear least squares fit program (FORTRAN code), where the parameters used varied according to the peak of interest. Basically, each peak was assumed to be a Gaussian: $Ce^{-(\frac{X-A}{W})^2}$ [70].

The parameters, C, A, and W, refer to the intensity, position of the centroid, and the width of a peak (Remember: $W = \sqrt{2}\ x\ \sigma$). X refers to a varying channel number which depends on the region of interest.

The background under pairs of peaks, $K_{\alpha 1}$ and $K_{\alpha 2}$, $K_{\beta 1}$ and $K_{\beta 3}$, and $K_{\beta 2}$ and the coherent scatter peak, was fitted by either a single or double exponential function. It had been previously shown that the optimum fit is achieved when the spectrum is divided into three regions and analyzed separately [70].

Since the background beneath $K_{\alpha 1}$ and $K_{\alpha 2}$ x-ray peaks has a Compton component which decreases rapidly with increasing energy, the background is best

approximated by a double exponential [70]. A single exponential was determined to be appropriate for the $K_{\beta 1}$ and $K_{\beta 3}$ x-ray peaks and the $K_{\beta 2}$ and the coherent scatter peaks [70]. As well, with respect to the beta peaks, the edge features from calcium and phosphorus or sulphur (person or phantom) were also modelled.

In order to be able to compare the peak amplitudes directly, a common photopeak width was used in all three regions. For the final determination of the lead concentration, an inverse variance weighted mean based on all the peaks (except $K_{\beta 2}$) was calculated. Such a mean was calculated, because it maximizes the spectral information that was gathered.

There is one slight quirk. Because of incomplete charge collection, there is a step in the Gaussian peak. (Figure 3.1) This step can be smoothed out using the complimentary error function (ERFC) which is a smooth step function derived from the error function (ERF).

$$ERF(Y) = \int_0^X \frac{1}{\sqrt{2\pi}} e^{-\frac{1}{2}x^2} dX \qquad (1)$$

$$ERFC(Y) = 1 - ERF(Y) \qquad (2)$$

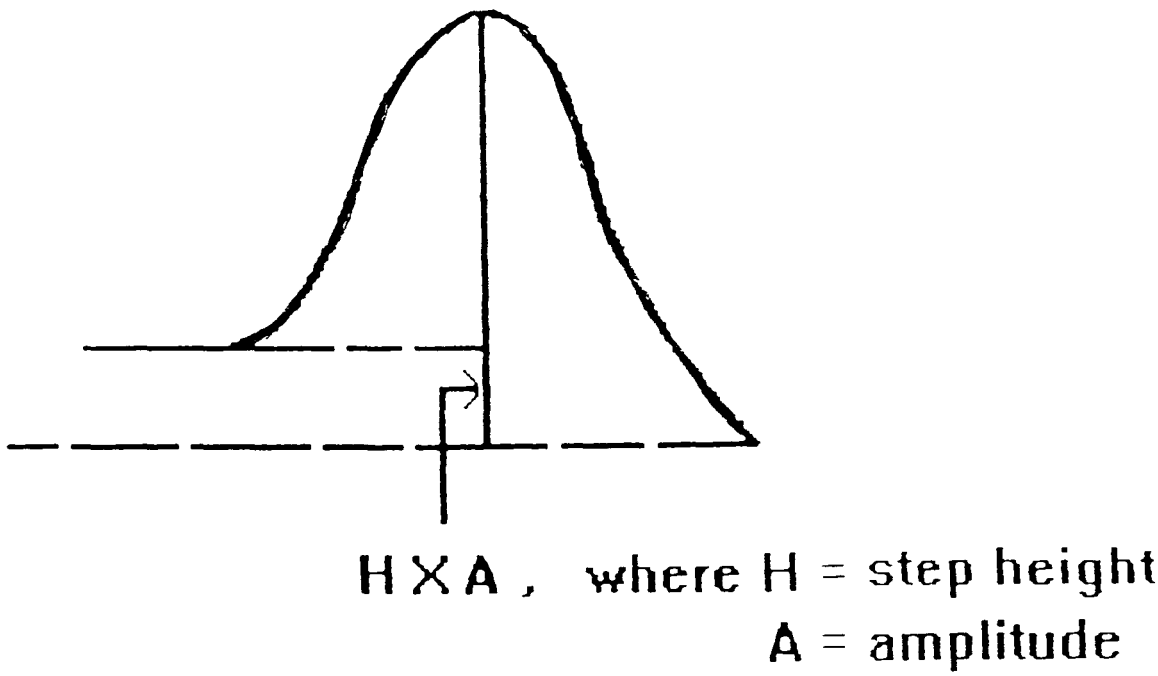

Figure 3.1: An illustration of the step observed in a Gaussian peak due to incomplete charge collection in the detector.

3.2 Non-Linear Least Squares Fitting Program

The non-linear least squares fitting program fits the non-linear parameterized function y(x) to data of values y_i. Such a concept was discussed at length in the book, Data Reduction and Error Analysis [83]. The subroutines of this program which dealt with peak analysis were modified in order to improve the fit.

Therefore, if one keeps in mind section 3.1 and the above paragraph, the following equations can be written:

$$y_\alpha = A(2)\,[e^{-Z^2} + H(ERFC(Z))] + A(3)\,[e^{-Y^2} + H(ERFC(Y))] + A(4)\,e^{A(5)x} + A(6)\,e^{A(7)x} \qquad (3)$$

where,

A(1) = position of α_1 peak

A(2) = amplitude of α_1 peak

A(3) = amplitude of α_2 peak

A(4) = amplitude of the first exponential background

A(5) = exponent coefficient for the first exponential background

A(6) = amplitude of the second exponential background

A(7) = exponent coefficient for the second exponential background

Z = (X - A(1)) / W

G = gain

Y = [X - (A(1) - 2165/G)] / W

$$y_C = A(2)\,[e^{-Z^2} + H(ERFC(Z))] + A(4)\,e^{A(5)X} \qquad (4)$$

$$+ A(3)\,[(e^{-Y^2} + H(ERFC(Y))) + 0.509\,(e^{-V^2} + H(ERFC(V)))]$$

where,

A(1) = position of coherent scatter peak

A(2) = amplitude of coherent scatter peak

A(3) = amplitude of β_2 peak

A(4) = amplitude of exponential background

A(5) = exponent coefficient for the exponential background

C = coherent peak using the fixed width and height model

Y = [X - (A(1) - 675/G)] / W

V = [X - (A(1) - 794/G)] / W

Z = (X - A(1)) / W

$$y_\beta = A(1)\,[e^{-D^2} + H(ERFC(D))] + A(2)\,[e^{-Y^2} + H(ERFC(Y)]$$

$$+ A(3)\,e^{A(4)X} + A(5)\,[e^{A(6)\,(POSCA)}\ (ERFC(CA)) \qquad (5)$$

$$+ 0.167\ (e^{A(6)\,(POSP)}\ (ERFC(P))]$$

where,

A(1) = amplitude of β_1

A(2) = amplitude of β_3

A(3) = amplitude of exponential background

A(4) = exponent coefficient for the exponential background

A(5) = amplitude of calcium edge

A(6) = exponential coefficient for calcium and phosphorus edges

CPOS = position of coherent peak

Ca = gaussian parameter for calcium edge (CA = POSCA / W)

POSCA = X - (CPOS - 4038/G)

D = [X - (CPOS - 3099/G)] / W

Y = [X - (CPOS - 3585/G)] / W

POSP = X - (CPOS - 2146/G)

P = POSP / W

The above equation is only used for people spectra. Plaster of Paris phantoms contain sulphur rather than phosphorus. The changes that would have to be made simply involve changing 0.167 to 0.37, POSP to POSS (POSS = X - (CPOS - 2472/G)), P to S, and ERFC(P) to ERFC(S).

a. DCWORK.FOR

The nonlinear least squares fitting routine begins with the program, DCWORK.FOR. This program allows one to input the initial start parameters (A(1), A(2),...etc.) for each peak region ($K\alpha_1$ and $K\alpha_2$, $K\beta_1$, and $K\beta_3$, $K\beta_2$ and the coherent scatter peak), determine the channel range, create output files, and calls the subroutine, FIT.FOR, which then calls the other necessary subroutines.

routine. First of all, it organizes the spectral data (x,y) into arrays and then reads the y value of the spectrum from the offset channel to channel 2048 (user determined limit). FIT.FOR then calls subroutine, FCHIS.FOR, to evaluate the χ^2 at the starting point of the search (CHISQ1) by calculating YFIT (equal to either y_α, y_c, or y_β) at each channel over the specified channel range using the appropriate version of the subroutine, FUNCT.FOR (alpha, beta, or coherent). FCHIS.FOR does this by calculating the χ^2 at each channel of the specified range using the equation:

$$CHISQ = CHISQ + (Y(I) - YFIT(I)) x (Y(I) - YFIT(I)) \; / \; YFIT(I)$$

where YFIT(I) is used to estimate the variance in Y(I).

The sum over all the required channels is then divided by the degrees of freedom where the number of degrees of freedom (FREE) equals the # of channels (NPTS) - # of parameters (NTERMS).

$$FREE = NPTS - NTERMS \qquad (7)$$

$$CHISQ1 = \frac{CHISQ}{FREE} \qquad (8)$$

It is important to note that the χ^2 is a **reduced** χ^2 which means that the χ^2 value is divided by the number of degrees of freedom.

Before continuing with the discussion of FIT.FOR, it is important to remember that the optimum values of the parameters, a_j, are obtained by minimizing the χ^2 with respect to each of the parameters simultaneously.

$$\frac{\partial \chi^2}{\partial a_j} = \frac{\partial}{\partial a_j} \sum \frac{[y_i - y(x_i)]^2}{\sigma_i^2} = 0 \qquad (9)$$

Experience has shown that one should consider χ^2 as a continuous function of the n parameters a_j describing a hypersurface in n-dimensional space and that the space must be searched for the appropriate minimum value of χ^2. The problem associated with such a search is that there may be more than one local minimum for χ^2 within a reasonable range of values for the parameters a_j with respect to an arbitrary function. Instead of expanding the function χ^2 to develop an analytical description of the hypersurface, one should expand the fitting function y(x) as a function of the parameters a_j and use the method of least squares to determine the optimum value of the parameter increments, δa_j.

It was Marquadt who developed an algorithm which combines the best features

of a gradient search with the method of linearizing the fitting routine by increasing the diagonal terms of the curvature matrix by a factor, λ [84]. The following paragraphs will discuss this method in great detail.

FIT.FOR first evaluates the weights at each channel in the portion of the spectrum that is being analyzed. In other words, FIT.FOR provides a measure of the accuracy of the fit in each channel and is equal to the inverse of the variance in the observed value of y ($1 / \sigma_i^2$).

In order to be able to solve the equation, $\frac{\partial \chi^2}{\partial a_j}$, a matrix inversion

technique must be used. That is, the alpha and beta matrices must be evaluated. The alpha matrix, a symmetrical curvature matrix, measures the curvature of the χ^2 hypersurface.

$$\alpha_{j,k} = \sum \frac{1}{\sigma_i^2} \frac{\partial y(x_i)}{\partial a_j} \frac{\partial y(x_i)}{\partial a_k} \qquad (10)$$

$$\alpha'_{j,k} = \alpha_{j,k}(1 + \lambda) \text{ when } j = k \text{ or } \alpha'_{j,k} = \alpha_{j,k} \text{ when } j \neq k$$

The beta matrix is a row matrix and its elements are defined as:

$$\beta_k = \sum \frac{1}{\sigma_i^2} \left[y_i - y(x_i) \right] \frac{\partial y(x_i)}{\partial a_k} \qquad (11)$$

Therefore, when λ is large, the diagonal element dominates and then the matrix equation reduces to $\beta_i = \lambda \, \delta a_j \, \alpha_{i,j}$.

One can thus write:

$$\delta a_j = \sum_{k=1}^{n} (\beta_k \, \epsilon'_{j,k}) \qquad (12)$$

where $\epsilon'_{j,k}$ is the inverse of $\alpha'_{j,k}$.

FIT.FOR calls the subroutine, FDERV.FOR, to calculate the values of the partial derivatives, $\frac{\partial y(x_i)}{\partial a_j}$, in order to determine the elements for these matrices.

The next step involves using the program MATINV.FOR for inverting the $\alpha'_{j,k}$ matrix to find the parameter increments according to equation 12.

The new parameters are accumulated as follows:

$$B(J) = a_j + \delta a_j \qquad (13)$$

These parameters are then used to recalculate YFIT using the subroutine, FUNCT.FOR, which assigns new values for the expected y's for all channels. The new YFIT values are used to calculate the reduced χ^2 (CHISQR) using the FCHIS.FOR subroutine. Next, the difference between the new χ^2 (CHISQR) and the χ^2 calculated at the starting point (CHISQ1) is calculated to determine whether the χ^2 has decreased. If the χ^2 has decreased or remained unchanged, the constant factor, λ, is reduced by a factor of 10 and the values for the new parameters B(J) are assigned to the variables A(J). Therefore, when the change in χ^2 ($\Delta \chi^2$) is greater than (0.001) x (new χ^2), FIT.FOR reevaluates the alpha and beta matrices using the new values, A(J) and λ to find even more accurate parameter increments. If $\Delta \chi^2$ is less than (0.001) x (new χ^2), then CHISQR is adequate and is kept. The last case to consider is when the χ^2 increases. If the χ^2 has increased and $\Delta \chi^2$ is less than or equal to 1×10^{-3}, then the difference is insignificant, but if the $\Delta \chi^2$ is greater than 1×10^{-3}, then the difference cannot be ignored. λ is thus increased by a factor of 10 and used to recalculate the parameter increments as discussed above.

c. FUNCT.FOR

The subroutine, FUNCT.FOR, is the peak analysis portion of the program. It has three different versions, alpha peaks, beta peaks, and the coherent scatter peak. In all cases, the peaks are considered to be Gaussian in nature. FUNCT.FOR takes into consideration for each specific case the relevant peaks and backgrounds. Using these equations, the program calculates the expected values of y and YFIT(I).

d. FDERV.FOR

As indicated previously, FDERV.FOR evaluates the partial derivatives of the function y(x) with respect to each parameter and appears in the equations for the elements of the alpha and beta matrices in the FIT.FOR subroutine.

e. MATINV.FOR

MATINV.FOR inverts the symmetrical $\alpha'_{j,k}$ matrix of NORDER (number of parameters) and calculates its determinant which then allows one to calculate the increment values for the parameters.

f. FCHIS.FOR

FCHIS.FOR is a very useful subroutine that FIT.FOR relies upon heavily and was discussed in great detail in part b of section 3.2.

g. ERFC.FOR

ERFC.FOR is the subroutine which calculates ERFC(Y) and allows one to correct for the step observed in the peaks due to incomplete charge collection in the detector. ERFC.FOR is also used to model the calcium, phosphorus, and sulphur edges.

3.3 Spectral Analysis of the Nova Pb Bone Lead Survey

3.3.1 General Peak Analysis

Using the people and phantom data from the first day of the Nova Pb bone lead survey, the following models were used to analyze the data. For an illustration of the different peaks, one is referred to figures 3.2 and 3.3.

a.) Coherent scatter peak

- Floating width and height
- Fixed width and height

b.) Beta peaks

- Unlinked β_1 and β_3 amplitudes
- Linked β_1 and β_3 amplitudes

c.) Alpha peaks

- Unlinked α_1 and α_2 amplitude
- Linked α_1 and α_2 amplitudes

a. Coherent Peak

With respect to the coherent scatter peak, figure 3.1 illustrates what is meant by the terms, width and height. At this point, it is important to recall that the width is due to the resolution of the detector while the height is due to incomplete charge collection. In the floating width and height case (FLWH), both the width and the

height were included in the initial start parameters for the non-linear least squares fitting routine. For both phantom and people data, the average value for the width was determined and used in the final analysis (fixed width and height - FWH). Since the height depends on how the detector operates, it should be the same for both phantoms and people, but in people, there is an oxygen edge which varies in amplitude with the amount of soft tissue in view and interferes with the height. Therefore, one used the average phantom height value for all cases. The main reasons for fixing the width and the height were to improve the χ^2 and decrease the statistical uncertainty. In summary, for people, a mean width of 9.69 +/- 0.10 was determined and a mean value of 0.053 +/- 0.008 for the height. For the phantoms, a mean width of 9.43 +/- 0.04 was determined and a mean height of 0.030 +/- 0.002.

The results of the coherent scatter peak analysis are best summarized if one looks at two separate groups, people and phantoms.

(i.) People

The mean χ^2 value (ν=63) for the FWH model was 1.018 +/- 0.174 which is numerically less than the mean χ^2 for the FLWH model, 1.024 +/- 0.159. However, the two are not significantly different at the 5% test of significance level using a paired t test approach. Similarly, neither χ^2 value is significantly greater than 1, the optimum value for a reduced χ^2, but the uncertainties in both the values for the position and amplitude of the coherent scatter peak are less in the FWH case than the

FLWH case. At the 5% test of significance level, the uncertainties are statistically different. Therefore, there is definite improvement in the uncertainties if one uses the FWH model. The following table illustrates the differences in the uncertainties for the position and amplitude of the coherent scatter peak using the FLWH and FWH models.

TABLE 3.1

*With respect to data file, NPB01T (first person (tibia) measured in survey).

	FLWH	FWH
POSITION	431.480 +/-0.059	431.450 +/- 0.057
AMPLITUDE	1442.1 +/- 12.7	1444.6 +/- 10.6

(ii.) Phantoms

With respect to the phantoms, the χ^2 (ν=63) was 1.126 +/- 0.171 using the FLWH model and 1.145 +/- 0.202 using the FWH model. The χ^2 values are nearly identical, but the trend is in the opposite direction as was observed in the people case. Although, they are within uncertainty range of each other. Like before, the χ^2 are not statistically different from each other and are within uncertainty range of 1. Although the values for the positions are quite similar, the uncertainties using the FWH model are less than the uncertainties obtained from using the FLWH model. The uncertainties are statistically different from one another which implies that it is better

to use the FWH model for increased precision. As well, lower uncertainties were obtained for the amplitude values using the FWH model which further emphasizes the point that precision can be gained by fixing both the width and height. Table 3.2 illustrates the differences in the uncertainties for the position and amplitude using the FLWH and FWH models.

TABLE 3.2

*With respect to data file, A069 (69 ppm phantom).

	FLWH	FWH
POSITION	431.900 +/- 0.038	431.920 +/- 0.036
AMPLITUDE	2936.5 +/- 17.2	2944.6 +/- 14.6

There is still more work that needs to be done with respect to the coherent scatter peak. That is, it would be interesting to only fix the height and have a floating width, because the results of the FLWH model with respect to the entire phantom data set indicate that there were slight but noticeable variations in the width which would result in higher χ^2 values. Such an experiment would help to fine tune the non-linear least squares fitting routine. It would ensure that the coherent scatter peak is being properly analyzed so that the maximum amount of information is being obtained and used.

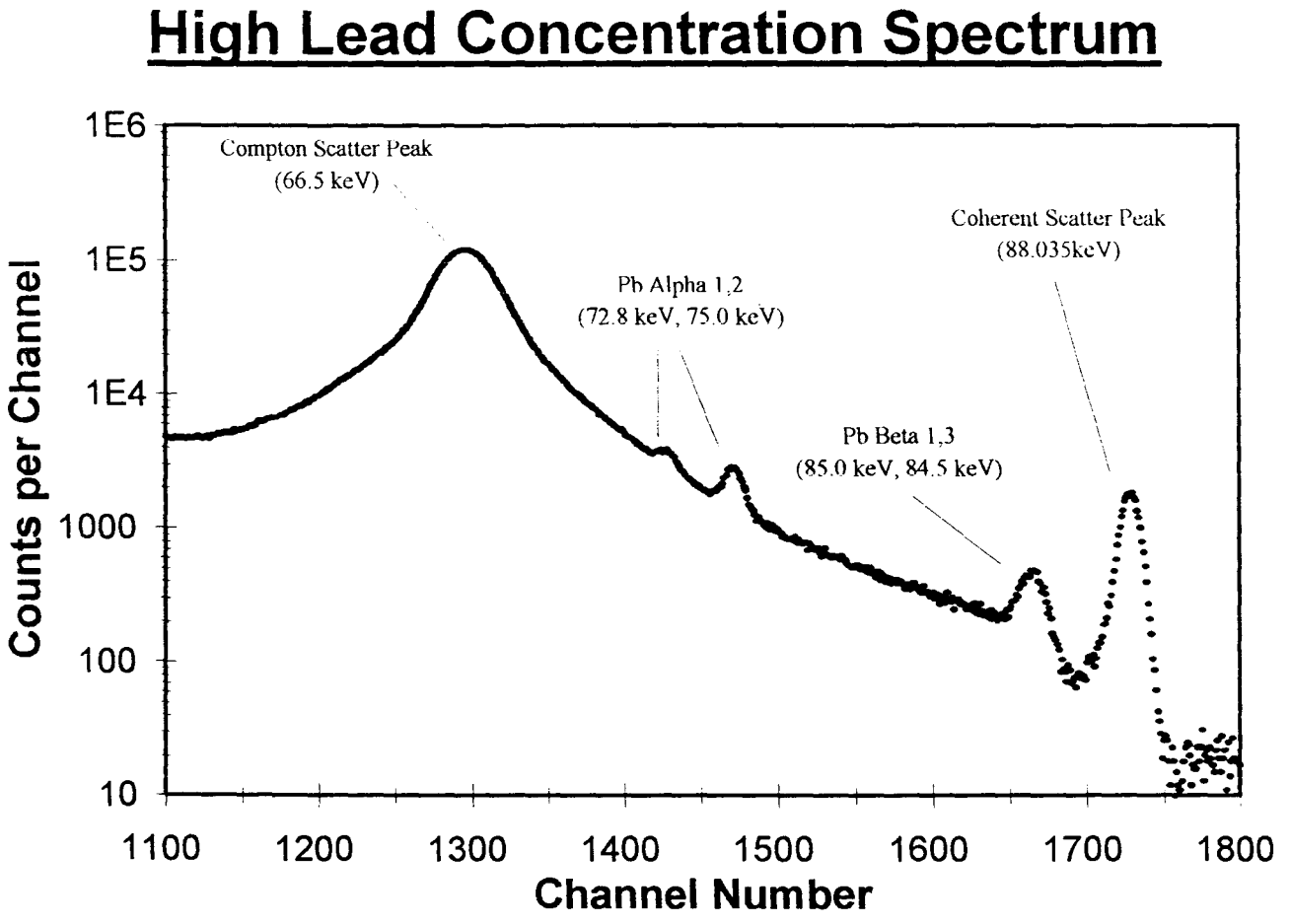

Figure 3.2: A High Lead Concentration Spectrum.

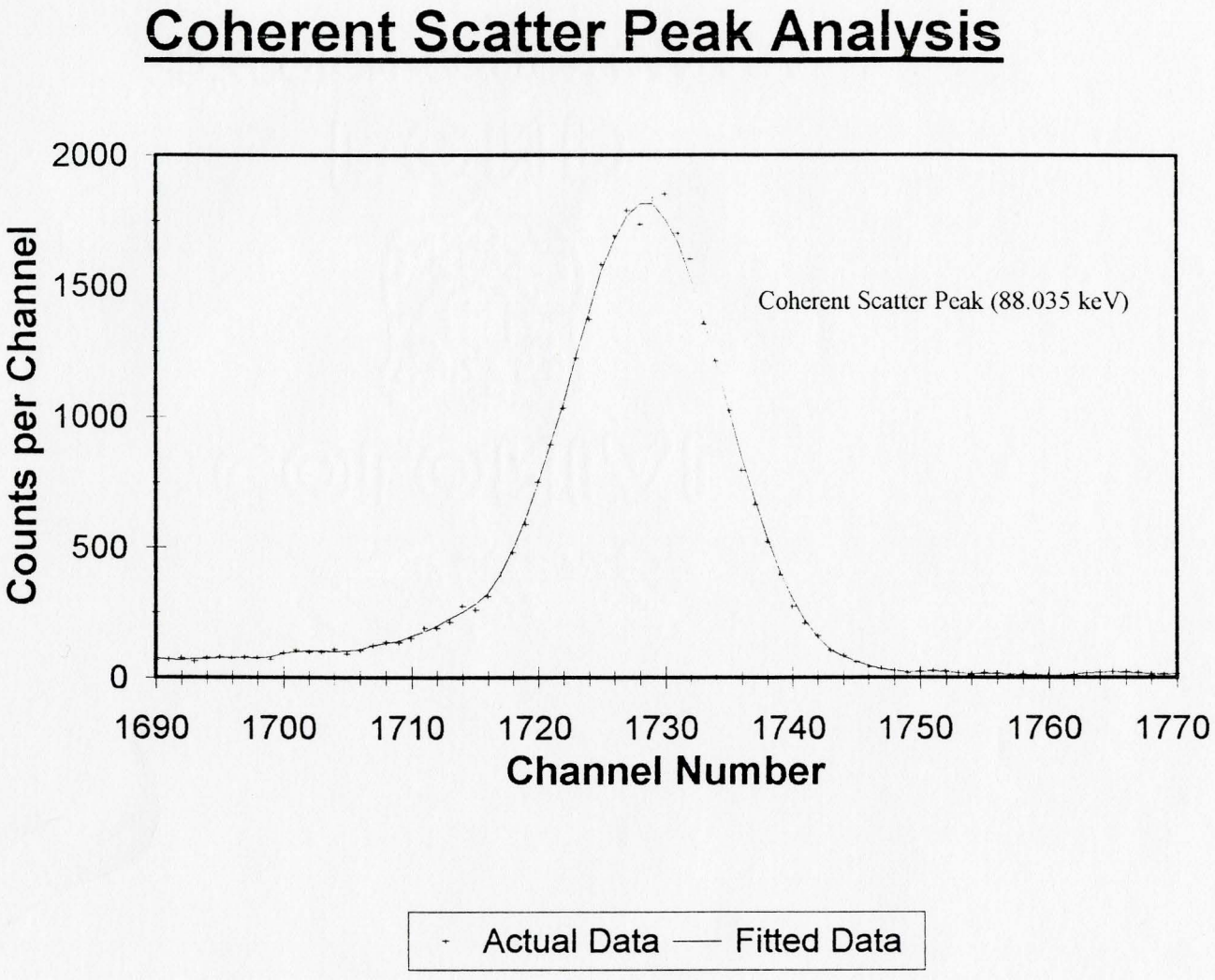

A.) Coherent Peak.

Alpha Peak Analysis

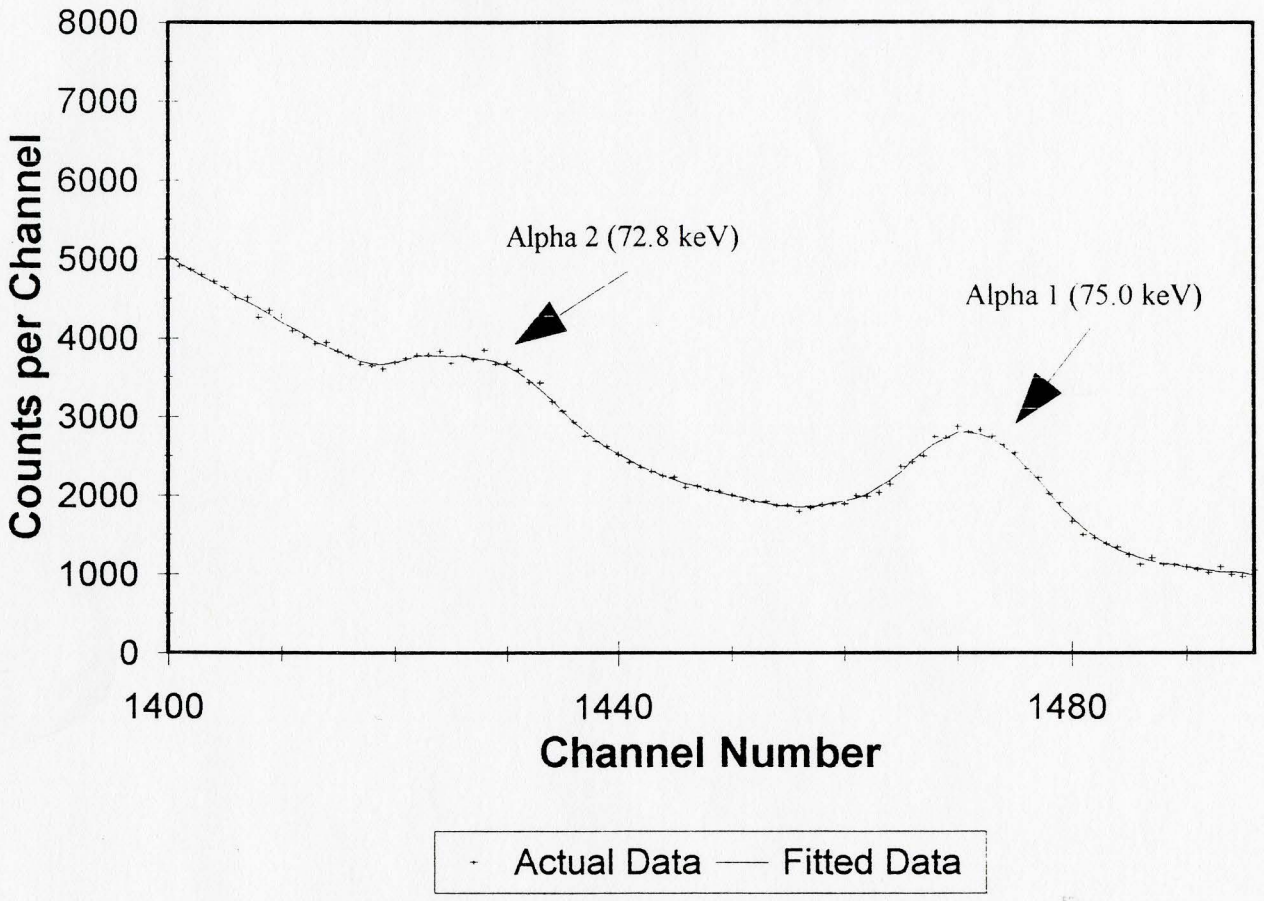

B.) Alpha Peaks.

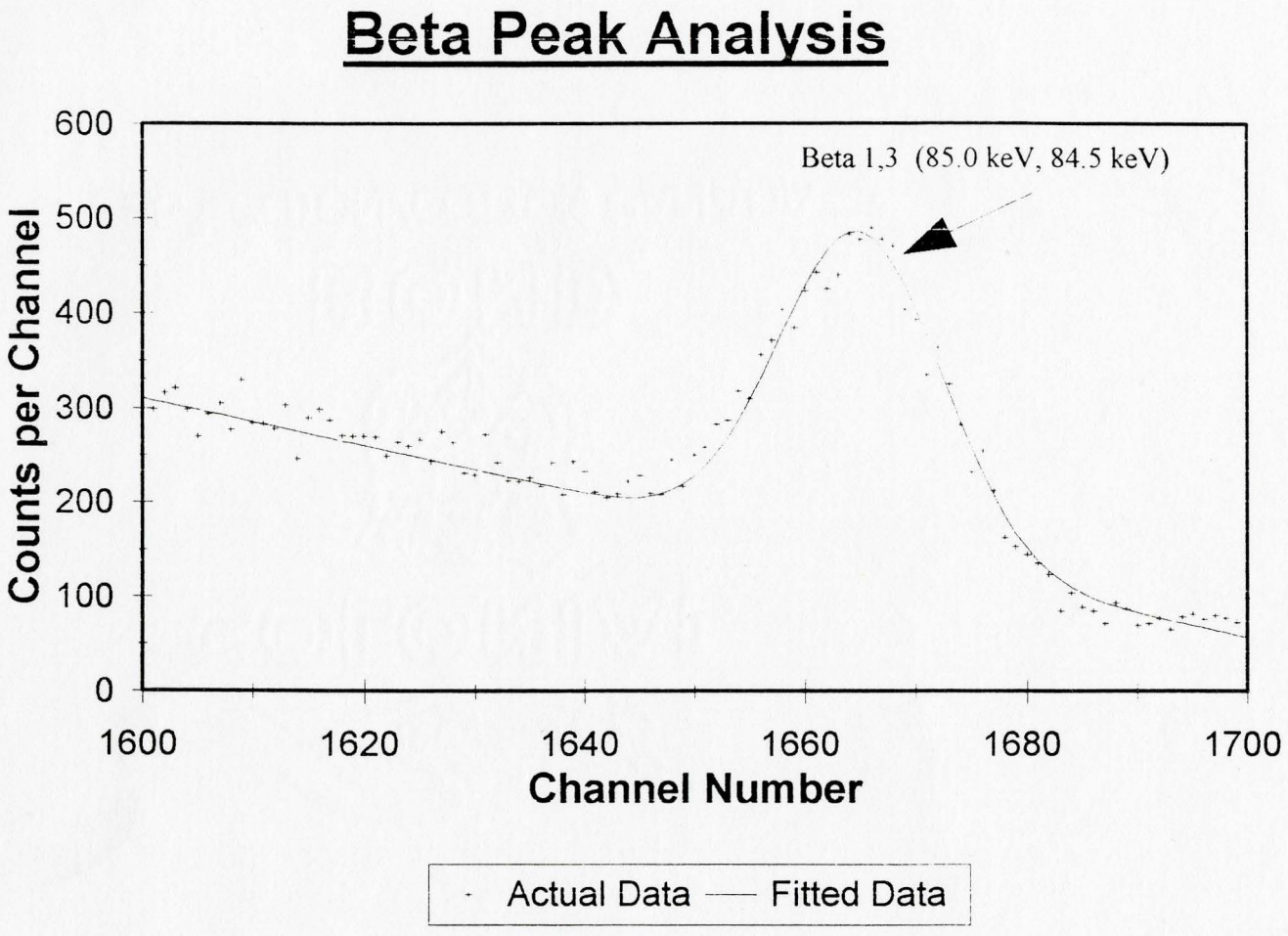

C.) Beta Peak.

Figure 3.3: Illustrations of the Fitted Peak Regions.

b. Alpha peaks

As indicated in the first paragraph of section 3.3, two different models were used to analyze the alpha peaks, linked and unlinked alpha amplitudes. In the Table of Isotopes, one can look up the relationship between the α_1 and α_2 lead peaks. Quite simply, for the linked model, one replaced the amplitude of α_2 with the following relationship:

$$\alpha_2 = \alpha_1 \times 0.593 \qquad (14)$$

(i.) People

The mean χ^2 value is greater in the linked case than the unlinked (1.080 +/- 0.134 versus 1.046 +/- 0.114 , ν=174 versus ν=173) but are within uncertainty range of each other and the ideal value of 1. Interestingly enough, when the individual χ^2 values were compared between different models using a paired t test, they were statistically different. As well, the uncertainties in the position of the α_1 peak are statistically higher in the linked than the unlinked model. Even though the uncertainties differ, the values for the position are not statistically different. See table 3.3.

TABLE 3.3

*With respect to data file, NPB01T.

	LINKED	UNLINKED
POSITION	133.59 +/- 1.38	134.10 +/- 1.27

Using the following equation, one can combine the alpha amplitudes in the unlinked model, so that comparisons can be made with the linked version ($\alpha_{1,2}$). See table 3.4.

$$\frac{\frac{A_1}{(\alpha_1)^2} + \frac{A_2/RATIO}{(\alpha_2/RATIO)^2}}{\frac{1}{(\alpha_1)^2} + \frac{1}{(\alpha_2/RATIO)^2}} \; +/- \; \sqrt{\frac{1}{\frac{1}{(\alpha_1)^2} + \frac{1}{(\alpha_2)^2}}} \qquad \textbf{(15)}$$

TABLE 3.4

***The numbers refer to Nova Pb bone lead survey measurements, and T and C are the symbols used to distinguish between tibia and calcaneus measurements.**

FILE	COMBINED $\alpha_{1,2}$	LINKED $\alpha_{1,2}$
01T	100.699 +/- 16.675	97.875 +/- 17.850
01C	64.110 +/- 15.638	62.924 +/- 16.641
02T	89.652 +/- 17.540	88.775 +/- 18.555
02C	138.803 +/- 16.480	134.400 +/- 17.521
03T	171.410 +/- 19.245	164.290 +/- 26.397
03C	85.316 +/- 14.082	86.143 +/- 14.802
04T	94.810 +/- 19.450	89.741 +/-20.852
04C	73.368 +/- 16.835	67.152 +/- 17.939
05T	246.057 +/- 19.020	237.720 +/- 20.172
05C	145.670 +/- 17.552	133.400 +/- 18.644

Similar to the trend observed with the position of the α_1 peak, the uncertainties in the amplitudes are statistically greater in the linked model. As well, the values for the amplitude obtained using the linked model are less than the unlinked model. At this point, one must be wondering if the linked model has any benefit. Based on the results of the unlinked model, one can calculate the ratio of α_2/α_1 to be 1.102 +/- 0.102 which is definitely not close to the correct value of 0.593. At this point, it should be emphasized that the α_2/α_1 values quoted for the data set as a whole are based on an inverse weighted mean of the data set used. See table 3.5. These results clearly illustrate why the combined amplitudes are greater than the linked. In conclusion, it is better to have a slightly higher χ^2 with an accurate ratio than an unacceptable value for the α_2/α_1 ratio.

TABLE 3.5

UNLINKED ALPHA AMPLITUDES

FILE	α_2/α_1
01T	1.190 +/- 0.398
01C	0.942 +/- 0.534
02T	0.726 +/- 0.378
02C	1.134 +/- 0.281
03T	1.168 +/-0.267
03C	0.467 +/- 0.295
04T	1.705 +/- 0.628
04C	2.415 +/- 0.951
05T	1.142 +/- 0.182
05C	1.707 +/- 0.371

(ii.) Phantoms

Similar to the people case, the mean χ^2 value associated with the linked model ($\nu=174$) is slightly greater than the value obtained using the unlinked model ($\nu=173$), but the values are definitely within uncertainty range of each other and 1. Although, the χ^2 are not statistically different.

Unlike the people case, there is not the obvious trend that the uncertainty in the position of the α_1 peak is greater in the linked case than the unlinked. This makes sense, because the only difference is that the amplitudes have been linked. The observation of such a trend with the people data set might be due to the fact that the alpha peaks are not as clear in people as in most phantoms. Contrary to what was observed in the people case, the ratio of α_2/α_1 is 0.588 +/- 0.009 which is definitely within range of the theoretical value (Table 3.6). Therefore, it is not obvious which method is preferable. Since measuring lead in human bones is the primary concern, then the linked model is the best choice and was used to analyze the Nova Pb bone lead measurements.

TABLE 3.6

UNLINKED ALPHA AMPLITUDES

LEAD CONCENTRATION (PPM)	α_2/α_1
0	0.783 +/- 1.748
69	0.537 +/- 0.034
28	0.420 +/- 0.079
200	0.594 +/- 0.013
9	1.047 +/- 0.254
200 - Hollow	0.595 +/- 0.015
0 - Hollow	0.338 +/- 0.576

c.) Beta Peaks

(i.) People

When analyzing the beta peaks (unlinked or linked), it was observed that the amplitude of the calcium edge was sensitive to the initial start parameters in that abnormally low values were obtained. After making slight changes to the initial start parameters based on the previous results, reasonable values were obtained for the amplitude of the calcium edge using either model. See table 3.7.

TABLE 3.7

DEPENDENCE OF CALCIUM EDGE ON START PARAMETERS

UNLINKED BETA AMPLITUDES

FILE	INITIAL	IMPROVED
01T	26.698 +/- 4.288	66.049 +/- 4.241
01C	-0.718 +/- 10.267	30.436 +/- 3.125
02T	45.658 +/- 4.637	83.434 +/- 4.614
02C	-17.397 +/- 4.292	12.898 +/- 3.083
03T	70.052 +/- 4.653	76.669 +/- 4.659
03C	-6.465 +/-4.570	19.805 +/- 2.674
04T	81.191 +/- 5.204	126.790 +/- 5.282
04C	5.639 +/- 2.640	42.458 +/- 3.656
05T	14.484 +/-4.074	92.432 +/- 4.533
05C	-23.195 +/- 3.978	11.380 +/- 2.746

Table 3.8 further emphasizes this point.

TABLE 3.8

THE SENSITIVITY OF THE β_3 / β_1 RATIO TO THE START PARAMETERS

UNLINKED BETA AMPLITUDES

FILE	INITIAL	IMPROVED
01T	0.312 +/- 0.387	0.982 +/- 0.343
01C	0.178 +/- 0.634	0.915 +/- 0.263
02T	0.041 +/- 0.312	0.679 +/- 0.270
02C	-0.235 +/- 0.312	0.246 +/- 0.235
03T	0.605 +/- 0.150	0.648 +/- 0.148
03C	-0.351 +/- 0.268	0.285 +/- 0.189
04T	2.103 +/- 1.256	2.174 +/- 0.730
04C	-0.568 +/- 0.764	0.813 /- 0.428
05T	0.046 +/- 0.170	0.688 +/- 0.133
05C	0.125 +/- 0.173	0.437 +/- 0.158

Using the initial start parameters, the inverse weighted mean for the ratio of β_3 to β_1 is 0.181 +/- 0.008 which is definitely not within range of the theoretical value (0.523) while for the improved set of start parameters, a value of 0.593 +/- 0.066 was obtained. Even though this value is not within range of the theoretical value, it is much more probable than the value obtained using the initial start parameters.

In order to link the beta amplitudes, one had to look up relative intensities in the Table of Isotopes.

$$\beta_3 = \beta_1 \times 0.523 \qquad (16)$$

For the linked model, one had to remove the amplitude of β_3 from the initial start parameters and incorporate the above relationship between the beta amplitudes into the Fortran code which fits the beta peaks. Similar to what was observed with respect to the alpha peaks, numerically lower χ^2 values, although not significantly different, were obtained with the unlinked model than the linked ($\nu=164$ versus $\nu=165$). Opposite to what was observed in the alpha peak case, the uncertainties in the amplitudes of $\beta_{1,3}$ were statistically lower than the uncertainties of the combined. See table 3.9. Also, the values for the amplitudes do not follow the trend observed for the alpha peaks, since the inverse weighted mean of β_3/β_1 is not substantially greater than the theoretical value.

TABLE 3.9

FILE	COMBINED $\beta_{1,3}$	LINKED $\beta_{1,3}$
01T	24.927 +/- 4.552	25.069 +/- 4.011
01C	17.065 +/- 3.772	14.551 +/- 3.303
02T	25.974 +/- 4.816	25.167 +/- 4.226
02C	19.258 +/- 4.324	21.112 +/- 3.771
03T	49.933 +/- 5.212	49.035 +/- 4.574
03C	18.575 +/- 3.360	20.335 +/- 2.933
04T	32.434 +/- 5.341	33.318 +/- 4.677
04C	16.324 +/- 4.279	16.447 +/- 3.754
05T	54.436 +/- 5.200	50.391 +/- 4.548
05C	33.223 +/- 4.416	34.361 +/- 3.818

Except for the slight improvement ($\sim 12\%$) in precision and that the linked model is physically correct, there is no other reason to prefer the linked model. Although, reasonably accurate values for the ratio of $\beta_{1,3}$ / $\alpha_{1,2}$ (theoretical value = 0.222) are obtained using the linked model and that the linked model is definitely preferable in the alpha amplitude case.

TABLE 3.10

LINKED AMPLITUDES

FILE	$\beta_{1,3}/\alpha_{1,2}$
01T	0.256 +/- 0.068
01C	0.231 +/- 0.062
02T	0.283 +/- 0.076
02C	0.157 +/- 0.035
03T	0.298 +/- 0.046
03C	0.236 +/- 0.053
04T	0.371 +/- 0.101
04C	0.245 +/- 0.086
05T	0.212 +/- 0.026
05C	0.258 +/- 0.048

Earlier it was mentioned that the calcium edge was very sensitive to the initial start parameters. This dependence is, of course, undesirable and must be corrected. One way to tackle this problem is to link the amplitude of the calcium edge to the amplitude of the coherent peak. In the next section, an experiment designed to explore this problem will be discussed in detail.

(ii.) Phantoms

With respect to the phantom data, there are several interesting observations to note. With both sets of start parameters, reasonable values were obtained for the amplitude of the calcium edge in both models (linked and unlinked) which is contrary

to the results observed in the people data set. Although, the values obtained using the two different sets of start parameters are statistically different at the 5% test of significance level in the unlinked case. See table 3.11.

TABLE 3.11

DEPENDENCE OF CALCIUM EDGE ON START PARAMETERS
UNLINKED MODEL

LEAD CONCENTRATION (PPM)	INITIAL	IMPROVED
0	100.460 +/- 4.136	111.980 +/- 3.877
69	95.232 +/- 4.909	110.730 +/- 3.982
28	100.420 +/- 3.922	127.080 +/- 3.936
200	83.887 +/- 5.597	99.245 +/- 4.176
9	102.380 +/- 4.194	112.050 +/- 3.900
200 - Hollow	115.590 +/- 5.155	118.100 +/- 5.188
0 - Hollow	127.030 +/- 4.254	173.120 +/- 4.588

It is also interesting to note that the inverse weighted mean ratio for the initial set of start parameters (β_3/β_1) is 0.527 +/- 0.014 and is within range of the theoretical value. Using the improved start parameters, the inverse weighted mean ratio is 0.563 +/- 0.014 which is not within range of the theoretical answer. Such observations emphasize the point that the beta component of the fitting program is sensitive to the start parameters and that the amplitude of the calcium edge is a problem that must be dealt with if people and phantom data are going to be analyzed using the same start parameters.

3.3.2 **Calcium Edge Experiment**

In section 3.3.1, it was mentioned that the amplitude of the calcium edge in people was very sensitive to the initial start parameters. Such dependence is obviously undesirable, and one way to solve the problem is to link the amplitude of the calcium edge to the amplitude of the coherent scatter peak by calculating the ratio of the amplitude of the calcium edge to the coherent scatter peak (Ca/Coh). This was done by measuring three plaster of Paris phantoms (blank, 100 ppm, and 28 ppm) and two calcaneus bone samples at a distance of 20 mm from the source for 14 hours. The 28 ppm and 100 ppm were made by Katrina Cake (KMC) while the blank was made by Chris Gordon (CLG). The calcaneus bone samples were borrowed from Chris Gordon and were numbered #1 and #5. The reason for the large acquisition times is that a large number of counts will be detected and therefore ensure good statistics when calculating the Ca/Coh ratio. It is important to note that this is only a preliminary experiment, the results of which indicate that further work must be done.

First, the floating width and height program was used to analyze the coherent scatter peak. For bone samples, the mean value for the width was calculated to be 9.77 and the mean height 0.02. The mean value for the width of the phantoms series was 9.70 and the mean height was 0.03.

(i) Phantoms

When analyzing bone lead measurements, it is common procedure to fix the width and the height. Therefore, for this experiment, the width and the height were fixed, after using the FLWH coherent peak analysis subroutine to determine the mean width and height. Dramatically higher χ^2 values were obtained using the FWH subroutine. The message here is that fixing both the width and the height of the coherent scatter peak worsens the fit. This was not apparent when analyzing the Nova Pb bone lead survey data, but the acquisition time was 28 times shorter than the time used for the calcium edge experiment. In other words, the calcium edge files contain more information which enables the fitting program to model the spectral data more accurately.

Out of curiosity, the data was analyzed using the floating width but fixed height (FLWFH) subroutine. The χ^2 values were very similar to the results obtained using the FLWH subroutine but were slightly larger numerically. Based on a t-test analysis, the χ^2 values were significantly different at the 5% test of significance level.

TABLE 3.12

χ^2 VALUES USING DIFFERENT MODELS

#1 - CLG → 0 ppm, #2 - KMC → 100 ppm, #3 - KMC → 28 ppm

SAMPLE	FLWH	FWH	FLWFH
#1	2.758	12.430	3.063
REPEAT	4.159	8.191	4.232
REPEAT	2.777	3.151	2.881
#2	3.028	3.523	2.993
REPEAT	2.937	3.088	3.113
REPEAT	2.603	3.173	2.943
#3	3.001	7.678	3.267
REPEAT	3.365	8.906	3.543
REPEAT	2.827	7.482	3.008

Such results emphasize the point that fixing parameters does not always improve the fit if the parameter is one that tends to vary. If a parameter does not change very much, then fixing it should improve the fit, since it is one less parameter that the fitting routine must take into consideration. Unfortunately, the widths tend to vary over time. It was observed in the Nova Pb bone lead survey that the widths of both people and phantom data gradually worsened. Therefore, fixing the width would not be appropriate unless a daily mean width was calculated. During the current survey (Brunswick), the pole-zero adjustment on the amplifier was checked everyday

and sometimes adjusted to maintain similar widths. It would be interesting to see if there is any benefit to be gained from using the FLWFH over the FWH with respect to the recent survey. But, more importantly, it is important to determine if such substantial differences between the FLWH and the FWH occur when one is sure that the pole-zero is properly adjusted and similar widths maintained. With respect to the calcium edge experiment, there was a gradual increase in the widths. These measurements were 14 hours long, and each phantom was measured three times. The pole-zero was not checked during this time. Therefore, it would be ideal to repeat this experiment keeping in mind the above observations. Then, it would also be useful to compare the positions and amplitudes of the coherent peak as determined by the different models.

Since the previously discussed work on the issue of linking alpha and beta amplitudes had shown that it was advantageous, the beta linked version of the beta peak analysis subroutine was used.

With respect to the beta peak analysis, the sample #1 files have noticeably higher χ^2 than the others except for the first repeat of sample #3 and may be due to differences in phantom size. The high χ^2 value associated with this measurement may be due to a false local minimum and would thus imply that the fit should be tried again.

TABLE 3.13

CA/COH RATIOS

#1 - CLG → 0 ppm, #2 - KMC → 100 ppm, #3 - KMC → 28 ppm

SAMPLE	χ^2	CA/COH ($x10^{-2}$)
#1	3.947	4.091 +/- 0.017
REPEAT	4.158	4.026 +/- 0.017
REPEAT	4.156	4.005 +/- 0.017
#2	1.319	3.133 +/- 0.021
REPEAT	1.488	3.123 +/- 0.021
REPEAT	1.201	3.134 +/- 0.020
#3	1.347	3.167 +/- 0.020
REPEAT	10.340	3.429 +/- 0.019
REPEAT	1.343	3.224 +/- 0.021

Except for the sample #1 files, the values for the Ca/Coh ratio are quite similar. It is important to remember that the sample #1 files are CLG phantoms while the rest are KMC phantoms.

(ii.) Calcaneus Bone Samples

Since calcaneus bone samples were measured rather than people's tibia and calcaneus (*in-vivo*), one is not worried about the oxygen edge. Therefore, the mean height as determined by the FLWH subroutine can be used. For *in-vivo* measurements, the phantom mean height must be used due to the oxygen edge artificially increasing the height.

Unlike the phantom case, the χ^2 values obtained using the FWH model are not very different from the χ^2 values obtained using the FLWH except for one measurement. The second repeat of sample #4 had a χ^2 of 10.13. The same can be said about comparing the FWH subroutine with the FLWFH, except for the first repeat of sample #4 which has a high χ^2 value, 11.03, when using the FLWFH subroutine.

TABLE 3.14

DIFFERENCES IN χ^2 VALUES USING DIFFERENT MODELS

#4 - Bone Sample → labelled #5 by CLG, #5 - Bone Sample → labelled #1 by CLG

SAMPLE	FLWH	FWH	FLWFH
#4	1.763	2.416	1.758
REPEAT	2.641	2.928	11.030
REPEAT	2.246	10.130	2.200
REPEAT	2.984	3.042	2.907
#5	2.259	2.149	2.163
REPEAT	2.155	2.076	2.082
REPEAT	1.913	1.951	1.850

With respect to people, the χ^2 values for the fixed case were not as bad as was observed for the phantoms which is most likely due to the fact that the mean width was very close to the value determined by the FLWH subroutine.

TABLE 3.15

CA/COH RATIOS

#4 - Bone Sample → labelled #5 by CLG, #5 - Bone Sample → labelled #1 by CLG

SAMPLE	χ^2	CA/COH ($x10^{-2}$)
#4	1.681	3.656 +/- 0.027
REPEAT	1.858	3.662 +/- 0.026
REPEAT	1.466	3.681 +/- 0.026
REPEAT	1.476	3.645 +/- 0.026
#5	1.186	3.689 +/- 0.033
REPEAT	1.332	3.618 +/- 0.033
REPEAT	1.197	3.583 +/- 0.037

Very reasonable χ^2 values were obtained for the beta peak region analysis, and all the values for the Ca/Coh ratio are within uncertainty range of each other. Such results are very reassuring, because it implies that it is possible to link the amplitude of the calcium edge to the amplitude of the coherent scatter peak by determining a constant for the Ca/Coh ratio.

Chapter 4

Blood Lead Analysis: Calculating the Cumulative Blood Lead Index

4.1 **Introduction**

Exposure to lead is commonly assessed by monitoring the concentration of lead in whole blood, because the procedure (graphite furnace atomic absorption spectroscopy) is relatively inexpensive, confidence can be placed in the results, and there is an extensive amount of information against which such measurements can be interpreted. Unfortunately, the half-life of lead in blood is approximately 5 weeks and thus is only an indicator of recent exposure. As well, whole blood lead does not equate to the biologically most readily available compartment of lead, therefore great care must be taken in interpreting whole blood lead information. Although, one can calculate the cumulative blood lead index (CBLI) to gain additional information with respect to long-term effects. In sections 4.2 and 4.3, it will be discussed thoroughly how one calculates and interprets CBLI values.

4.2 **Cumulative Blood Lead Index (CBLI)**

Of the 65 individuals who had bone lead measurements done at the end of May 1993 (Nova Pb Bone Lead survey), 53 had blood lead records, but only 11 of the 53 individuals had complete blood lead records. In this case, a complete blood lead record implies that a blood lead measurement was made sometime during the first month of employment, but there may be gaps after that.

For those individuals who had complete blood lead records, the cumulative blood lead index (CBLI) can be defined as follows:

$$\int_0^T B(t)dt \qquad (17)$$

where B(t) is the blood lead level at time t and T is the total time of exposure.

Because the measurements were taken at nonuniform intervals, the integral had to be evaluated numerically using the trapezoidal rule:

$$\int_0^T B(t)dt = \sum \bar{B}_i \; x \; T_i \qquad (18)$$

where $\bar{B}_i$ is the mean of two successive blood lead measurements and T_i is the interval between them. When it was possible, one month intervals were used. Results are shown in Table 4.1.

TABLE 4.1

CBLI Values for Complete Blood Lead Records

#ID refers to a Nova Pb bone lead survey measurement

ID#	CBLI (μg yr dl^{-1})
NPB01	172.9
NPB04	210.6
NPB11	142.2
NPB12	165.8
NPB14	150.8
NPB19	298.1
NPB22	73.8
NPB26	305.9
NPB30	214.7
NPB37	65.1
NPB61	135.1

With respect to the incomplete blood lead records, five different methods were used to calculate the CBLI (μg y dl^{-1}). The first method will be referred to as CBA. It involved calculating a weighted blood lead over the measurement interval (B_{av}) and multiplying it by the time employed before blood lead measurements commenced (EPM). This was the strategy adopted by Somervaille et al. [85]

$$CBLI_{CBA} = B_{av} \; x \; EPM + \sum \bar{B}_i \; x \; T_i \qquad (19)$$

The second method, CBB, involved taking the average of the first few measurements (1st year), B_{av}^{1st}, and multiplying by EPM.

$$CBLI_{CBB} = B_{av}^{1st} \; x \; EPM + \sum \bar{B}_i \; x \; T_i \qquad (20)$$

The last three methods, CBC, CBD, and CBE, used extrapolation techniques. First, B_i versus T_i was plotted, and then the line of best fit was calculated using the following equation:

$$B(t) = mt + b \tag{21}$$

where m is the slope and b is the intercept.

Next, one extrapolated back for the region where there were no recorded blood lead measurements.

Method, CBC, was simply a combination of the first two equations where the region of integration was from 0 to EPM instead of 0 to T.

$$CBLI_{CBC} = \int_0^{EPM} B(t)dt + \sum \bar{B}_i \; x \; T_i \tag{22}$$

Both methods, CBD and CBE, took into account that there is an initial rise from background levels of blood lead (10 μg dl^{-1}) to occupational levels which range from 20 to 80 μg dl^{-1} by integrating the line of best fit in two parts. The difference between the two methods is in the initial rise time. Unfortunately, there were only 11 complete blood lead records on which to base the value for the rise time. As well, in 2 of the 11 records, the rise time was not obvious at all ; it was not possible to determine a value accurately. Therefore, based on the 9 complete blood lead records, the mean value for the rise time was calculated to be 2 +/- 1 months. In order to determine the sensitivity of the calculations to the choice in the rise time, the values, 2 (CBE) and 4 (CBD) months, were used for the rise time. For example, with respect to method, CBD, the area under the straight line beginning from 10 μg dl^{-1} to the value for the blood lead at 4 months was integrated and then the line of best fit from 4 months to EPM.

$$CBLI_{CBD} = \int_0^4 B_{initial}(t)dt + \int_4^{EPM} B(t)dt + \sum \bar{B}_i \; x \; T_i \qquad (23)$$

where $B_{initial}$ is the extrapolated value of whole blood at 2 or 4 months using the line of best fit equation but assuming a background level of 10 μg dl^{-1}.

Similarly, for method, CBE,

$$CBLI_{CBE} = \int_{0}^{2} B_{initial}(t)dt + \int_{2}^{EPM} B(t)dt + \sum \bar{B}_i \; x \; T_i \qquad (24)$$

Figure 4.1 is a pictorial representation of the above equations using the following simplified and fictitious data [86]:

Time (months)	Blood Lead (μg / l)
40	500
45	550
50	400
55	450
60	500
65	450
70	350
75	450
80	400
85	450
90	300
95	250
100	350
105	350
110	250
115	300
120	250

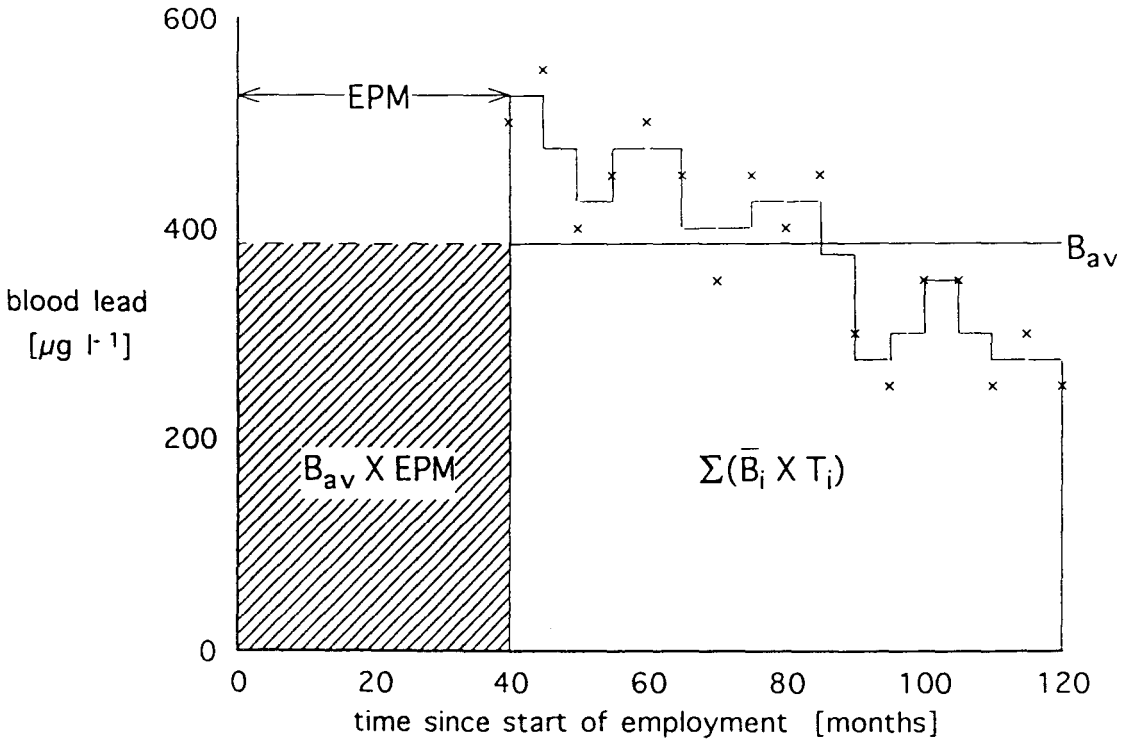
600
400
200
0
blood lead
[μg l⁻¹]
EPM
B_{av}
B_{av} X EPM
$\Sigma(\bar{B}_i \times T_i)$
0
20
40
60
80
100
120
time since start of employment [months]

a.) Method CBA

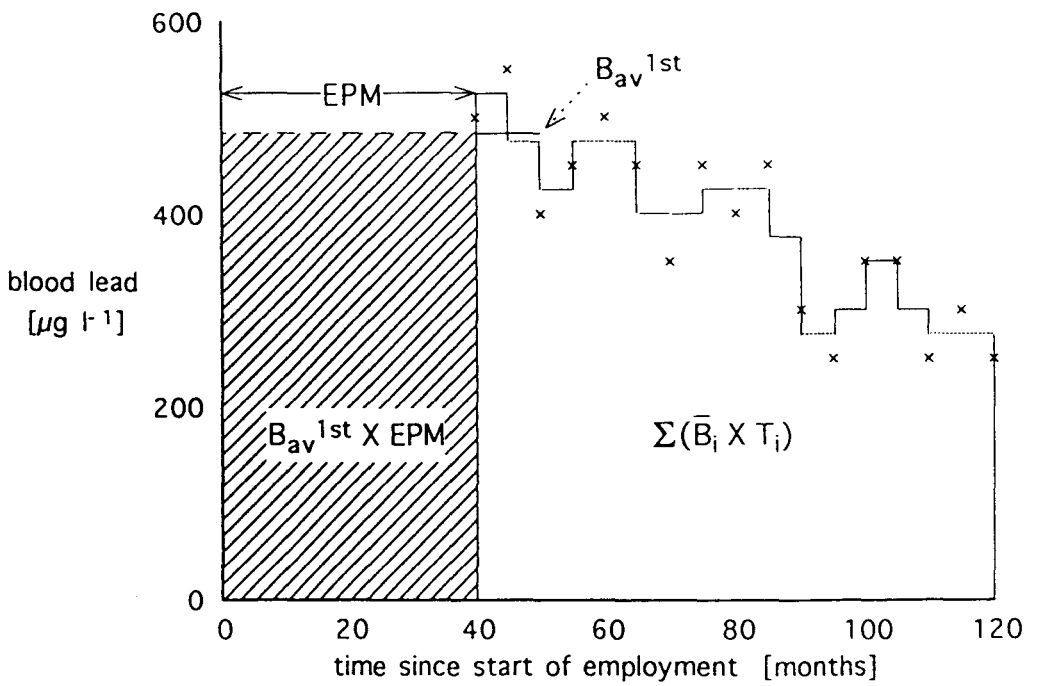
600
400
200
0
blood lead
[μg l⁻¹]
EPM
B_{av}^{1st}
B_{av}^{1st} X EPM
$\Sigma(\bar{B}_i \times T_i)$
0
20
40
60
80
100
120
time since start of employment [months]

b.) Method CBB

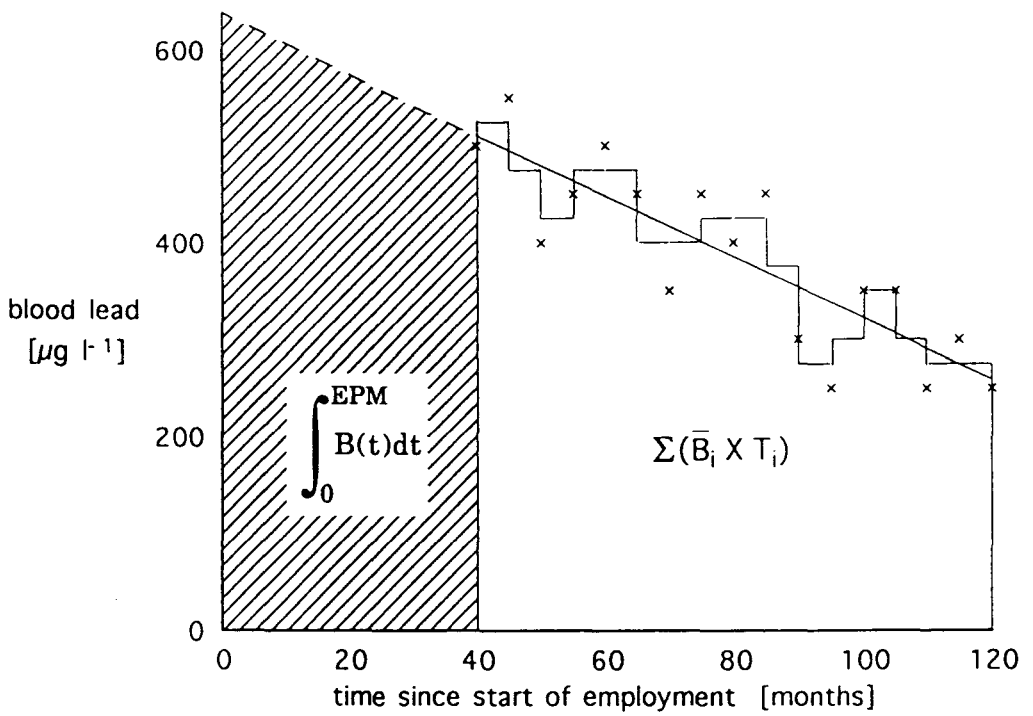
600
400
200
0
blood lead
[μg l⁻¹]
EPM
∫ B(t)dt
0
Σ(B̄ᵢ X Tᵢ)
0
20
40
60
80
100
120
time since start of employment [months]

c.) Method CBC

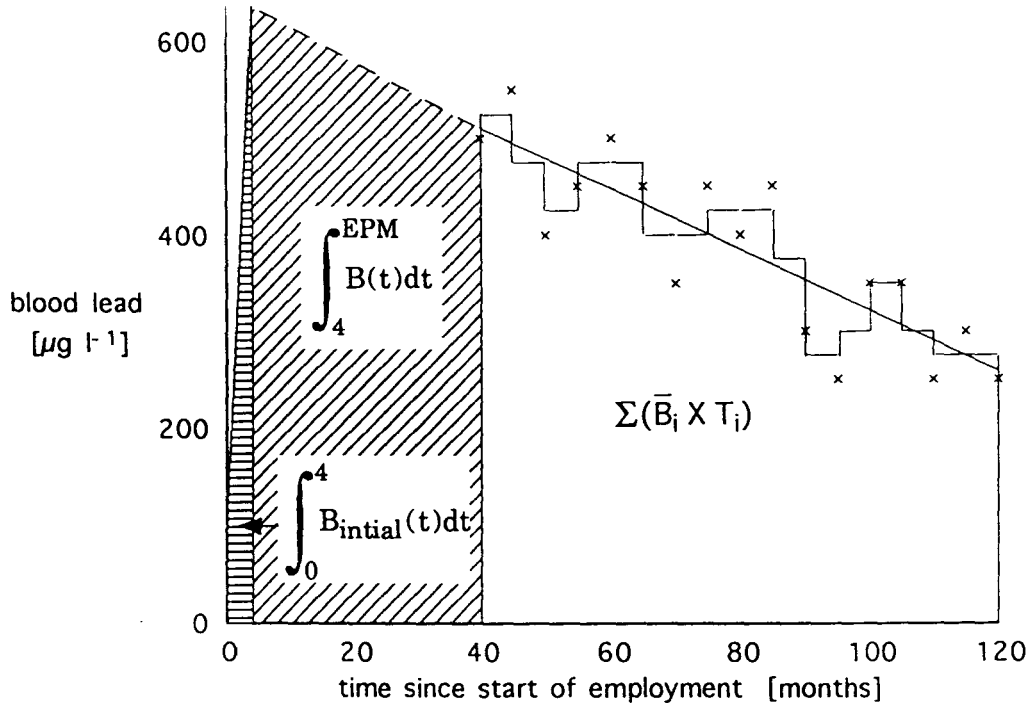
600
400
200
0
blood lead
[μg l⁻¹]
EPM
B(t)dt
4
Σ(B̄i X Ti)
4
Bintial(t)dt
0
0
20
40
60
80
100
120
time since start of employment [months]

d.) Method CBD

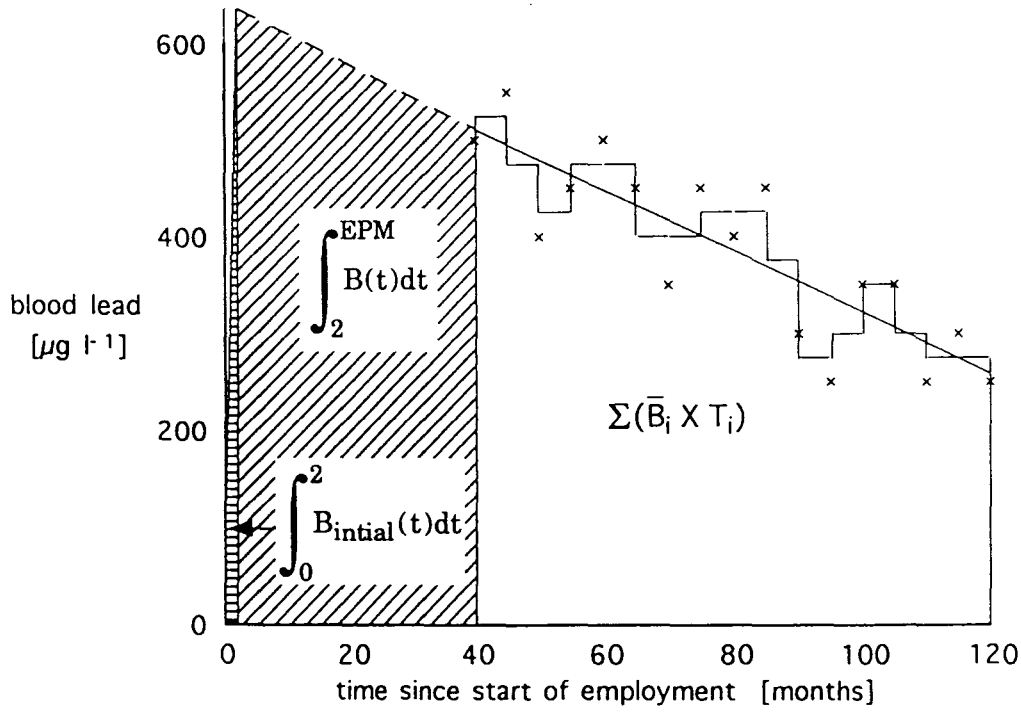

e.) Method CBE

Figure 4.1: A graphical representation of the equations used to calculate the CBLI.

4.3 Analysis and Discussion of CBLI Results

Due to the size of the data set, a computer program in QuickBASIC was written to calculate the CBLI values, plot blood lead versus time graphs, and to determine the line of best fit for incomplete blood lead data files.

Since improvements in occupational hygiene have achieved a reduction in lead exposure in the workplace, blood lead concentrations would be expected to fall with time. This pattern is observed in all but a very few of the individuals in this study. Specifically, 33 of the 42 incomplete blood lead records (79%) had a negative slope. Of the 9 positive slope results, only 3 were very distinct. The others were either characterized by not having a very steep slope (nearly horizontal) or by nearly being complete blood lead records so that the initial rise time period could have been biasing the results. More work needs to be done in investigating the yearly trends in the blood lead data, because there were obvious peaks in the blood lead versus time graphs. Since the x axis in the graphs of blood lead versus time is representative of the individuals employment time at the plant, the best approach would be to plot for each individual the blood lead measurement versus the calendar month for a given year.

Because of the general trend of negative slope for the line of best fit, methods, CBA and CBB, would both be expected to underestimate the true value for the CBLI. The extrapolation methods, CBD and CBE, should more accurately model the

observed behaviour of blood lead versus time by taking into account three identifiable regions where the blood lead data follows different trends. In general, the greatest estimate of the CBLI should be the CBC method, since one is not taking into account the initial rise from background levels of blood lead. There were three exceptions where CBB > CBC, but these cases were characterized by exceptionally high blood lead measurements during the first year. CBE will, of course, be larger than CBD, because the integration is over a larger region of the line of best fit. With respect to the positive slope files, CBA would give the highest estimate, since the positive slope results in lower values when one back extrapolates. Similar to the negative slope case, there are always exceptions, but it is due to either the slope not being particularly steep or more high blood lead levels during the first year. Table 4.2 summarizes the results obtained for the CBLI using the different methods.

TABLE 4.2

CBLI Values for Incomplete Blood Lead Records

ID#	CBA	CBB	CBC	CBD	CBE
NPB02	487	510	527	520	523
NPB03	572	560	531	527	529
NPB05	568	594	582	576	579
NPB06	606	624	645	637	641
NPB08	614	593	634	626	630
NPB09	631	648	653	646	649
NPB10	382	413	414	410	412
NPB15	448	467	450	444	447
NPB16	544	598	625	617	621
NPB17	347	363	401	396	399
NPB18	423	461	478	469	473
NPB20	335	339	342	336	339
NPB21	403	412	430	423	427
NPB23	481	483	455	452	454
NPB24	520	580	658	648	653
NPB25	575	625	631	624	628
NPB27	537	642	705	694	700
NPB28	247	261	274	270	272
NPB29	130	130	131	126	129
NPB31	455	492	520	513	516
NPB32	699	690	695	688	692
NPB33	339	347	346	340	343
NPB34	223	222	222	219	221
NPB35	639	649	706	697	701
NPB36	349	360	363	360	361
NPB38	127	128	128	123	125
NPB39	284	297	295	290	292
NPB40	603	603	618	610	614
NPB43	218	217	217	214	215
NPB44	340	337	336	331	333
NPB45	739	773	804	794	799
NPB46	682	703	768	759	763
NPB47	317	331	329	322	325
NPB48	538	614	724	711	718

NPB49	569	569	595	588	592
NPB50	633	641	654	648	651
NPB52	228	230	232	228	230
NPB54	525	539	541	535	538
NPB56	601	622	646	637	641
NPB57	42	42	43	39	41
NPB60	376	391	377	372	375
NPB64	248	249	249	245	247

Do the various methods for calculating the CBLI yield results which are statistically different from each other? In order to answer that question, a paired t-test analysis had to be done. Because the only difference between the methods was how the CBLI was determined, sets of paired samples can be formed. The raw data remained untouched. A computer program was written to calculate t values for the pairs, CBA-CBB, CBA-CBC, CBA-CBD, CBA-CBE, CBB-CBC, CBB-CBD, CBB-CBE, CBC-CBD, CBC-CBE, and CBD-CBE.

$$t = \frac{\bar{D}}{S_{\bar{D}}} \qquad (25)$$

$$S_{\bar{D}} = \frac{S_D}{\sqrt{n}} \qquad (26)$$

$$S_D = \sqrt{\frac{\sum d^2}{n-1}}, \; d = D - \bar{D} \qquad (27)$$

where $\bar{D}$ is the sample mean difference and D is the difference between the pairs.

Both 1% and 5% test of significance levels were taken into consideration. For example, a 5% test of significance implies that the probability of rejecting the null hypothesis when it is true is 5%. The results of the t-test are outlined in the following table:

TABLE 4.3

PAIR TYPE	5% TEST OF SIGNIFICANCE	1% TEST OF SIGNIFICANCE
CBA-CBB	REJECT	REJECT
CBA-CBC	REJECT	REJECT
CBA-CBD	REJECT	REJECT
CBA-CBE	REJECT	REJECT
CBB-CBC	REJECT	REJECT
CBB-CBD	**REJECT**	**ACCEPT**
CBB-CBE	REJECT	REJECT
CBC-CBD	REJECT	REJECT
CBC-CBE	REJECT	REJECT
CBD-CBE	REJECT	REJECT

In all cases, except for one, the null hypothesis has been rejected which implies that the values calculated for the CBLI are statistically different. Therefore, the importance of choosing the appropriate method is quite obvious. The one exception is the pair, CBB-CBD, at the 1% test of significance level.

Having established the fact that the methods yield statistically different results, it would be useful to establish how different the results are from one another. For example, one can look at the results for NPB02 and calculate the ratios of CBA/CBB, CBA/CBC, and so forth. One would expect the ratios to be equal to 1 if the methods yielded similar results.

As table 4.4 indicates, the calculated ratios based on NPB02 are not numerically very different from the ideal value of 1, although the ratios associated with the combinations of CBC, CBD, and CBE are much closer to 1 than the other ratios. This implies that the differences between methods CBC, CBD, and CBE are slight, but this is expected. All three methods involved variations on the extrapolation technique.

TABLE 4.4

	CBA/CBB	CBA/CBC	CBA/CBD	CBA/CBE	CBB/CBC
Ratio	0.955	0.925	0.937	0.931	0.968
Deviation from 1	-0.045	-0.075	-0.063	-0.069	-0.032

CBB/CBD	CBB/CBE	CBC/CBD	CBC/CBE	CBD/CBE
0.981	0.975	1.013	1.007	0.993
-0.019	-0.025	0.013	0.007	-0.007

Based on the above discussion of the different techniques for calculating the CBLI, the CBE method was thus used to calculate the CBLI's for the graphs which compare the CBLI with different bone lead concentrations.

Further evidence of the importance in choosing the correct method for the CBLI are the following tables of tibia and calcaneus bone lead concentrations versus CBA, CBB, CBC, CBD, and CBE which illustrate how the slope, intercept, and the correlation coefficient (R Val) varied from one model to the next. But, the values for the slopes and intercepts are well within range of each other if one takes their uncertainty into consideration. It is interesting to note that the extrapolation methods yielded uncertainties that were less than the values obtained using the other techniques, although the correlation coefficients had fallen slightly. The trend in slopes is not surprising considering the trend in the CBLI values as previously noted. It is also important to note that one would not expect a great difference in the slopes using methods, CBD and CBE, because the only difference between the two are the limits of integration.

TABLE 4.5

Tibia - no data rejection - Incomplete Blood Lead Records

METHOD	SLOPE	INTERCEPT	R VAL
CBA	(8.05 +/- 1.62) x 10^{-2}	8.03 +/- 7.69	0.618
CBB	(7.80 +/- 1.53) x 10^{-2}	7.80 +/- 7.58	0.626
CBC	(7.14 +/- 1.44) x 10^{-2}	9.79 +/- 7.38	0.617
CBD	(7.20 +/- 1.45) x 10^{-2}	9.95 +/- 7.35	0.617
CBE	(7.17 +/- 1.45) x 10^{-2}	9.87 +/- 7.36	0.617

TABLE 4.6

Calcaneus - Incomplete Blood Lead Records

METHOD	SLOPE	INTERCEPT	R VAL
CBA	0.15 +/- 0.03	4.86 +/- 12.15	0.682
CBB	0.14 +/- 0.02	5.04 +/- 12.04	0.685
CBC	0.13 +/- 0.02	9.36 +/- 11.85	0.668
CBD	0.13 +/- 0.02	9.67 +/- 11.82	0.668
CBE	0.13 +/- 0.02	9.51 +/- 11.84	0.668

When plotting tibia lead concentration versus CBLI for the entire data set (53 individuals), an apparent outlier was observed. This point was tested using the maximum normal residual (MNR) [87]:

$$MNR = \frac{\max | x - \bar{x} |}{\sqrt{\sum (x - \bar{x})^2}} \qquad (28)$$

In this expression, x is the value of the observed tibia lead and $\bar{x}$ is the tibia lead value predicted from the regression relationship of tibia lead with CBLI. The MNR value for the apparent outlier was 0.582, implying a probability of $< 1\%$ that it did indeed belong to the rest of the sample. It seems likely that this person had accumulated lead in his tibia during a period not covered by blood lead monitoring, perhaps on a previous job or even in childhood.

Figure 4.2 illustrates the impact of rejecting the outlier on the slope. The slope without rejecting any points is 0.066 +/- 0.011 with units of μg[g bone mineral]$^{-1}$/(μg y dl^{-1}) while the slope without the outlier is 0.059 +/- 0.009. Even though the slopes are within their uncertainty range of each other, the slope without the outlier has a lower uncertainty and more correctly fits the data as indicated by the correlation coefficients. (Table 4.7) The slope including the outlier is an obvious bias which is

wrongly inflating the value for the slope.

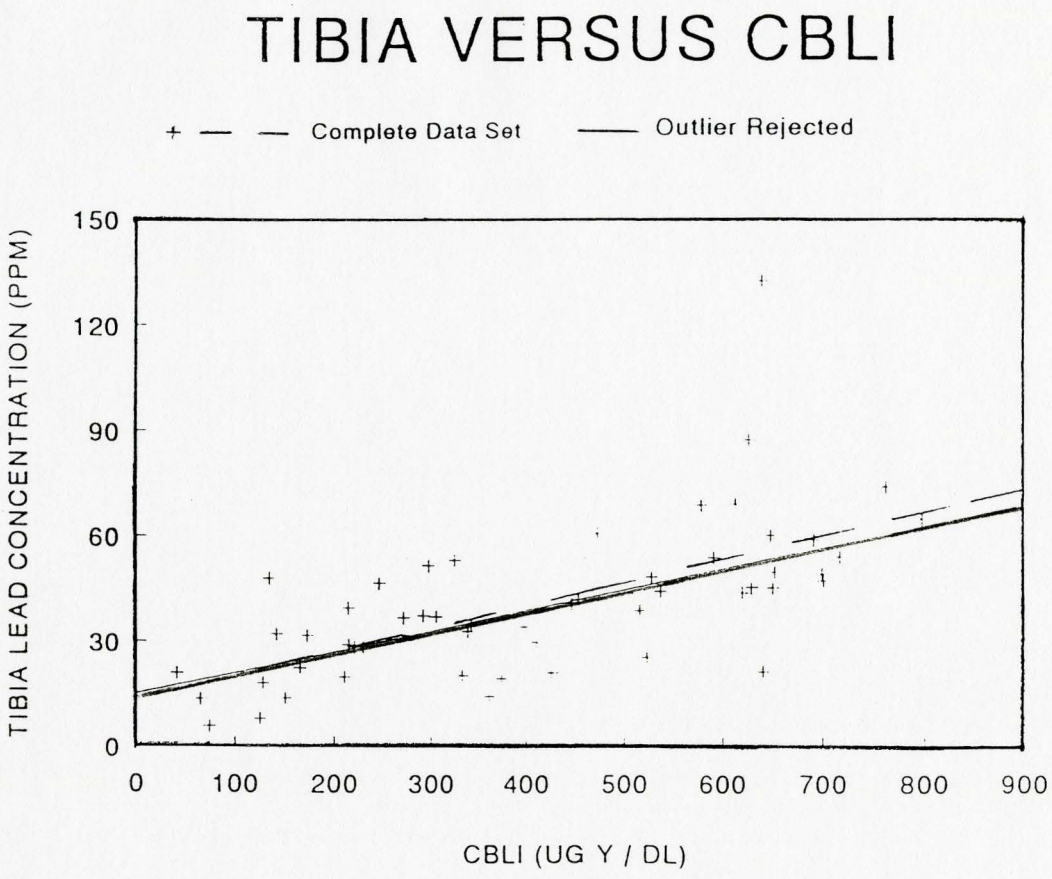

Figure 4.2: Tibia lead concentration versus CBLI for entire data set.

TABLE 4.7

Tibia - Data Rejection Comparison - Entire Data Set

	TIBIA	TIBIA - Outlier Rejected
SLOPE	$(6.63 \pm 1.10) \times 10^{-2}$	$5.85 \times 10^{-2} \pm 8.53 \times 10^{-3}$
INTERCEPT	13.35 ± 5.07	15.05 ± 3.90
RVAL	0.646	0.696

The differences in the slopes, intercepts, and correlation coefficients made by rejecting the outlier are quite dramatic. Tables 4.5 and 4.8 together further illustrates this point.

TABLE 4.8

Tibia - outlier removed - Incomplete Blood Lead Records

METHOD	SLOPE	INTERCEPT	RVAL
CBA	$(7.03 \pm 1.20) \times 10^{-2}$	10.69 ± 5.67	0.683
CBB	$(6.84 \pm 1.13) \times 10^{-2}$	10.34 ± 5.55	0.696
CBC	$(6.26 \pm 1.06) \times 10^{-2}$	12.07 ± 5.42	0.686
CBD	$(6.32 \pm 1.07) \times 10^{-2}$	12.20 ± 5.40	0.686
CBE	$(6.29 \pm 1.07) \times 10^{-2}$	12.14 ± 5.41	0.686

The relationship of calcaneus to CBLI has a steeper slope than that of the tibia, reflecting the generally higher lead concentration observed in more trabecular bone. See figure 4.3. The person, whose tibia result was an outlier, did not produce an outlying calcaneus result. This is consistent with the hypothesis of an earlier unmonitored exposure, given the generally shorter residence time of lead in trabecular than cortical bone.

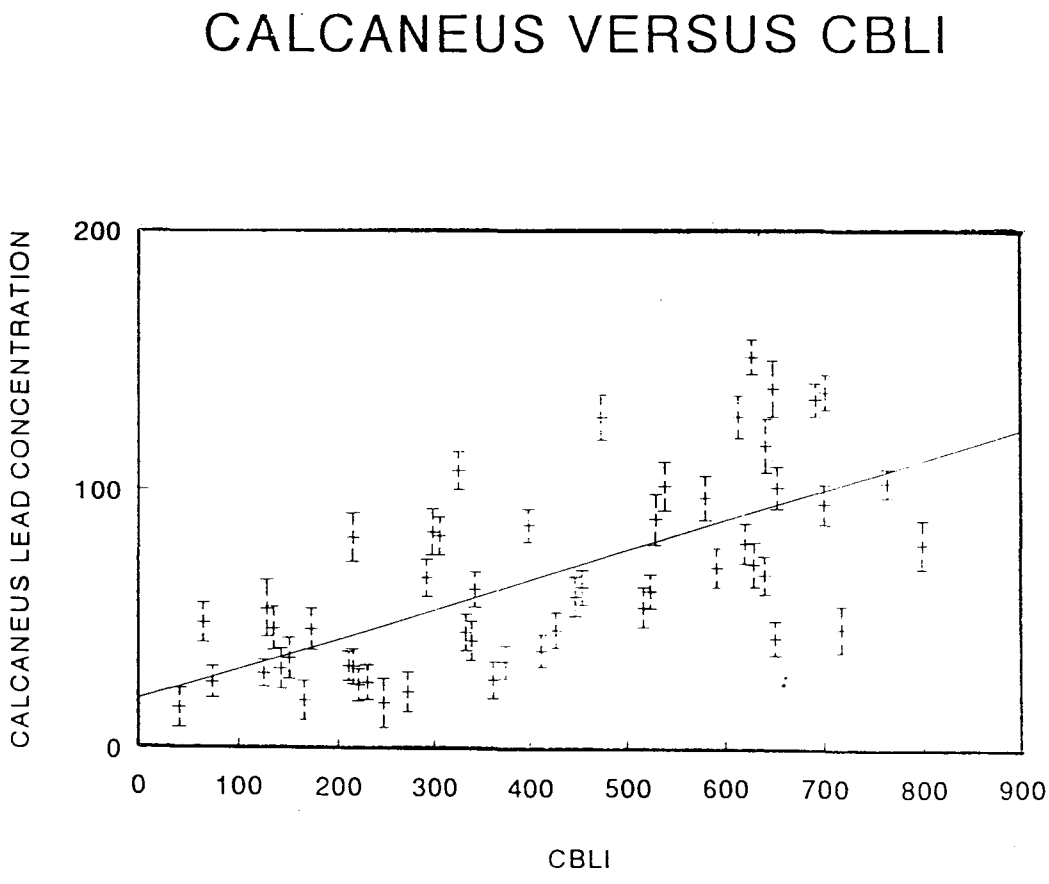

Figure 4.3: Calcaneus lead concentration versus CBLI for entire data set.

The following table summarizes the CBLI results of bone lead surveys in an occupational setting [85,88,89,90,91,92,93].

TABLE 4.9

reference	group	bone	size	slope	r
				$\frac{\mu gPb[g\ bone\ mineral]^{-1}}{\mu gPb\ y\ dl^{-1}}$	
Somervaille et al '88	factory B	tibia	88	0.060±0.005	0.82
	factory C	tibia	87	0.050±0.003	0.86
Armstrong et al '92	factory A '83	tibia	15	0.10±0.02	0.87
	factory A '88	tibia	11	0.10±0.02	0.91
	factory A '88-'83	tibia	7	0.052±0.021	-
Christoffersson et al '84		phalanx	43	0.17	0.41(r_s)
Börjesson et al '93		phalanx	~50	0.04	0.64
Hu et al '91		tibia	12	0.061±0.008	0.92
		patella	12	0.218±0.026	0.93
Erkkilä et al, '92	active	tibia	91	0.028±0.003	0.66
		calcaneus	90	0.073±0.013	0.53
	retired	tibia	13	0.061±0.012	0.85
		calcaneus	13	0.105±0.018	0.87
Gerhardsson et al, '93		tibia	100	0.022	0.60
		calcaneus	100	0.042	0.44
Cake '94		tibia	53	0.059±0.009	0.70
		calcaneus	53	0.117±0.018	0.68

The Nova Pb bone lead survey results agree and disagree with the work done by other researchers in this field, although the results of Cake et al agree with most of the others. It will be interesting when the data collected during the latest survey ($\sim$400 factory workers) is analyzed to see if the results confirm the above values for the slopes. It has been brought to my attention that the correlation coefficients are not very high and that it might be a good idea to investigate fitting the data with different models. Future work will look into this question, although the current (linear) fit does produce respectable results.

Chapter 5

Bone Lead Analysis

5.1 **Introduction**

In chapter 1, it was mentioned that the skeleton is the principal storage site for lead and therefore is indicative of cumulative lead exposure. This implies that bone lead can become a dominant source of lead (endogenous exposure) in retired lead workers. This issue will be discussed in more detail in chapter 7, where the interrelationships between whole blood, serum, and bone lead will be explored.

This chapter will look at the relationships between calcaneus and tibia bone lead concentrations and bone lead concentrations versus years exposed in order to increase one's understanding of human lead metabolism and an appreciation for the role played by the skeleton.

5.2 **General Results**

Table 5.1 summarizes the results obtained from the Nova Pb bone lead survey. One should note that the whole blood lead measurement referred to in the table was the one made closest to the time of the survey. Most were within one month of that time, but none was more than three months earlier. The whole blood lead

concentrations ranged from 165-552 μg/l. The serum samples were collected in late April and early June, and the values ranged between 1.72-12.32 μg/l. The tibia lead concentrations ranged from 5.7-132.32 μgPb[g bone mineral]$^{-1}$; the calcaneus lead concentration varied between 7.0-152.3 μgPb[g bone mineral]$^{-1}$. Unfortunately, there were only 49 factory workers who had all four measurements done.

TABLE 5.1

ID#	TIBIA LEAD (PPM)	CALCANEUS LEAD (PPM)	BLOOD LEAD (µg/l)	SERUM LEAD (µg/l)	YEARS EXPOSED
NPB01	31.63 +/- 3.78	46.6 +/- 8.06	345	4.96 +/- 0.12	4.6
NPB02	25.43 +/- 3.36	61.57 +/- 6.51	362	5.68 +/- 0.15	11.7
NPB03	48.23 +/- 3.63	89.38 +/- 9.92	469	8.03 +/- 0.28	13
NPB04	19.83 +/- 2.51	32.35 +/- 5.61	345	4.37 +/- 0.08	5.3
NPB05	68.63 +/- 4.23	97.66 +/- 8.55	428	6.71 +/- 0.03	13.5
NPB06	21.35 +/- 2.53	67.89 +/- 7.25	447	7.94 +/- 0.11	12.9
NPB07	44.29 +/- 3.18	77.04 +/- 6.89		10.92 +/- 0.16	7.2
NPB08	45.33 +/- 3.79	71.96 +/- 8.59	414	5.48 +/- 0.21	11.7
NPB09	60.12 +/- 3.76	140.02 +/- 10.74	474	9.82 +/- 0.75	13.5
NPB10	29.79 +/- 3.07	38.66 +/- 6.37	262	4.63 +/- 0.09	13
NPB11	32.05 +/- 3.21	31.16 +/- 7.94	322	3.23 +/- 0.16	4.6
NPB12	22.42 +/- 3.99	18.8 +/- 7.57	296	2.49 +/- 0.10	3.6
NPB13	58.95 +/- 2.99	83.43 +/- 5.98		5.89 +/- 0.08	10.9
NPB14	13.79 +/- 3.38	35.31 +/- 8.04	281	3.44 +/- 0.16	4.8
NPB15	40.71 +/- 3.18	59.61 +/- 7.55	552	10.50 +/- 0.28	9.7
NPB16	43.81 +/- 3.07	80.08 +/- 7.76	476	5.88 +/- 0.27	13.1
NPB17	34.05 +/- 3.51	87.04 +/- 6.35	246	3.88 +/- 0.16	12.4
NPB18	60.74 +/- 3.22	128.93 +/- 8.62	428	7.44 +/- 0.19	9.8
NPB19	51.43 +/- 4.24	84.18 +/- 8.95	403	8.30 +/- 0.08	6.4
NPB20	32.72 +/- 2.7	42.38 +/- 7.61	347	4.30 +/- 0.27	8.1
NPB21	21.07 +/- 2.7	46.65 +/- 6.88	362	3.66 +/- 0.16	9.8
NPB22	5.73 +/- 3.03	25.95 +/- 6.08	267	3.52 +/- 0.04	2.3
NPB23	41.88 +/- 3.15	63.11 +/- 6.55	335	4.82 +/- 0.09	13.3
NPB24	49.6 +/- 2.99	101.75 +/- 8.21	293	6.29 +/- 0.04	12.6
NPB25	87.33 +/- 3.51	152.31 +/- 6.72	370	8.58 +/- 0.60	13.6
NPB26	37.02 +/- 2.83	82.66 +/- 7.32	490	9.26 +/- 0.02	6.4
NPB27	49.15 +/- 3.15	95.24 +/- 7.87	370	6.06 +/- 0.16	13.6
NPB28	36.67 +/- 5.81	22.43 +/- 7.76	207	1.72 +/- 0.03	9.3
NPB29	18.12 +/- 3.21	54.54 +/- 10.9	283		3.6
NPB30	39.46 +/- 3.8	81.97 +/- 9.35	418		5
NPB31	38.76 +/- 2.84	55.41 +/- 7.65	341	6.78 +/- 0.21	11.7
NPB32	59.81 +/- 2.86	135.67 +/- 6.44	432		13.5
NPB33	34.59 +/- 3.18	62.13 +/- 6.71	461	9.99 +/- 0.22	7.8
NPB34	28.43 +/- 3.14	24.93 +/- 6.31	304		6.8
NPB35	47.14 +/- 3.17	138.69 +/- 6.66	432	8.52 +/- 0.34	12.7
NPB36	14.31 +/- 2.55	27.28 +/- 7.21	258	4.14 +/- 0.07	13.2
NPB37	13.5 +/- 3.81	49.07 +/- 7.64	275	3.86 +/- 0.10	2.5
NPB38	7.99 +/- 4.47	29.35 +/- 5.36	378	7.05 +/- 0.38	3.7
NPB39	37.32 +/- 3.31	66.4 +/- 7.03	364	4.16 +/- 0.12	8.2
NPB40	69.14 +/- 3.28	129.18 +/- 8.2	498	7.36 +/- 0.41	11.3
NPB41	22.7 +/- 3.06	50.79 +/- 7.37		11.83 +/- 0.16	3.6
NPB42	23.28 +/- 2.95	39.21 +/- 8.64		6.38 +/- 0.07	5.7
NPB43	29.07 +/- 2.95	32.15 +/- 6.89	300	6.05 +/- 0.70	6.8
NPB44	20.28 +/- 3.25	45.66 +/- 7.04	467	7.03 +/- 0.03	7.8
NPB45	64.7 +/- 3.55	79.56 +/- 9.43	507	9.05 +/- 0.15	13.2
NPB46	73.98 +/- 3.28	103.53 +/- 5.67	393	5.64 +/- 0.02	13.8
NPB47	52.93 +/- 3.12	108.0 +/- 7.32	387	7.41 +/- 0.19	8.1
NPB48	53.93 +/- 3.96	47.31 +/- 9.04	308	5.27 +/- 0.04	12.8
NPB49	53.81 +/- 4.93	70.66 +/- 7.6	300	5.10 +/- 0.10	13.5
NPB50	45.17 +/- 3.44	43.48 +/- 6.63	337	6.13 +/- 0.07	16
NPB51	9.71 +/- 3.47	43.93 +/- 8.56		4.19 +/- 0.09	2.8
NPB52	28.5 +/- 3.73	25.91 +/- 6.79	221	5.52 +/- 0.16	8
NPB53	7.46 +/- 5.9	6.98 +/- 8.67			11
NPB54	44.29 +/- 5.39	102.33 +/- 9.49	354	4.59 +/- 0.16	13.1
NPB55	16.88 +/- 3.34	20.46 +/- 7.76		4.44 +/- 0.13	2.7
NPB56	132.32 +/- 5.8	118.08 +/- 10.4	492	10.44 +/- 0.22	11.9
NPB57	20.89 +/- 4.12	15.75 +/- 7.57	215	2.64 +/- 0.05	1.7
NPB58	48.19 +/- 4.23	74.18 +/- 10.08		12.32 +/-0.24	9.9
NPB59	18.95 +/- 3.38	12.63 +/- 7.4		7.89 +/- 0.20	9.7
NPB60	19.34 +/- 4.51	34.21 +/- 6.34	414	4.12 +/- 0.10	10.2
NPB61	47.88 +/- 3.61	46.88 +/- 8.31	165	2.43 +/- 0.20	6.4
NPB62	78.2 +/- 6.18	32.8 +/- 9.46		2.20 +/- 0.11	2.9
NPB63	34.06 +/- 3.2	86.62 +/- 6.81		5.52 +/- 0.09	13.5
NPB64	46.46 +/- 4.8	18.02 +/- 9.53	238	2.57 +/- 0.14	8.1
NPB65	30.86 +/- 3.57	33.2 +/- 8.10			14

5.3 Calcaneus Lead Concentration versus Tibia Lead Concentration

Since better precision can be obtained with tibia measurements than calcaneus, it is more advantageous to plot calcaneus versus tibia instead of the other way around. The plot of calcaneus versus tibia for the entire data set is quite interesting. See figure 5.1. There are two obvious outliers which deviate from the otherwise linear fit to the data set. The slope is 1.143 +/- 0.150 with an intercept of 18.492 +/- 6.693 and a correlation coefficient of 0.693. The MNR data rejection technique described in chapter 4 with a slight variation was used to test the two outliers, NPB56 and NPB62.

TABLE 5.2

FILE	TIBIA (PPM)	CALCANEUS (PPM)
NPB56	132.32	118.08
NPB62	78.2	32.8

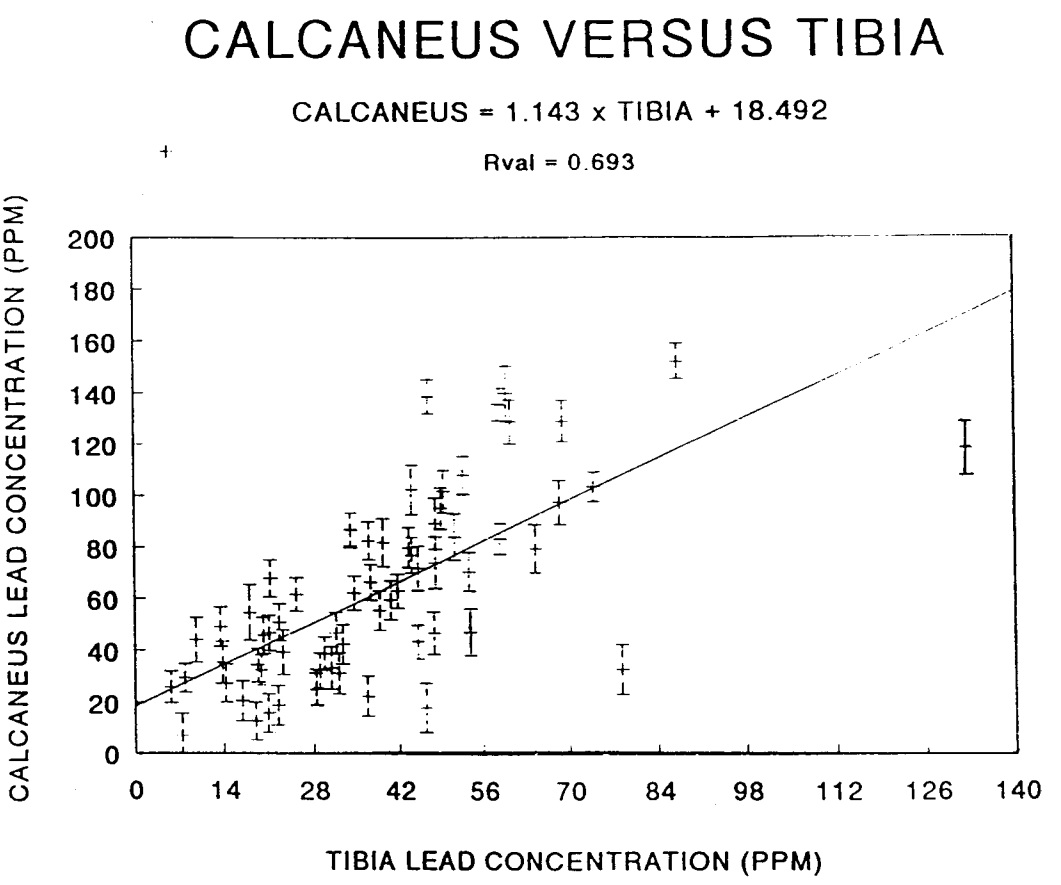

Figure 5.1: Calcaneus Lead Concentration versus Tibia Lead Concentration.

The slight variation is due to the fact that there are two outliers to test. Two suspicious outliers may be tested by repeated use of the MNR technique. First, the most extreme value is tested, and then the second most extreme value is tested in the sample size, n - 1, formed by omitting the most extreme outlier. Both tests must be made no matter what the verdict of the first test is, because a second outlier may mask a first outlier if both are on the same side of the line of best fit. If one considers (132.32, 118.08) as the most extreme value, the resulting MNR value for the first test is 0.191 (n=65) and 0.105 (n=64) for the second test. At the 1% level of significance, the MNR values are 0.455 and 0.456 for n = 65 and n = 64 respectively. Both tests support the statement that a deviate of the size observed here or larger occurs more than 1% of the time. If one considered (78.2, 32.8) as the most extreme value, the MNR results were 0.106 for the first test and 0.190 for the second. Again, both tests support the statement that the suspect data points cannot be rejected.

The following table summarizes the work done with respect to the relationship between the calcaneus and the tibia (Calcaneus versus Tibia graph).

TABLE 5.3

REFERENCE	GROUP	SIZE	SLOPE	INTERCEPT
Gerhardsson et al., 1993 [93]	Mixed -- active and retired	100	1.23	48.0
Erkkila et al., 1992 [92]	Active	91	1.67	41.4
	Retired	16	1.58	22.4
Somervaille et al., 1989 [94]	Mixed -- active and retired	120	2.50	-14.7
Cake, 1994	Active	65	1.14	18.5
	Drop Outliers**	63	1.55	5.6

**N.B. Unfortunately, it has been shown that the outliers cannot be rejected.

Earlier it was mentioned that the tibia was chosen to be the x variable because it is a more precise measurement. There is another good reason as well. The volume of blood delivered per unit time is greater for trabecular bone than cortical, and the

rate of bone turnover is greater in trabecular bone than cortical bone. This results in higher lead concentrations in the calcaneus than the tibia. The tibia lead concentration is a more static measurement which will slowly increase with time compared to the calcaneus and is not as affected by sudden changes of lead intake.

5.4 Bone Lead Concentration versus Years Exposed

(i.) Tibia Lead versus Years Exposed

When plotting tibia lead concentration versus years exposed, there were two obvious outliers. See figure 5.2. Again, the MNR technique was used to test these suspect points where the most extreme point was tested first and then the second. The most extreme observation is (132.32, 11.9), tibia lead concentration and years exposed. The second most extreme observation was (78.2, 2.9). With respect to the first test, the MNR value was calculated to be 0.535. For 65 measurements, the MNR value for the 1% level of significance is 0.455. Thus, based on the first test, the most extreme point can be rejected. With respect to the second suspect point, the results of the MNR test did not allow for data rejection. The MNR value for a data set of 64 measurements (n - 1) where the most extreme observation was removed was calculated to be 0.276 which is much less than the MNR value of 0.456 for 64 measurements at the 1% significance level. The following table outlines the results.

TABLE 5.4

	SLOPE	INTERCEPT	RVAL
ALL POINTS	2.572 +/- 0.622	15.501 +/- 6.207	0.462
DATA POINT REJECTED	2.329 +/- 0.519	16.378 +/- 5.168	0.495

The values for the slopes and the intercepts are within uncertainty range of each other and the values for the correlation coefficient are not substantially different. Thus, the benefit gained from the rejecting the data point is not clear.

The tibia lead concentration does increase with years exposed, although not perfectly linearly. It seems as if it is quite linear from 0 to 9 years exposed. After that, it seems as if the steepness of the slope decreases. It would be a good idea to plot tibia lead concentration versus years exposed per job, but because of the size of this data set, it would be difficult to get meaningful results. The Brunswick bone lead survey will be very useful in answering this question because of the large data set. It is important to remember that different jobs at a lead smelter are exposed to different levels of lead exposure.

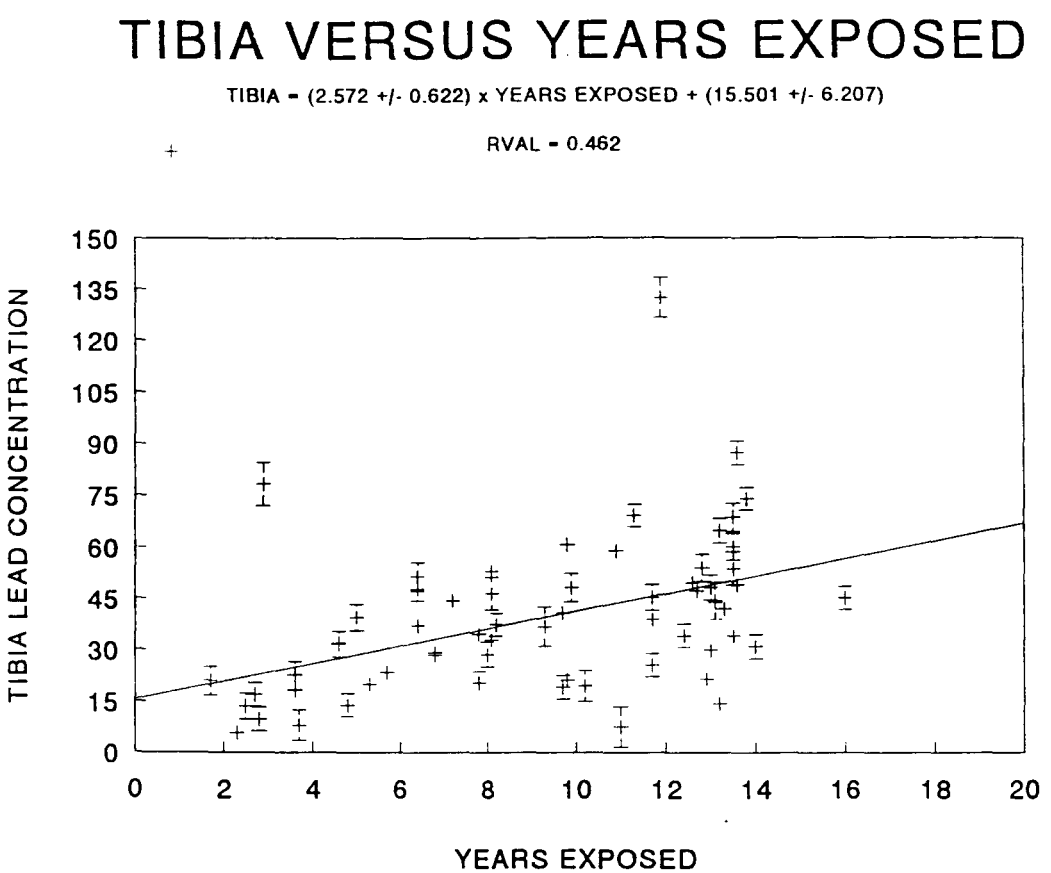

Figure 5.2: Tibia Lead Concentration versus Years Exposed -- All Points

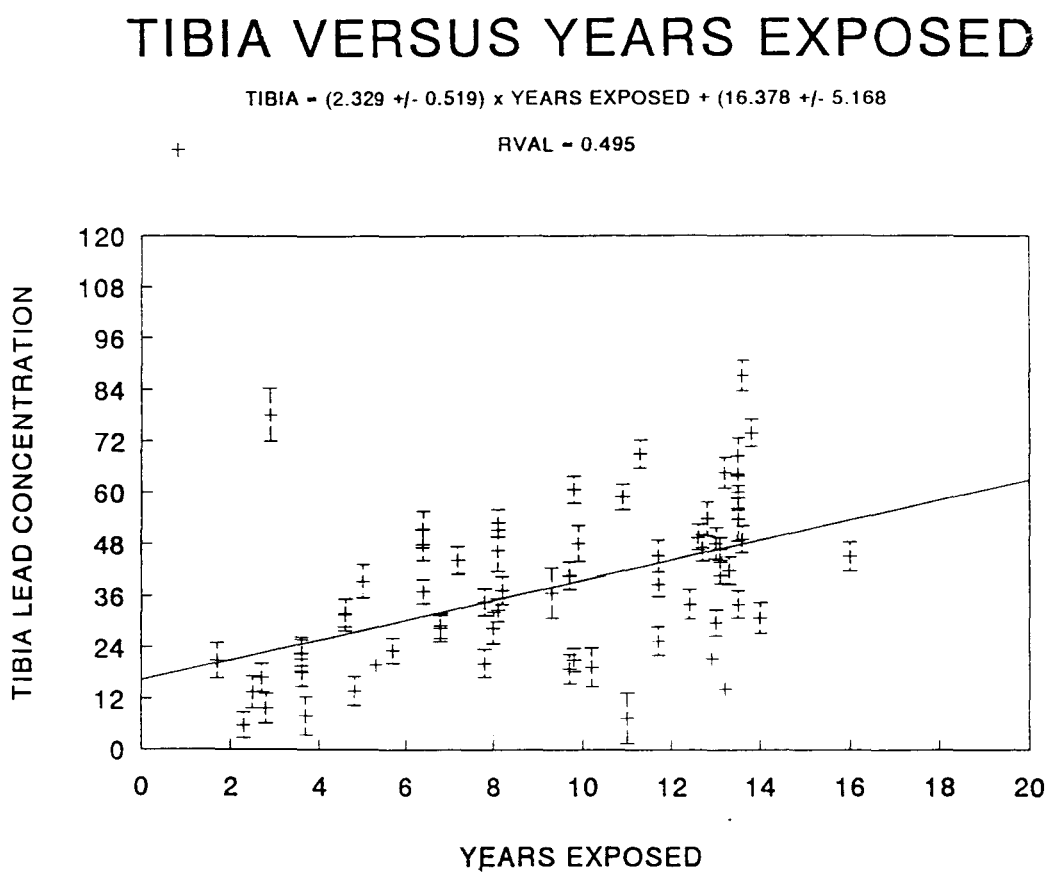

Figure 5.3: Tibia Lead Concentration versus Years Exposed -- Most Extreme Outlier Rejected

(ii.) Calcaneus Lead versus Years Exposed

Similar to what was observed with respect to the tibia, the calcaneus lead concentration is increasing with age, but the slope is much steeper. See figure 5.4. This makes sense since the calcaneus is an example of trabecular bone.

The correlation coefficient was 0.514 for a linear fit to the data points with a slope of 4.711 +/- 0.991 and an intercept of 19.917 +/- 9.899. It is also interesting to note that there are no outliers as was observed for the tibia case. As mentioned before, it would be ideal to separate the measurements according to job, but one is limited by the size of the data set.

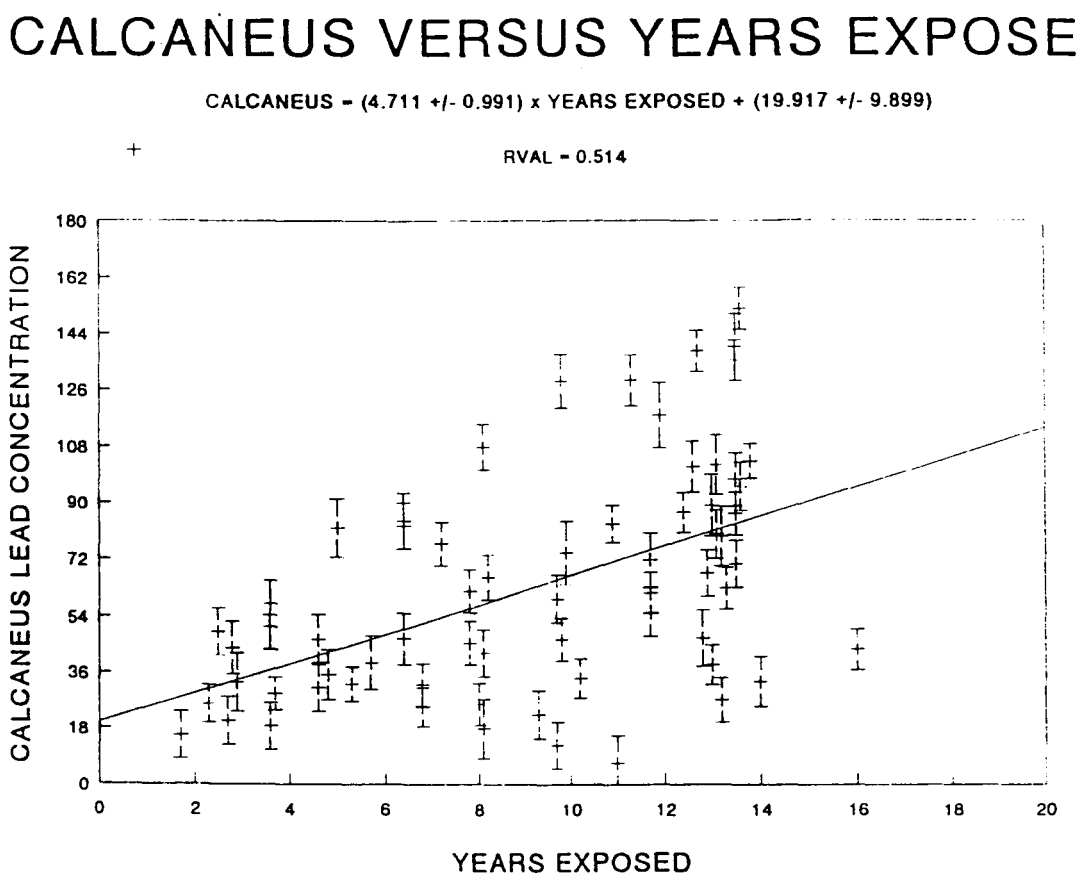

Figure 5.4: Calcaneus Lead Concentration versus Years Exposed

Chapter 6

Serum lead Analysis

6.1 **Introduction**

Plasma is considered to be the biologically most readily available compartment of lead. The difference between the terms, plasma and serum, is that plasma contains fibrinogen, but with respect to lead, plasma and serum are essentially the same. Even though the significance of lead in serum is widely recognized, the concentration of lead in serum is not routinely measured, because the lead concentration is low which makes it difficult to quantitate accurately. Serum lead concentrations lie in the range of 0.5 - 5% of whole blood lead concentration [95,96]. Therefore, difficulties can quickly arise from the lysis of a small number of red cells, minor external contamination, and inadequate measurement sensitivity. Regardless of the potential problems, it is still useful to measure serum lead concentration in order to further existing knowledge of human lead metabolism.

The serum samples collected for the Nova Pb bone lead survey were analyzed by Bowins and McNutt [77]. Essentially, 0.10 ml of 100 ng/ml, 99.73% ^{204}Pb solution was added to 1.00 ml of each serum sample which was acidified with 0.10 ml of 15 M nitric acid. 10 μl aliquots were then volatilized in a graphite furnace and introduced to an inductively coupled plasma mass spectrometer. Unfortunately, the

accuracy of the method is difficult to assess with complete confidence due to the lack of certified standard materials. Although, it is believed that the inaccuracy is relatively small, because the serum lead concentrations for a group of non-occupationally exposed subjects using this technique ranged from 0.37 - 1.27 $\mu g\ l^{-1}$ [97] which are very similar to the values reported by Manton and Cook, 0.32 - 1.20 $\mu g\ l^{-1}$ [96].

6.2 Serum Lead versus Endogenous and Exogenous Exposure

First of all, the terms, endogenous and exogenous exposure, should be defined. Endogenous exposure is best described by considering your own body as a source of lead while the source, in the case of exogenous exposure, is current environmental conditions. In order to estimate the endogenous contribution to whole blood lead, one used the equations determined by Gerhardsson et al based on the data obtained from retired lead workers [98].

$$whole\ blood = 0.00654\ \frac{\mu mol\ l^{-1}}{\mu g\ g^{-1}}\ x\ tibia\ Pb \qquad (29)$$

$$whole\ blood = 0.00324 \frac{\mu mol\ l^{-1}}{\mu g\ g^{-1}} x\ calcaneus\ Pb \quad (30)$$

**N.B. One needs to multiply the slopes of the above equations by 207.2 in order to convert the units of whole blood lead to μg/l.

For example, NPB33,

tibia = 34.59 μg g^{-1}

calcaneus = 62.13 μg g^{-1}

measured whole blood = 461 μg l^{-1}

Thus, due to endogenous exposure:

whole blood $_{tibia}$ = 46.87 μg l^{-1}

whole blood $_{calcaneus}$ = 41.69 μg l^{-1}

mean whole blood lead = 44.28 μg l^{-1} ~ 44 μg l^{-1}

Therefore, the mean whole blood lead due to endogenous exposure is 44 μg l^{-1}. Since the measured whole blood lead is 461 μg l^{-1}, then the contribution in whole blood due to exogenous exposure is 417 μg l^{-1}. Table 6.1 outlines the results.

TABLE 6.1

ID#	SERUM LEAD (μg/l)	ENDOGENOUS (μg/l)	EXOGENOUS (μg/l)
NPB01	4.96 +/- 0.12	37	308
NPB02	5.68 +/- 0.15	38	324
NPB03	8.03 +/- 0.28	63	406
NPB04	4.37 +/- 0.08	24	321
NPB05	6.71 +/- 0.03	79	349
NPB06	7.94 +/- 0.11	37	410
NPB08	5.48 +/- 0.21	55	359
NPB09	9.82 +/- 0.75	88	386
NPB10	4.63 +/- 0.09	33	229
NPB11	3.23 +/- 0.16	32	290
NPB12	2.49 +/- 0.10	21	275
NPB14	3.44 +/- 0.16	21	260
NPB15	10.50 +/- 0.28	48	504
NPB16	5.88 +/- 0.27	57	419
NPB17	3.88 +/- 0.16	52	194
NPB18	7.44 +/- 0.19	84	344
NPB19	8.30 +/- 0.08	63	340
NPB20	4.30 +/- 0.27	36	311
NPB21	3.66 +/- 0.16	30	332
NPB22	3.52 +/- 0.04	13	254
NPB23	4.82 +/- 0.09	50	285
NPB24	6.29 +/- 0.04	68	225
NPB25	8.58 +/- 0.60	110	260

NPB26	9.26 +/- 0.02	53	437
NPB27	6.06 +/- 0.16	65	305
NPB28	1.72 +/- 0.03	32	175
NPB31	6.78 +/- 0.21	45	296
NPB33	9.99 +/- 0.22	44	417
NPB35	8.52 +/- 0.34	78	354
NPB36	4.14 +/- 0.07	19	239
NPB37	3.86 +/- 0.10	26	249
NPB38	7.05 +/- 0.38	15	363
NPB39	4.16 +/- 0.12	48	316
NPB40	7.36 +/- 0.41	90	408
NPB43	6.05 +/- 0.70	30	270
NPB44	7.03 +/- 0.03	29	438
NPB45	9.05 +/- 0.15	71	436
NPB46	5.64 +/- 0.02	85	308
NPB47	7.41 +/- 0.19	72	315
NPB48	5.27 +/- 0.04	52	256
NPB49	5.10 +/- 0.10	60	240
NPB50	6.13 +/- 0.07	45	292
NPB52	5.52 +/- 0.16	28	193
NPB54	4.59 +/- 0.16	64	290
NPB56	10.44 +/- 0.22	129	363
NPB57	2.64 +/- 0.05	19	196
NPB60	4.12 +/- 0.10	25	389
NPB61	2.43 +/- 0.20	48	117
NPB64	2.57 +/- 0.14	38	200

The correlation coefficient for the graph of serum lead versus exogenous exposure was quite high, 0.728. The slope was 0.0205 +/- 0.0028 with an intercept of -0.530 +/- 0.906. See figure 6.1. The correlation coefficient calculated for the relationship between serum lead and endogenous exposure was not as high, 0.616. The slope for such a graph was calculated to be 0.0556 +/- 0.0104 with an intercept of 3.073 +/- 0.580. See figure 6.2. It is interesting to note that the slope is higher for the graph of serum lead versus endogenous exposure than for the graph of serum lead versus exogenous exposure. This implies that the proportion of circulating lead in the serum is greater when the source of lead is internal (bone) than when the source of lead exposure is external.

The fact that exogenous exposure correlates better than endogenous exposure implies the serum lead is more reflective of current, external exposure than the slow release from bone (endogenous exposure). This makes sense, since the half-life of lead in serum is approximately 8 hours. As well, all the individuals measured for the Nova Pb bone lead survey were active lead workers, therefore one would expect better correlation with exogenous exposure. It will also be interesting to analyze the data collected during the Brunswick bone lead survey which dealt with retired and active lead workers. For retired lead workers, one would expect the plasma lead to correlate more strongly with endogenous exposure since the bone is the only influence except for background environmental conditions.

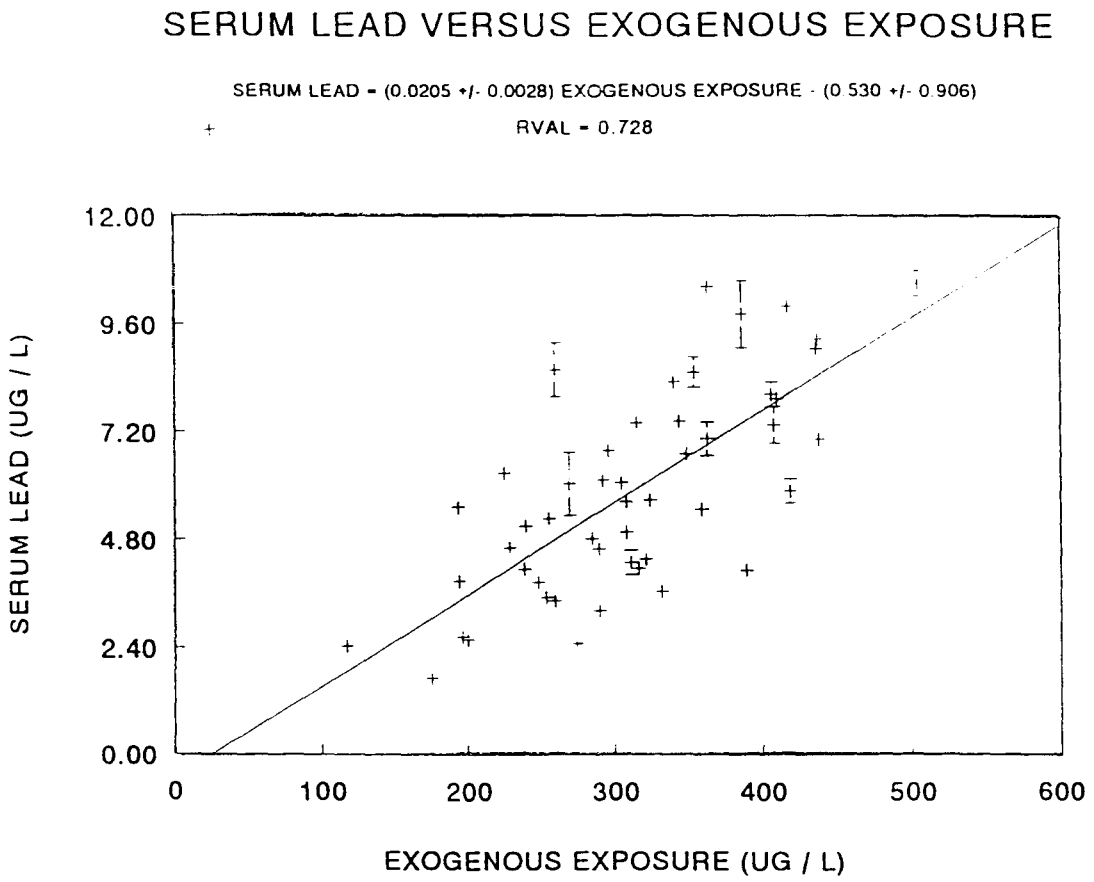

Figure 6.1: Serum lead Concentration versus Exogenous Exposure.

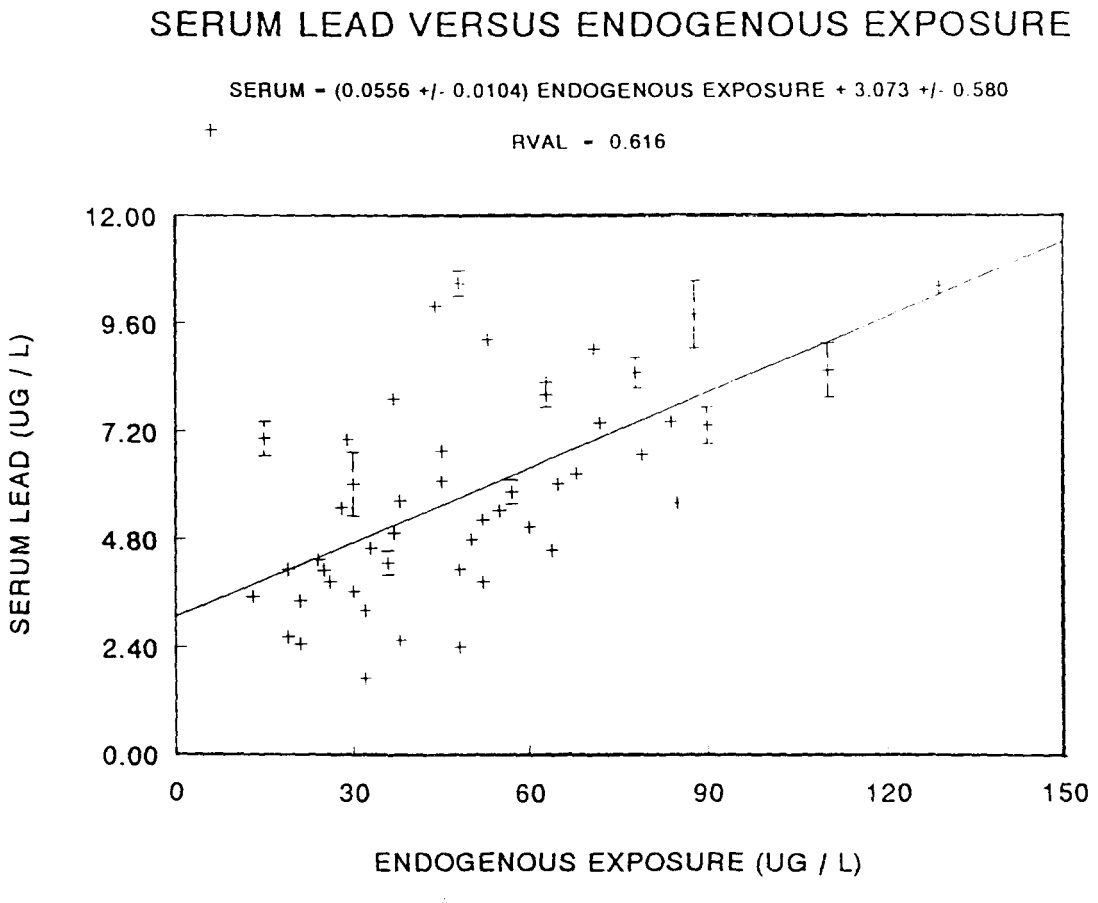

Figure 6.2: Serum Lead Concentration versus Endogenous Exposure.

Exogenous exposure does not correlate ($r_{1,2}$ = 0.261) significantly with endogenous exposure. See figure 6.3. This observation has important implications. One should first remember that serum correlated partly with exogenous exposure (r_1 = 0.728) and partly, but separately, with endogenous exposure (r_2 = 0.616). To a first approximation, one could say that the total proportion of variation in serum by exogenous and endogenous exposure is equal to $r_1^2 + r_2^2$, 0.909. This is a maximum estimate, because some of the variation could be due to the weak relationship between endogenous and exogenous exposure. Therefore, the minimum proportion of variation would be equal to $r_1^2 + r_2^2 - r_{1,2}^2$, 0.841. Based on the lowest estimate, 84% of the variation in serum lead can be explainable through its relationship with endogenous and exogenous exposure. It will be interesting to see if similar results are obtained with the Brunswick survey data.

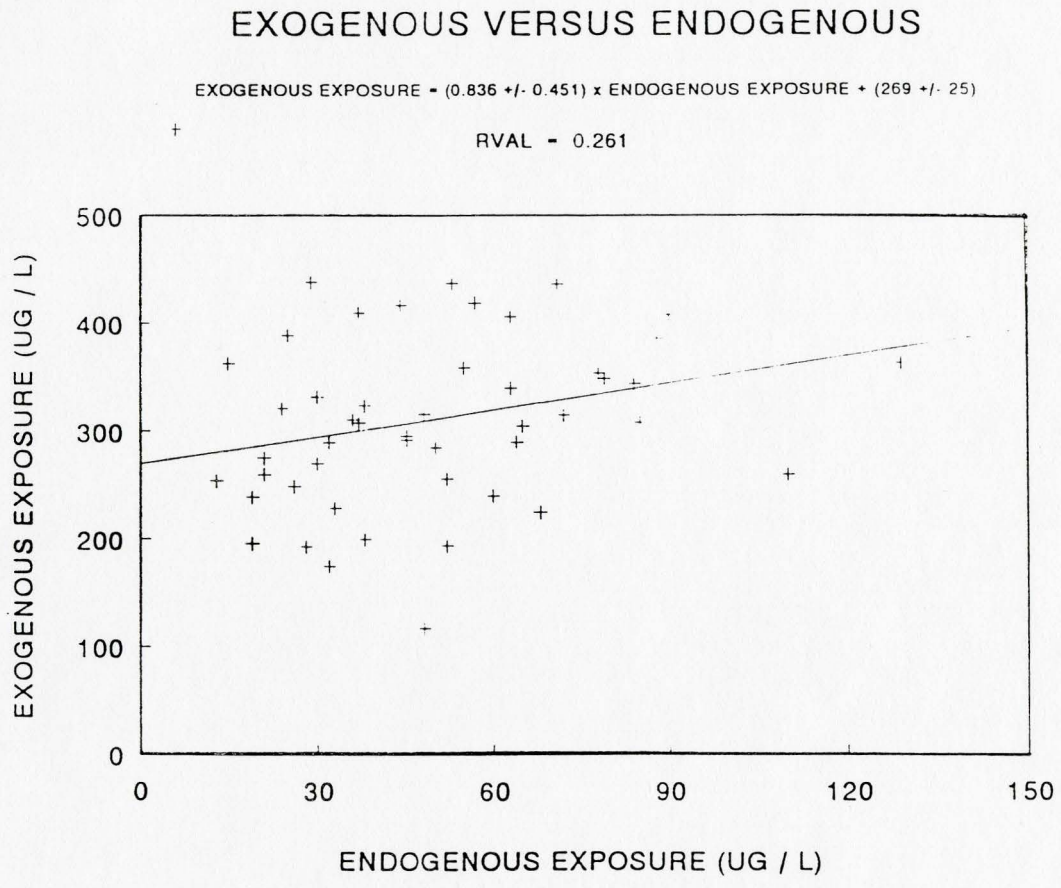

Figure 6.3: Exogenous Exposure versus Endogenous Exposure.

Chapter 7

Closing Remarks

7.1 **Interrelationships between Whole Blood, Serum, and Bone Lead**

In chapter 5, it had already been mentioned that only 49 factory workers had serum lead, whole blood lead, tibia lead, and calcaneus lead measurements done. It is also important to remember that the whole blood lead measurement used was the one made closest to the time of the bone lead survey.

The interrelationships were studied by performing pairwise regressions amongst the four parameters. The following equations summarize the results, where the units for bone lead is μg Pb [g bone mineral]$^{-1}$ and μg/l for both whole blood lead (WB) and serum lead. As well, one should note that the abbreviation, CALC, will occasionally be used for the word, calcaneus, due to space requirements.

$$CALCANEUS = (1.17 +/- 0.16)\ x\ TIBIA + (18.3 +/- 7.6)$$

$$r = 0.721,\ t = 7.138,\ p < 0.001 \qquad (29)$$

$$WHOLE\ BLOOD = (1.61 +/- 0.55)\ x\ TIBIA + (295 +/- 25)$$

$$r = 0.394,\ t = 2.942,\ 0.001 < p < 0.01 \qquad \textbf{(30)}$$

$$WHOLE\ BLOOD = (1.42 +/- 0.30)\ x\ CALCANEUS + (267 +/- 23)$$

$$r = 0.567,\ t = 4.719,\ p < 0.001 \qquad \textbf{(31)}$$

$$SERUM = (0.0522 +/- 0.0128)\ x\ TIBIA + (3.72 +/- 0.60)$$

$$r = 0.509,\ t = 4.058,\ p < 0.001 \qquad \textbf{(32)}$$

$$SERUM = (0.0408 +/- 0.0070)\ x\ CALCANEUS + (3.14 +/- 0.53)$$

$$r = 0.648,\ t = 5.833,\ p < 0.001 \qquad \textbf{(33)}$$

$$SERUM = (0.0206 +/- 0.0021)\ x\ WHOLE\ BLOOD - (1.58 +/- 0.78)$$

$$r = 0.820,\ t = 9.817,\ p < 0.001 \qquad \textbf{(34)}$$

With respect to the above equations, r refers to the correlation coefficient, t is the t value based on 47 degrees of freedom, and p refers to the probability that there is no relationship between the two variables. Except for the relationship between whole blood and tibia which achieves significance at the 1% level, the rest are all significant at the 0.1% level.

It is interesting to note that the relationship between serum lead and either bone lead is significant. As well, the correlation coefficients are numerically higher in the relationships between serum and bone lead than whole blood and bone lead which makes sense since lead that comes out of bone goes to the plasma compartment first before the red blood cells. The strong correlation of serum lead with bone lead is reflective of the release of lead from bone stores, endogenous exposure.

The intercepts in the regression equations of (serum lead / whole blood lead) versus bone lead are estimates of this ratio in the case of exogenous exposure.

$$\frac{SERUM}{WB} = [(6.74 +/- 2.38)x\ 10^{-5}]\ x\ TIBIA + (0.0132 +/- 0.0011)$$

$$r = 0.382,\ t = 2.835 \qquad \textbf{(35)}$$

$$\frac{SERUM}{WB} = [(5.04 +/- 1.40) x 10^{-5}] \; x \; CALC + (0.0126 +/- 0.00111)$$

$$r = 0.464, \; t = 3.596 \qquad \textbf{(36)}$$

The values for the intercepts are 0.0132 and 0.0126 for the tibia and the calcaneus. Similarly, the intercepts in the relationships between whole blood and bone lead are estimates of the amount of whole blood lead due to exogenous exposure. Also, the intercepts in the regression equation of serum lead versus bone lead are numerically similar, 3.72 μg/l and 3.14 μg/l, for the tibia and calcaneus, and are estimates of the impact of exogenous exposure.

When the bone lead was high, it was observed that serum lead tended to be a higher proportion of whole blood lead. Further evidence for such an observation is the fact that the ratio of serum lead to whole blood lead correlated significantly with either bone lead.

The ratio of the slopes of the graphs of serum lead versus bone lead and whole blood lead versus bone lead are 0.0324 and 0.0287 for the tibia and calcaneus. This result and the fact that the ratio of serum lead over whole blood lead correlates

significantly with bone lead implies that the amount of lead circulating in the serum is greater when the source of lead is endogenous than exogenous. Therefore, one can conclude that endogenous exposure results in serum lead being 0.0306 of whole blood lead while for exogenous exposure the proportion is 0.0129. This hypothesis is also reinforced by comparing calcaneus and tibia lead concentrations. Since the calcaneus is an example of trabecular bone which has a shorter biological half-life than the tibia, cortical bone, endogenous exposure would be expected to relate more closely to the calcaneus lead concentration than the tibia. Such a statement is supported by the fact that the correlation coefficients for the graphs of serum, whole blood, and serum/whole blood versus bone lead are all numerically higher for the calcaneus than the tibia.

Further work needs to be done to test the hypothesis that endogenous exposure to lead results in a different partitioning of lead between serum and red blood cells than that resulting from exogenous exposure. An excellent way to test this hypothesis would be to study retired workers, since the dominant contributor to whole blood lead would only be endogenous exposure. If the hypothesis is confirmed, it implies that endogenous exposure results in 2-3 times as much lead in serum as would be predicted from whole blood lead measurements alone. Usually, more concern is placed on the health hazard represented by exogenous exposure, but these results indicate that one should be concerned about the health risk associated with endogenous exposure.

7.2 **Future Work**

In each "result" chapter (chapter 3 and onwards), future work that needs to be done with respect to a specific area was discussed. Such work should eventually lead to improvements in the techniques used to analyze bone lead measurements and hopefully answer a few questions about human lead metabolism.

This thesis has looked at the essential components of any human lead metabolism model, bone, whole blood, and serum, and the interrelationships between them. The next step is to start to piece together all the information in order to create a plausible model.

Human lead metabolism models can be divided into two groups, compartmental and diffusion. Most of the research that has been done in studying lead metabolism has focussed heavily upon the compartmental models [99], but the general consensus now is that the diffusion model [100] more accurately reflects what is being observed in the human body. Both types of models have their strengths and weaknesses, thus the best approach would be to combine the positive qualities associated with each model. Unfortunately, the limited size of the Nova Pb bone lead survey data set, sporadic blood lead records, and the fact that not everyone had a serum lead measurement done makes it difficult to design such a model. With respect to the Brunswick bone lead survey, there should be enough information to accurately design a model for human lead metabolism. Consistent blood lead records, serum

samples from all volunteers, and a large data set make the latest survey very attractive for modelling prospects.

REFERENCES AND BIBLIOGRAPHY

[1] Hamilton, A., Exploring the Dangerous Trade, Boston: Little Brown, 1943.

[2] Schutz, A. and Skerfving, S., "Effect of a Short, Heavy Exposure to Lead Dust Upon Blood Lead Level, Erythrocyte δ-Aminolevulinic Acid Dehydratase Activity and Urinary Excretion of Lead, δ-Aminolevulinic Acid, and Coproporphyrin. Results of a 6 Month Follow-up of Two Male Subjects"; Scand. J. Work Environ. Health, 3, pp. 176-84, 1976.

[3] Meredith, R.A. et al., "Delta-Aminolevulinic Acid Metabolism in Normal and Lead Exposed Humans"; Toxicology, 9, pp. 1-9, 1978.

[4] Hernberg, S., "Biochemical and Clinical Effects and Responses as Indicated by Blood Lead Concentration"; Lead Toxicity, Edited by R.L. Singal et al., Urban and Schwarzenberg, Baltimore, pp. 367-99, 1980.

[5] Piomelli, S., "A Micromethod for Free Erythrocyte Prophyrins: the FEP Test"; J. Lab. Clin. Med., 81, pp. 932-40, 1973.

[6] Putnam, R.D., "Review of Toxicology of Inorganic Lead"; Am. Ind. Hyg. Assoc. J., 47, 11, pp. 700-3, 1986.

[7] Ratcliffe, J.M., Lead in Man and the Environment, Connecticut: Eastern Graphics Inc., pp. 35, 1981.

[8] Araki, S. and Honma, T., "Relationship Between Lead Absorption and Peripheral Nerve Conduction Velocities in Lead Workers"; Scand. J. Work Environ. and Health, 4, p. 225, 1976.

[9] Seppalainen, A.M. et al., "Relationship Between Blood Lead Levels and Nerve Conduction Velocities"; Neurotoxicology, 1, p. 313, 1979.

[10] Wedeen, R.P. et al., "Occupational Lead Nephropathy"; Am. J. Med., 59, pp. 630-41, 1975.

[11] Lilis, R. et al., "Kidney Function and Lead: Relationships in Several Occupational Groups with Different Levels of Exposure"; Am. J. Ind. Med., 1, pp. 405-12, 1980.

[12] Verschoor, M. et al., "Influence of Occupational Low-Level Lead Exposure on Renal Parameters"; Am. J. Ind. Med., 12, pp. 341-51, 1987.

[13] Rosen, J.F. et al., "Reduction in 1,2,5 - Dihydroxyvitamin D in Children with Increased Lead Absorption"; N. Engl. J. Med., 302, pp. 1128-31, 1980.

[14] Landrigan, P.J., "Toxicity of Lead at Low Dose"; Br. J. Ind. Med., 46, pp. 593-6, 1989.

[15] Rom, W.N., "Effects of Lead on Reproduction"; Proceedings of a Workshop on Methodology for Assessing Reproductive Hazards in the Workplace, Edited by P.F. Infante and M.S. Legator, National Institute for Occupational Safety and Health, Washington DC, 1980.

[16] Lancranjan, I. et al., "Reproductive Ability of Workers Occupationally Exposed to Lead"; Arch. Environ. Health, 30, pp. 396-401, 1975.

[17] Bornschein, R.L. et al., "The Cincinnati Prospective Study of Low-Level Lead Exposure and its Effects on Child Development: Protocol and Status Report"; Environ. Res., 38, pp. 4-18, 1985.

[18] Bellinger, D. et al., "Longitudinal Analyses of Prenatal and Postnatal Lead Exposure and Early Cognitive Development"; N. Engl. J. Med., 316, pp. 1037-43, 1987.

[19] McMichael, A.J. et al., "Port Pirie Cohort Study: Environmental Exposure to Lead and Children's Abilities at the Age of Four Years"; N. Engl. J. Med., 319, pp. 468-75, 1988.

[20] Rabinowitz, M. et al., "Absorption, Storage, and Excretion of Lead by Normal Humans"; Trace Substances in Environmental Health, Edited by D.D. Hemphill, University of Missouri Press, Missouri, pp. 361-8, 1975.

[21] Fielding, J.E. and Russo, P.K., "Exposure to Lead: Sources and Effects"; N. Engl. J. Med., 297, pp. 943-5, 1977.

[22] Rabinowitz, M.B. et al., "Effect of Food Intake and Fasting on Gastrointestinal Lead Absorption in Humans"; Am. J. Clin. Nutr., 33, pp. 1784-8, 1980.

[23] Watson, W.S. et al., "Food Iron and Lead Absorption in Humans"; Am. J. Clin. Nutr., 44, pp. 248-56, 1986.

[24] Aub, J.C. et al., "Significance of Bone Trabeculae in the Treatment of Lead Poisoning. Lead Studies XVII"; Am. J. Public Health, 22, pp. 825-30, 1932.

[25] Sobel, A.E. et al., "The Biochemical Behaviour of Lead. I. Influence of Calcium, Phosphorus, and Vitamin D on Lead in Blood and Bone"; J. Biochem., 132, pp. 239-65, 1940.

[26] McLean, R. et al., "Migration of Inorganic salts in Bone as Measured by Radioactive Lead and by Alizarin"; Arch. Ind. Hyg. Occup. Med., 9, pp. 113-121, 1954.

[27] Lindh, U. et al., "Microprobe Analysis of Lead in Human Femur by Proton Induced X-Ray Emission (PIXE)"; Sci. Total Environ., 10, pp. 31-7, 1978.

[28] Hu, H. et al., "X-ray Fluorescence Issues Surrounding the Application of a New Tool for Measuring Burden of Lead"; Environ. Res., 49, pp. 295-317, 1989.

[29] Jones, K.W. et al., "Distribution of Lead in Human Bone. III. Synchrotron X-Ray Microscope Measurements"; Advances in In vivo Composition Studies, Edited by S. Yasumura et al., Plenum Press, New York, pp. 275-80, 1990.

[30] Gong, J.K. et al., "The Density of Organic and Volatile and Non-Volatile Inorganic Components of Bone"; Anat. Rec., 149, pp. 319-24, 1964.

[31] Johnson, L.C., Bone Biodynamics, Edited by H.M. Frost, Boston: Little Brown, 1964, pp. 543-654.

[32] O'Flaherty, E.J., "Physiologically Based Models for Bone-Seeking Elements. I. Rat Skeletal and Bone Growth"; Toxicology and Applied Pharmacology, 111, pp. 299-312, 1991.

[33] Smith, F.A. and Hursh, J.B., "Bone Storage and Release"; Handbook of Physiology Reactions to Environmental Agents, Edited by S.R. Geiger et al., Williams and Wilkins, Baltimore, pp. 469-82, 1977.

[34] Rabinowitz, M.B. et al., "Kinetics of Lead Metabolism in Healthy Humans"; J. Clin. Invest., 58, pp. 260-70, 1976.

[35] Barry, P.S.I., "A Comparison of Concentrations of Lead in Human Tissues"; Br. J. Ind. Med., 32, pp. 119-39, 1975.

[36] International Commission on Radiological Protection, "Report of the Task Group on Reference Man:; Publication 23, Pergamon Press, Oxford, 1975, pp. 73.

[37] Gamblin, C. et al., "In Vivo Measurements of Bone Lead Content in Residents of Southern Ontario"; to be published.

[38] U.S. EPA, "Air Quality Criteria for Lead"; EPA-60018-83-028, Environmental Criteria and Assessment office, Research Triangle Park, NC., June, 1986.

[39] Kehoe, R.A., "The Metabolism of Lead in Man in Health and Disease: the Normal Metabolism of Lead"; J. R. Inst. Public Health Hyg., 24, pp. 81-97, 1960.

[40] Heard, M.J. and Chamberlain, A.C., "Effects of Minerals and Food Uptake of Lead from the Gastrointestinal Tract in Humans"; Hum. Toxicol., 1, pp. 411-5, 1982.

[41] Rabinowitz, M.B., "Toxicokinetics of Bone Lead"; Environ. Health Perspec., 91, pp. 33-7, 1991.

[42] Marcus, A.H. and Schwartz, J., "Dose-Response Curves for Erythrocyte Protoporphyrin vs. Blood Lead: Effect of Iron Status"; Environ. Res., 44, pp. 221-7, 1987.

[43] Barry, P.S.I. and Mossman, D.B., "Lead Concentrations in Human Tissues"; Br. J. Ind. Med., 27, pp. 339-51, 1970.

[44] Barry, P.S.I., "Concentrations of Lead in Tissues of Children"; Br. J. Ind. Med., 38, pp. 61-71, 1981.

[45] Gerhardsson, L. et al., " Kidney Effects in Long-Term Exposed Lead Smelter Workers"; Br. J. Ind. Med., 49, pp. 186-92, 1992.

[46] Nilsson, U. et al., "Kinetics of Lead in Bone and Blood After the End of Occupational Exposure"; Pharmacol. Toxicol., 69, pp. 477-84, 1991.

[47] Lagerkvist, B.J. et al., "Kadmiumhalter Hos Gravida "; Abstract, Annual General Meeting of the Swedish Medical Association, 1990.

[48] Silbergeld, E.K. et al., "Lead and Osteoporosis: Mobilization of Lead from Bone in Postmenopausal Women"; Environ. Res., 47, pp. 79-94, 1988.

[49] Osterloh, J. and Berker, C.E., "Pharmacokinetics of $CaNa_2EDTA$ and Chelation of Lead in Renal Failure"; Clin. Pharmacol. Ther., 40, pp. 686-93, 1986.

[50] Hammond, P.B., "The Effects of Chelating Agents on the Tissue Distribution and Excretion of Lead"; Toxicol. Appl. Pharmacol., 18, pp. 296-310, 1971.

[51] Castellino, N. and Aloj, S., "Effects of Calcium Sodium Ethylenediaminetetra-Acetate in the Kinetics of Distribution and Excretion of Lead in the Rat"; Br. J. Ind. Med., 22, pp. 172-80, 1965.

[52] Germain, M.J. et al., "Failure of Chelation Therapy in Lead Nephropathy"; Arch. Intern. Med., 144, pp. 2419-20, 1984.

[53] Westerman, M.P. et al., "Concentrations of Lead in Bone in Plumbism"; N. Engl. J. Med., 273, pp.1246-50, 1965.

[54] Batuman, V. et al., "Reducing Bone Lead Content by Chelation Treatment in Chronic Lead Poisoning: an In Vivo X-Ray Fluorescence and Bone Biopsy Study"; Environ Res., 48, pp.70-5, 1989.

[55] Tell, I. et al., "Chelated Lead and Bone Lead"; Scand. J. Work Environ. Health, 18, pp. 113-9, 1992.

[56] Wedeen, R.P. et al., "Lead Nephropathy: In Vivo X-Ray Fluorescence (XRF) for Assessing Body Lead Stores"; In Vivo Body Composition Studies, Edited by K.J. Ellis et al., Bocardo Press, Oxford, pp. 357-62, 1987.

[57] Ahlgren, L. et al., "X-Ray Fluorescence Analysis of Lead in Human Skeleton In Vivo"; Scand. J. Work Environ. Health, 2, pp. 82-6, 1976.

[58] Price, J. et al., "In Vivo X-Ray Fluorescence Estimation of Bone Lead Concentrations in Queensland Adults."; Br. J. Radiol., 57, pp. 29-33, 1984.

[59] Bloch, P. et al., "Measurement of Lead Content of Children's Teeth in situ by X-ray Fluorescence"; Phys. Med. Biol., 22, 1, pp. 56-63, 1977.

[60] Chettle, D.R. et al., "Measurements of Trace Elements In Vivo"; In Vivo Body Composition Studies, Edited by S. Yasumura et al., Plenum Press, New York, pp. 247-57, 1990.

[61] Chettle, D.R. et al., "Improvements in the Precision of In Vivo Bone Lead Measurements"; Phys. Med. Biol., 34, 9, pp. 1295-1300, 1989.

[62] Wielopolski, L. et al., "Feasibility of Non Invasive Analysis of Lead in the Human Tibia by Soft X-Ray Fluorescence"; Med. Phys., 10, pp. 248-51, 1983.

[63] Robinson, J.W., ed., Handbook of Spectroscopy, Second Edition, Bora Raton, Florida, CRC Press, 1979.

[64] Woodard, H.Q., "The Elementary Composition of Human Cortical Bone"; Health Physics, 8, pp. 513-517, 1962.

[65] International Commission on Radiological Protection, "Report on the Task Group of Reference Man"; Publication 23, Pergamon, Oxford, 1975.

[66] Chettle, D.R. et al., "Lead in bone: Sampling and Quantitation Using K X-Rays Excited by ^{109}Cd"; Environ. Health Perspec., 91, pp. 49-55, 1991.

[67] Kornylo, D.J., illustration of lead detection system, internal communication, McMaster University, 1994.

[68] Thomas, B.J., "Equipment Design Issues for the In Vivo X-Ray Fluorescence Analysis of Bone Lead"; Environ. Health Perspec., 91, pp. 39-43, 1991.

[69] Hubbell, J.H. and Overbo, I., "Relativistic Form Factors and Photon Coherent Scattering Cross Sections"; J. Phys. Chem. Ref. Data, 8, pp. 69-105, 1979.

[70] Somervaille, L.J. et al., "In Vivo Measurement of Lead in Bone Using X-Ray Fluorescence"; Phys. Med. Biol., 30, 9, pp. 929-43, 1985.

[71] Todd, A.C. and Chettle, D.R., "In Vivo X-Ray Fluorescence of Lead in Bone: Review and Current Issues"; Environ Health Perspec., 102, pp. 172-7, 1994.

[72] Wittmers, L.E. et al., "Lead in Bone. IV. Distribution of Lead in the Human Skeleton"; Arch. Environ. Health, 43, 6, pp. 381-91, 1988.

[73] Somervaille, L.J. et al., "Comparison of Two In Vitro Methods of Bone Lead Analysis and the Implications for In Vivo Measurements"; Phys. Med. Biol., 31, pp. 1267-74, 1986.

[74] Somervaille, L.J. et al., "X-Ray Fluorescence of Lead In Vivo: Simultaneous Measurements of a Cortical and a Trabecular Bone in a Pilot Study"; In Vivo Body Composition Studies, Edited by S. Yasumura et al., Institute of Physical Sciences in Medicine, London, pp. 325-33, 1987.

[75] Canberra Industries Inc., "Germanium Detectors - User's Manual"; Meridan, Ct., 1991.

[76] Todd, A.C. et al., "In Vivo X-ray Fluorescence of Lead in Bone Using K X-Ray Excitation with ^{109}Cd Source: radiation Dosimetry Studies"; Environ Res., 57, pp. 117-132, 1992.

[77] Bowins, R.J. and McNutt, R.H., "Analyses of Pb in Human Serum and Urine by Graphite-Furnace Isotope-Dilution ICP/MS"; (in press, 1994).

[78] Canberra Industries Inc., One State Street, Meriden, Ct., U.S.A., 06450.

[79] Aptec Engineering Limited, East-50B Caldari Road, Concord, Ontario, Canada, L4K 4N8.

[80] EG & G Nuclear Instruments, 100 Midland Road, Oak Ridge, Tn., U.S.A., 37831.

[81] Knoll, G.F., Radiation Detection and Measurement, Second Edition, U.S.A.: John Wiley and Sons, 1989.

[82] Chettle, D.R., internal communication, McMaster University, 1993.

[83] Bevington, P.R., Data Reduction and Error Analysis for the Physical Sciences, U.S.A.: McGraw-Hill Inc., 1969.

[84] Marquadt, D.W., "An Algorithm for Least-Squares Estimation of Nonlinear Parameters"; J. Soc. Ind. Appl. Math, 11, 2, pp. 431-41, 1963.

[85] Somervaille, L.J. et al., "In Vivo Tibia Lead Measurements as an Index of Cumulative Exposure in Occupationally Exposed Subjects"; Br. J. Ind. Med., 45, pp. 174-81, 1988.

[86] Chettle, D.R., internal communication, McMaster University, 1994.

[87] Snedecor, G.W. and Cochran, W.G., Statistical Methods, Iowa: Iowa State University Press, 1989.

[88] Armstrong, R. et al., "Repeated Measurements of Tibia Lead Concentrations by In Vivo X-Ray Fluorescence in Occupational Exposure"; Br. J. Ind. Med., 49, pp. 14-6, 1992.

[89] Christoffersson, J.O. et al., "Lead in Finger Bone Analysed In Vivo in Active and Retired Lead Workers"; Am. J. Ind. Med., 6, pp. 447-57, 1984.

[90] Borjesson, J. et al., "In vivo matning au bly i ben hos langtids exponerade blyarbetare"; Presented at the Annual Meeting of the Swedish Society of Medicine, Stockholm, December 1993.

[91] Hu, H. et al., "Effect of Repeated Occupational Exposure to Lead, Cessation of Exposure, and Chelation on Levels of Lead in Bone"; Am. J. Ind. Med., 20, pp. 723-35, 1991.

[92] Erkkila, J. et al., "In Vivo Measurements of Lead in Bone at Four Anatomical Sites: Long Term Occupational and Consequent Endogenous Exposure"; Br. J. Ind. Med., 49, pp. 631-44, 1992.

[93] Gerhardsson, L. et al., "In Vivo Measurements of Lead in Bone in Long-Term Exposed Lead Smelter Workers"; Arch. Environ. Health, 48, pp. 147-56, 1993.

[94] Somervaille, L.J. et al., "In Vivo Measurements of Bone Lead - a Comparison of Two X-Ray Fluorescence Techniques Used at Three Different bone Sites"; Phys. Med. Bio., 34, pp. 1833-45, 1989.

[95] deSilva, P.E., "Determination of Lead in Plasma and Studies on its Relationship to Lead in Erythrocytes"; Br. J. Ind. Med., 38, pp. 209-17, 1981.

[96] Manton, W.I. and J.D. Cook, "High Accuracy (Stable Isotope Dilution) Measurements of Lead in Serum and Cerebrospinal Fluid"; Br. J. Ind. Med., 41, pp. 313-19, 1984.

[97] Cake et al., "The Partition of Circulating Lead Between Serum and Red Cells is Different for Internal and External Sources of Lead"; to be published.

[98] Gerhardsson, L. et al., "In Vivo Measurements of Lead in Bone in Long-Term Exposed Lead Smelter Workers"; Arch. Environ. Health, 48, pp. 147-56, 1993.

[99] Leggett, R.W., "An Age-Specific Kinetic Model of Lead Metabolism in Humans"; Environ. Health Perspec., 101, pp. 598-616, 1993.

[100] O'Flaherty, E.J., "Physiologically Based Models for Bone-Seeking Elements IV. Kinetics of Lead Disposition in Humans"; Toxicology and Applied Pharmacology, 118, pp. 16-29, 1993.